Dual-Stage Boosting Systems: Modeling of Configurations, Matching and Boost Control Options

by

Byungchan Lee

A dissertation submitted in partial fulfillment
of the requirements for the degree of
Doctor of Philosophy
(Mechanical Engineering)
in The University of Michigan
2009

Doctoral Committee:

Professor Dionissios N. Assanis, Co-Chair
Assistant Professor Dohoy Jung, Co-Chair
Research Professor Zoran S. Filipi
Assistant Professor Matthias Ihme

ACKNOWLEDGEMENTS

I would like to acknowledge the technical and financial support of the Automotive Research Center (ARC) by the National Automotive Center (NAC) located within the US Army Tank-Automotive Research, Development and Engineering Center (TARDEC) in Warren, Michigan. The ARC is a U.S. Army Center of Excellence for Automotive Research at the University of Michigan, currently in partnership with 6 other Universities.

TABLE OF CONTENTS

LIST OF TABLES

LIST OF FIGURES

LIST OF ABBREVIATIONS

BDC : bottom dead center
BSFC : brake specific fuel consumption
EIVC : early intake valve closure
LIVC : late intake valve closure
MBT : maximum brake torque
TDC : top dead center
VGT : variable geometry turbine
VNT : variable nozzle turbine
N_e : engine speed
V_d : engine displacement volume
T : temperature
p : pressure
η : compressor/turbine efficiency
γ : heat capacity ratio
ε : intercooler effectiveness
$\dot{W}$: power
$\dot{m}$: mass flow rate
$\dot{m}_{corr}$: corrected mass flow rate
c_p : constant pressure specific heat
η_{mech} : turbocharger mechanical efficiency
η_{vol} : volumetric efficiency
ρ : density
A/F : air-fuel ratio
R : gas constant
D : diameter of turbomachinery
T_{01} : inlet stagnation temperature
p_{01} : inlet stagnation pressure
T_{02} : outlet stagnation temperature
p_{02} : outlet stagnation pressure
μ : dynamic viscosity

Subscripts and Superscripts

amb : ambient
LPC : low pressure compressor
LPT : low pressure turbine
HPC : high pressure compressor
HPT : high pressure turbine
a : air
f : fuel

t : total
1-2 : from state 1 to 2
$\overline{X}_{1-2}$: average value of X from state 1 to 2

CHAPTER 1. INTRODUCTION

1.1. Overview

For millions of years, the changes in the climate have been driven by forces of nature, but in recent years, the average temperature of the Earth has been rising faster than ever before. The consensus in science is that much of that change has been driven by the significant increase of greenhouse gases in the atmosphere. These greenhouses gases are known to increase the average temperature of the atmosphere by trapping the heat radiated from the surface of the Earth. Scientists are now certain that human activities are changing the composition of the atmosphere, and that increasing the concentration of greenhouse gases will change the global climate at a rate that is unparalleled for the last many millions of years.

According to EPA, human activities have increased the concentration of CO_2, one of the direct greenhouse gases, by 36% globally since the Industrial Revolution, principally due to the combustion of fossil fuels. In 2006, CO_2 contributed 84.8% of the total greenhouse gases in the United States. The total CO_2 emission has increased by 18% from 1990 to 2006. The sources of CO_2 vary by region, but most researchers cite transportation for about 33%. Electric power generation in the US produces about another third, while heating our homes, manufacturing, agriculture and clearing forests account for the rest.

Due to current concern over global warming and the connection between fuel consumption and emissions of the greenhouse gases such as CO_2, improving the fuel economy of internal combustion engines for automotive applications has a higher priority this decade than at any time since the Oil Crisis in the 1970s. The seriousness of the issue is gaining ground, and the sense of urgency is growing around the need to address the issue in an effective way.

Various new or improved power train technologies are being exploited to reduce CO_2 emission by improving vehicle fuel economy. Among many technical innovations and improvements in power train technologies, engine downsizing (reduction in displacement volume and/or the number of cylinders) is one of the most effective methods to reduce fuel consumption, i.e. CO_2 emission [1-10]. Engine downsizing, the use of a smaller capacity engine operating at higher specific engine loads, is achieved by running with high levels of pressure boosting at full load using a supercharger or turbocharger.

In fact, most technical advances in automotive engineering can be viewed as means to allow engine downsizing as they improve the specific output of the engine. For example, in the past, one of the main limitations to maximum power for small Diesel engines was the ability to provide enough fuel in a limited injection period. Modern high pressure injection systems, such as common rail, have solved this problem significantly, allowing further downsizing of the engine.

Cantore *et al.* [2] have shown that the downsized 1.8 *l* Diesel engine with two-stage boosting system can achieve up to 24% of fuel economy improvement over the baseline 2.5 *l* turbocharged Diesel engine while meeting or exceeding the performance

targets of the baseline engine. Guzzella *et al.* [4] have concluded in their study that the downsized engine not only improves the fuel economy but also improves drivability of the vehicle by reducing overall vehicle weight as the smaller engine requires smaller and lighter engine subcomponents in the vehicle. The reduction in overall vehicle weight also contributes to even more improvement in fuel economy. Engine downsizing and subsequent downsizing of other related components are also advantageous in packaging, and frees up more space in the engine compartment for other features such as vehicle safety enhancement and allows better aerodynamic design of the vehicle.

Hybrid power train technologies are also emerging as a highly practical and efficient way to reduce fuel consumption [11-22]. In passenger cars, the application of hybrid systems seems to be beneficial in terms of CO_2 and fuel consumption reduction, at least as long as the vehicle is operated predominantly at part load conditions. Toussaint [11] has shown 19 to 31% improvement in fuel economy with a parallel hybrid electric vehicle consisting of a downsized engine and electric motor. The use of hybrid powertrain is also proven to be advantageous with city buses (21% improvement over Diesel engine counterpart [12], and up to 75% in [13]) in their very transient driving conditions.

However, in heavy duty applications, especially for long haul operation, the use of hybridization seems to be less attractive at least according to actual common understanding. Katrasnik [14] has shown that the improvement in the fuel economy of hybrid powertrains increases with decreasing test cycle average load and the powertrains incorporating internal combustion engines with smaller swept volume provide more fuel economy improvements for decreasing test cycle average load. The study concludes that

the hybrid powertrains perform best for the test cycles with lower average load, i.e. light duty application, whereas heavy duty application requires powertrains with low hybridization factor resulting in smaller benefits in the fuel consumption. Takada *et al.* [15] conducted an experiment on fuel economy improvement with a medium duty hybrid truck in real traffic conditions, and concluded that the hybrid truck did not show improvement in fuel economy in high way trip even though fuel economy improvement of 20% was observed for the urban trip where there were many traffic stops. Considering that the improvement in fuel economy of the hybrid powertrain also comes from the engine downsizing, even though part of the improvement is the result of advanced power management and regenerative braking, engine downsizing is a more fundamental method to reduce fuel consumption.

Engine downsizing by increasing the air available for fuel combustion with turbocharger improves the thermal efficiency of the engine and reduces the fuel consumption through a number of mechanisms, including:

- Reducing pumping losses as less volume is swept on each engine revolution.
- Using the compressor (powered by waste exhaust enthalpy) to force the piston down under boosted conditions to further reduce pumping losses, and to produce useful work during induction.
- An improvement in mechanical efficiency due to reduction in friction.
- Improved in-cylinder turbulence (tumble and swirl patterns) due to higher intake pressures and gas velocities which promote faster burning rates and hence improved combustion.
- Reduced fuel consumption at idle and part load conditions.

- Reduced overall heat losses due to exhaust heat recovery and reduced surface areas for heat transfer.

However, when the displacement of the engine is reduced substantially, its dependence on boosting system increases as the engine torque under naturally aspirated operation is lower and it needs high boost pressure to produce enough torque for acceleration. Although very effective, some characteristics of the turbocharged engines remain unsatisfactory and matching an engine to a turbocharger to achieve efficient turbocharger operation over a wide range of engine speed is a difficult and often a compromising process. For example, at low engine speed, turbocharged engine produces less torque than naturally aspirated engine with comparable power as the available exhaust energy is simply not enough to supply sufficient power to the compressor at low speed. In addition, transient response of the turbocharged engine is much slower than that of the naturally aspirated engine since the centrifugal compressor needs to reach substantial rotational speed to produce usable boost [23-24]. In Diesel engine applications, combined with smoke-limited fueling, both the steady-state low end torque and the transient response become even worse. In order to solve this inherent weakness of engine downsizing through turbocharging, various technologies have been developed for the turbocharger itself such as inertia reduction, aerodynamics and bearing improvements [25], variable geometry on both compressor and turbine sides [26], and electrically assisted turbocharger [27], as well as for the charging system architecture such as twin-turbo system [28], sequential system [29], and dual-stage system [30]. Also a number of alternative charging systems, such as positive displacement supercharger and electric compressor, are used in some applications either by themselves [31-33] or in combination

with the turbocharger [27, 34-35]. Even thought these devices generally increase fuel consumption, the benefits of using them can outweigh their shortcomings in some cases depending on the system design philosophy and the type of applications as they substantially reduce the turbo-lag associated with the exhaust driven turbochargers.

1.2. Literature Review on Air Charging Systems

1.2.1. Positive displacement supercharger

The most appealing asset of a positive displacement supercharger is its simplicity. It is easy to install and doesn't require complicated controls in most cases. It draws power through mechanical connection to the crankshaft, and its rotational speed is directly proportional to the rotational speed of the engine. The engine-compressor matching is relatively easy, and the boost pressure is almost constant over the entire range of engine operating speeds. Therefore, the torque curve is flat, and the turbo-lag problem is completely overcome. In effect, a supercharged engine behaves as a naturally aspirated engine with a larger displacement volume.

It is this linearity that makes designing and predicting its boosting characteristics relatively easier than turbocharging. However, a supercharged engine consumes more fuel than a turbocharged engine with comparable power since the supercharger draws power directly from the engine crankshaft. Another weakness of the supercharger, the parasitic loss, also comes from its simplicity. Since it is always connected to the crankshaft even when the boost is not needed, the parasitic losses become problematic especially at idle and part load conditions. Miyagi *et al.* [36] showed that for a Lysholm compressor, 70-80% of the parasitic losses come from unnecessary pumping. Therefore, it is important to minimize the airflow losses for these superchargers.

The most common types of positive displacement superchargers are the Roots blower and the Lysholm compressor. They are also known as the Roots type supercharger and screw type supercharger, respectively. The screw type compressor has two rotors, a male and a female, forming a set of chambers between themselves and the housing. The volume of the chamber decreases during the rotation and thus compresses the air that is trapped inside the chamber. The shapes of the two male and female rotors are very complex and difficult to manufacture. Thus, the cost of the Lysholm compressor is considerably higher than that of the Roots blower, making it less common. Unlike the Lysholm compressor, the Roots type blower has two similar rotors forming discrete volumes but with constant volume. Modern Roots type blowers have three lobes instead of two, and twisted lobes have become more common.

The Lysholm compressor has higher adiabatic (η_{ad}) and total (η_{total}) efficiency than the Roots type blower. Takabe *et al.* [37] shows η_{total} = 70% for the Lysholm compressor and η_{total} = 50% for the Roots blower, in spite of the lower mechanical efficiency of the Lysholm compressor due to its higher step up gear ratio. The difference in efficiency comes from their distinctive compression mechanisms. Unlike the near adiabatic internal compression of Lysholm compressor, for the Roots blower, the compression takes place at the outlet as the air exits the blower. This condition is more comparable to isochoric condition (constant volume process) than adiabatic condition, thus resulting in lower efficiency and higher heat loss.

However, the actual efficiency of the Lysholm compressor varies with engine operating condition. In order to fully utilize the higher efficiency of Lysholm compressor, the charge pressure at the compressors outlet has to be same as the intake manifold

pressure. Otherwise, the discharged air must go through either isochoric compression or isochoric expansion inside the intake manifold, which is known to be less efficient. As a result, the overall efficiency becomes somewhere between adiabatic and isochoric efficiency.

1.2.2. Centrifugal compressor as a supercharger

The centrifugal compressor is another type of supercharger that works on a different principle. It is a dynamic machine, whereas the Lysholm compressor and the Roots type blower are both positive displacement pumps. The air is accelerated very rapidly by the impeller and then carefully diffused to recover the kinetic energy as static pressure. Therefore, the centrifugal compressor operates on internal compression. The isentropic efficiency of the centrifugal compressor matches or sometimes exceeds that of the Lysholm compressor [38]. It is very compact in size and significantly less expensive to manufacture compared to the other types of superchargers.

However, the boosting characteristics of the centrifugal compressor are very non-linear and peaky when operating with internal combustion engines. It also requires very high speed to achieve useful boost. In addition, in order to achieve such high speed, well above 100,000 rpm, in a short period of time, substantial portion of the power must be wasted on just overcoming the inertia of the compressor during acceleration. The high speed also demands a gearbox. Therefore, the engine must overcome the combined inertia of the compressor and the gearbox. This requires that the gearbox must have very low inertia and can handle very high speed. Therefore, the cost of such gearbox offsets the cost savings from the compressor unit. This is why this type of compressor is less common than the other types.

1.2.3. Electrically driven supercharger

Electric assist has been used in two ways, either by having an extra electrically driven supercharger supporting the turbo at low loads and during transients or by having the electric motor attached directly on the turbocharger shaft. In this study, a centrifugal compressor is driven electrically by directly attached electric motor to support the turbocharger at low speeds and transient conditions. This type of arrangement offers a faster response due to the fact that the rotor of the electric motor can have a lower inertia because it is not connected to the turbine wheel. It also offers the possibility of higher boost pressures without variable compressors if it is fitted in series with the regular turbocharger. A third advantage is that the electric motor doesn't have to stand as high temperature as for the electrically assisted turbocharger since it is not in direct contact with the hot exhaust gas.

1.2.4. Single-stage turbocharging

The transient behavior of a single-stage turbocharger can be improved by turbocharger development. However, optimizing the flow through blade angles etc. is a continuous process that has been going on for many years, so no dramatic improvements are to be expected within a small time frame.

A fixed geometry turbine is not capable of supplying enough power to the compressor for the boost pressure required for low speed and during transient conditions. In addition, the flow range of a centrifugal compressor is a limiting factor, and if higher boost pressures are demanded, it will be even more difficult to achieve satisfactory width of the usable range since the width of the compressor map becomes narrower as the boost pressure approaches its maximum.

The primary motive for using variable geometry turbines in automotive applications is to reduce turbo-lag. Even though both the spark ignition engine and the Diesel engine benefit from this technology, the high exhaust gas temperature in spark ignition engines have prevented the variable geometry mechanism from being widely used [39].

Variable geometry turbocharging in Diesel engines has largely overcome the turbo-lag issue. The dominant VGT technology for Diesel applications is the Variable Nozzle Turbine (VNT), which is a system that uses pivoting vanes to change the speed and angle of the exhaust gas as it enters the turbine rotor.

By using variable geometry turbine, the exhaust energy absorbing capabilities of the turbine is increases substantially, resulting in vast improvements especially during transients. This is what lies behind the success of passenger car Diesel engines during the decade. Many research papers are published about the variable geometry turbines [26, 39-42]. The flow range of the compressor can also be improved though the use of variable nozzle compressor [43].

As the turbine power increases at low speeds, and subsequently on low mass flows, the compressor will eventually run into surge. In order to avoid surge, the compressor maps must be widened. One of the methods to widen the compressor map is to use variable geometry guide vanes at the compressor inlet. With the variable inlet guide vanes, the compressor can operate at higher boost level for lower mass flows without surge.

SEQUENTIAL SYSTEMS - The primary purpose of sequential turbocharging is to improve transient response at low engine speed. Twin turbocharging also improves the

transient response due to the lower inertia compared to the single turbocharger with similar flow capacity. However, the improvement is much more significant with sequential turbocharging since only one turbocharger is used at low engine speed instead of two. Tashima *et al.* [29] showed that the new sequential twin turbocharger used in Mazda RX-7 reached the maximum boost pressure 30% faster than the conventional turbocharger used in the previous model in acceleration test, and improved engine maximum power by 25% as well.

Backlund *et al.* [44] claimed that the series-sequential system was preferable to parallel-sequential system due to rough transition from single to twin turbocharger operation of the parallel-sequential system. However, Tashima *et al.* [29] showed that the pressure drop during the transition was almost eliminated in the parallel-sequential system by allowing the secondary turbocharger to accelerate before the change-over. Additionally, the parallel-sequential system has wider flow range than the series-sequential system. The series-sequential system is essentially a two-stage turbocharging system, and thus has narrower flow range while it allows for higher boost. Therefore, the parallel-sequential system is suitable for applications that require wider flow range but lower boost pressure, such as spark ignition engines, and the series-sequential system for higher boost applications such as Diesel engines.

1.2.5. Dual-stage turbocharging

Dual-stage turbocharging offers several advantages over single-stage turbocharging when it is applied properly. Improved specific power level across a broad speed range is an immediate benefit of the dual-stage turbocharging applied to Diesel engines [2, 9, 30], as the boost level reached with dual-stage turbocharging system is

much higher than single-stage turbocharging system can provide. Unlike spark ignition engines, Diesel engines benefit from increased boost level in excess of 4 bar as the boost level is only limited by the peak cylinder pressure.

Dual-stage turbocharging also provides better overall efficiency at high intake manifold pressure compared to single-stage turbocharging as the compression is done in two stages instead of one. At high intake manifold pressure in excess of 3.5 bar or more, the efficiency of single-stage turbocharger becomes unacceptably low whereas the dual-stage turbocharger operates more efficiently as the pressure ratio at each stage is well within the efficient region in the performance map. This two stage compression also effective reduces the likelihood of compressor surging. Since the pressure ratio is divided into two smaller steps while the mass flow rate is unaffected, the compressor operation is more robust in terms of surge limit.

In addition, transient behavior of a dual-stage turbocharged engine is improved because of the combination of a smaller high pressure turbocharger and a larger low pressure turbocharger [9, 30]. By configuring a relatively small high pressure turbocharger with a much larger low pressure turbocharger, the dual-stage turbocharging system provides significantly better boosting characteristics at both steady state and transient conditions. The smaller turbine at high pressure stage provides more power to the compressor compared to the single stage counterpart, thus enabling higher boost at both the early stage of acceleration and the steady state low speed operation. Lower moment of inertia of the smaller high pressure turbocharger also contributes to the overall fast response of the dual stage turbocharger performance.

1.3. Motivation and objectives

Considering that the fuel efficiency and CO_2 reduction are at the top of the agenda as the fuel cost continues to escalate and concerns grow over future energy supply and global warming, the recent popularity of Diesel engines seems quite natural. However, the specific power of Diesel engines are inherently inferior to the spark ignition engines, and they have been notorious for NVH related issues and emissions. Even though recent advancements in Diesel engine technologies such as variable geometry turbines, common rail injection systems, and multiple injection strategies have mostly solved the problems, the deficiency in specific power has yet to be addressed. In order to increase the specific power of modern Diesel engines, dual-stage turbocharging must be applied as the air supply to the engine is the only remaining limiting factor.

Even though dual-stage turbocharging offers many advantages over single-stage turbocharging, increased cost, complexity of the system, and very challenging nature of matching procedure have prevented them from widely spread use so far. Furthermore, in most of the published studies on dual-stage turbocharging, matching procedure has been very rarely discussed as the matching is mostly done by combining available turbochargers in a trial-and-error fashion [9, 45], even though careful matching of the turbochargers is very important to achieve optimal engine performance. A non-optimal matching of dual stage turbochargers will lead to poor performance at low speed, part load conditions, since the pressure ratio per stage is even lower than a single-stage system [38].

Interestingly, the most recent comprehensive study on dual-stage turbocharger matching dates back to 1970s by Benson *et al.* [46]. In their study, the matching was

done using a lookup table type engine model based on the experimental data obtained with externally blown air supply. However, the lookup table type engine model used in the study lacked the fidelity and resolution required for accurate prediction of turbocharger performance even with the comprehensive set of experimental data used to construct the engine model. Since the matching for dual-stage turbocharger involves two sets of turbochargers and interactions between high pressure and low pressure stages as well as interactions between compressors and turbines, and the error in predicting turbocharger operation multiplies as it affects the other stages as well, the accuracy of the engine system model is more crucial for dual-stage turbocharger matching. More recent advances in modeling and simulation, as well as availability of turbomachinery capable of providing cost-effective solutions for dual stage systems motivates a new approach pursued in this study.

Dual-stage turbocharging system with only fixed geometry turbochargers on both stages still needs improvement when it is to be used in place of larger displacement engines especially at low engine speed and transient conditions. Although it is preferable to use exhaust driven turbochargers in terms of efficiency, by joining several different types of charging devices with the fixed geometry turbocharger, some of the shortcomings of each devices can be reduced or cancel their drawbacks.

Turbochargers usually lack the low speed boost, as centrifugal compressors require substantially high rotational speed in order to produce meaningful boost. This is where the other types of charging systems can enhance the overall boosting characteristics of the system. Mechanically driven superchargers can provide adequate boost even at low engine speed taking advantage of its direct connection to the output

shaft. The combined effect of the whole system is more consistent boost over the entire operating range of the engine.

Therefore, the objectives of this research are

- Develop dual-stage turbocharger matching method for a downsized 4.5 *l* V6 Diesel engine in order to achieve a dual-stage system that performs well both in low engine speed and transient conditions as well as in the rated condition compared to the baseline 6.0 *l* V8 engine in order to achieve engine downsizing without severe compromise in performance.
- Demonstrate the effectiveness of the matching method by showing efficient operations of both the high pressure and low pressure turbochargers in a downsized engine with dual-stage turbocharging system.
- Study the effect of different types of boost control options for a dual-stage system on the engine performance.
- Investigate hybridization of the dual-stage boosting systems (utilizing different types of boosting devices) to further improve the low end torque and transient response, which are often problematic when the engine is aggressively downsized.
- Investigate various types of hybrid boosting systems and compare them with dual-stage turbocharging system to provide fundamental understandings of dual-stage boosting options.

CHAPTER 2. SIMULATION OF TURBOCHARGED DIESEL ENGINE

2.1. Introduction

The engine system model used in the study is a physics-based thermodynamic zero-dimensional model originally developed by Assanis *et al.* [47], and has been used very successfully for predictions of steady-state engine operation. The model contains simplified physical descriptions of combustion based on phenomenological models and engineering correlations that have been validated against test results from Diesel engines of various sizes, ranging from highway truck engines [47] to large locomotive engines [48]. An engine dynamics sub-model is added to the model to further extend its capability to transient performance predictions on crank-angle basis [49]. It is then modified to include the dual-stage boosting systems in order to evaluate and analyze the interaction between the boosting system and the engine. Considering that the dual-stage boosting systems evaluated in this study are mostly non-existent and require extensive matching and system tuning, the simulation based approach is a cost-effective alternative to an experimental procedure.

In the engine model, it is assumed that the properties of the gas inside the cylinder is uniform and depends only on the pressure, temperature and fuel contents. Compared to the computational fluid dynamics and multi-dimensional engine simulation models, the zero-dimensional model used in this study is computationally much faster and often more reliable as this type of model is based on empirical correlations, and can be used in the

analysis of the transient characteristics of the boosting systems. However, it is not capable of predicting emissions related results, and gas dynamics effect. Therefore, the effect of cylinder-to-cylinder variation and tuning effect (dynamic resonance effect) cannot be studied with this type of engine simulation models.

2.2. Description of the simulation model

The engine system model used in the study consists of multiple engine cylinder modules linked with external component modules such as intake and exhaust manifolds, compressors and turbines, intercooler and air filter as shown in Figure 1. The cylinder control volume is open to the transfer of mass, enthalpy and energy in the form of work and heat. The cylinder contents are treated as a continuous medium which is uniform in pressure and temperature, characterized by an average equivalence ratio.

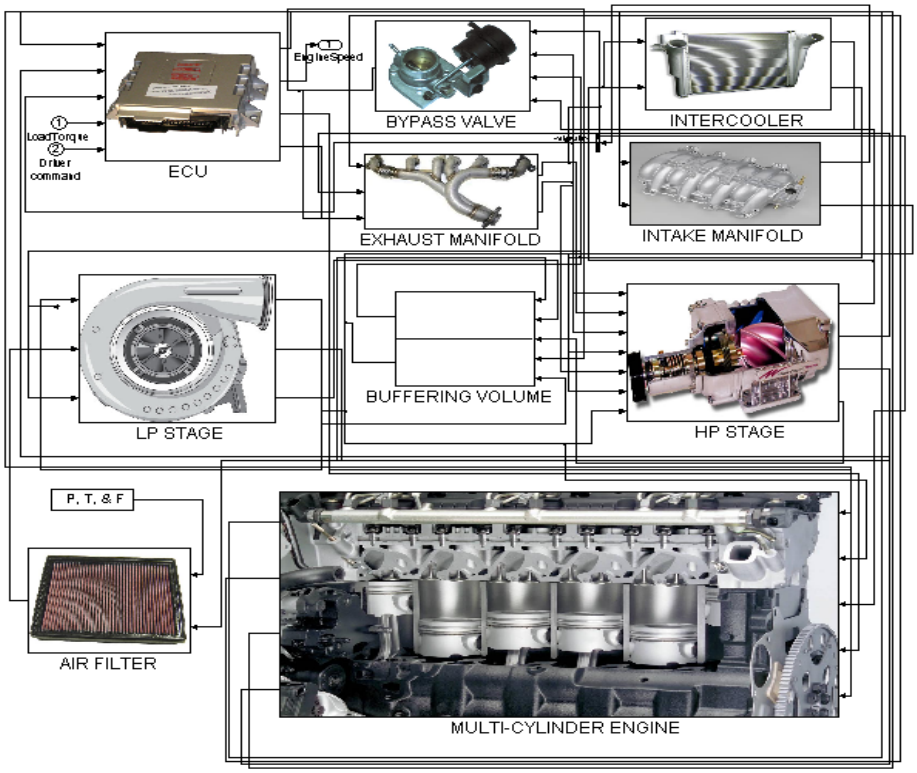

Figure 1. Diesel Engine System Model

Thermodynamic properties of the cylinder contents are obtained by empirical correlation based on the composition of the fuel-air mixture. Throughout the cycle, the cylinder is treated as a variable volume plenum, spatially uniform in pressure. Furthermore, the cylinder contents are represented as one continuous medium by defining an average equivalence ratio and temperature at all times. The cyclic processes in the cylinders are represented by more fundamental and phenomenological models of turbulence, combustion and heat transfer. The filling and emptying approach is applied to the intake and exhaust manifolds.

The Diesel four-stroke cycle is treated as a sequence of continuous processes: intake, compression, combustion (including expansion), and exhaust. The intake process begins when the intake valve opens and ends when the intake valve closes. The compression process begins at the intake valve closing and ends at the time of ignition. The combustion process begins when ignition occurs and ends when the exhaust valve opens. The exhaust process begins upon exhaust valve opening and ends when the intake valve opens and not when the exhaust valve closes.

Mass flow rate through intake and exhaust valves are determined by quasi-steady, adiabatic, one-dimensional compressible flow equations. Watson correlation is used to represent the combustion process as a uniformly distributed heat release process. Unlike intake, exhaust, and compression processes, where the convection is the only mode of heat transfer, during the combustion process, heat transfer from the gas to the cylinder wall occurs in two modes, convection and radiation. The convective heat transfer rate is predicted from a Nusselt-Reynolds number correlation for steady turbulent flow in a pipe based on the characteristic velocity concept [47]. The radiative heat transfer rate is

calculated from the apparent radiant temperature and wall temperature. The specifications of the engine are summarized in **Table 1**.

Table 1. Engine Specification

Engine Type	Diesel, 4-Stroke
Displacement	4.5 *l* V6
Bore	95 mm
Stroke	105 mm
Connecting Rod Length	176 mm
Compression Ratio	16.0 / 18.0
Maximum Speed	3300 rpm
Intake Valve Opening	-38^{o}
Intake Valve Closing	252 ^{o} / 150 ^{o}
Exhaust Valve Opening	464 ^{o}
Exhaust Valve Closing	768o

2.2.1. Air filter model

Air filter is modeled as a flow restriction. The mass flow through the air filter is a quasi-one dimensional, adiabatic, steady, inviscid flow through a nozzle [50, 51].

$$\dot{m}_{AF} = \frac{A_{AF\_eff}\, p_0}{\sqrt{RT_0}} \gamma^{\frac{1}{2}} \left(\frac{p_{AF}}{p_0}\right)^{\frac{1}{\gamma}} \sqrt{\frac{2}{\gamma-1}\left[1-\left(\frac{p_{AF}}{p_0}\right)^{\frac{\gamma-1}{\gamma}}\right]} \quad \text{for } \frac{p_{AF}}{p_0} > \left(\frac{2}{\gamma+1}\right)^{\frac{\gamma}{\gamma-1}} \tag{1}$$

$$\dot{m}_{AF} = \frac{A_{AF\_eff}\, p_0}{\sqrt{RT_0}} \gamma^{\frac{1}{2}} \sqrt{\left(\frac{2}{\gamma+1}\right)^{\frac{\gamma+1}{\gamma-1}}} \quad \text{for } \frac{p_{AF}}{p_0} \le \left(\frac{2}{\gamma+1}\right)^{\frac{\gamma}{\gamma-1}} \tag{2}$$

The flow area and discharge coefficient of the air filter is lumped together as

$$A_{AF\_eff} = C_{D\_AF} \times A_{AF} \tag{3}$$

in the flow rate equation. The ratio of pressure in the air filter to ambient pressure determines whether the flow is choked or not. Mass flow rate increases as the pressure ratio increases until the speed of the flow reaches the speed of sound at the throttle. Then the flow becomes choked. This critical pressure ratio is about 0.528 for ambient air. The pressure ratio also determines whether the flow is forward or backward. The flow is

reversed when the pressure ratio is greater than 1. Same set of governing equations are also used to model exhaust system in order to simulate exhaust back pressure.

2.2.2. Turbocharger model

Compressor and turbine operating maps are used to determine the mass flow rate and efficiency from the rotor speed and the pressure ratio across the turbomachinery at every time step. The power consumed by the compressor and the power developed by the turbine are calculated from the mass flow rate and the enthalpy change across the device. The compressor and turbine modules are linked by turbocharger dynamics module that determines the rotor speed from the energy balance between the compressor and the turbine.

The boosting system is then connected in a series configuration. The boost control is achieved utilizing either a bypass valve between high and low pressure turbines or other means with the hybrid configurations. The bypass valve is activated when the boost reaches a preset level in order to keep the peak cylinder pressure below the maximum allowable limit (180 bar).

Buffering volume modules are placed between the compressors and the turbines, which determine inlet and outlet conditions for each turbomachinery. The buffering volume modules take mass and energy fluxes as inputs and calculate pressure and temperature within the control volume. They are then used as outlet conditions for upstream turbomachinery and inlet conditions for downstream turbomachinery. The temperature drop in the intercooler is determined from the inlet air temperature, specified wall temperature and cooling efficiency. The pressure drop in the intercooler is calculated using an orifice model.

2.2.3. Intake/Exhaust manifold model

Intake and exhaust manifold model is a filling-and-emptying model. Equations for the conservation of mass and energy are developed for the contents of open thermodynamic systems such as the reciprocator cylinder, intake and exhaust manifolds. The control volumes of the thermodynamic systems are shown in Figure 2.

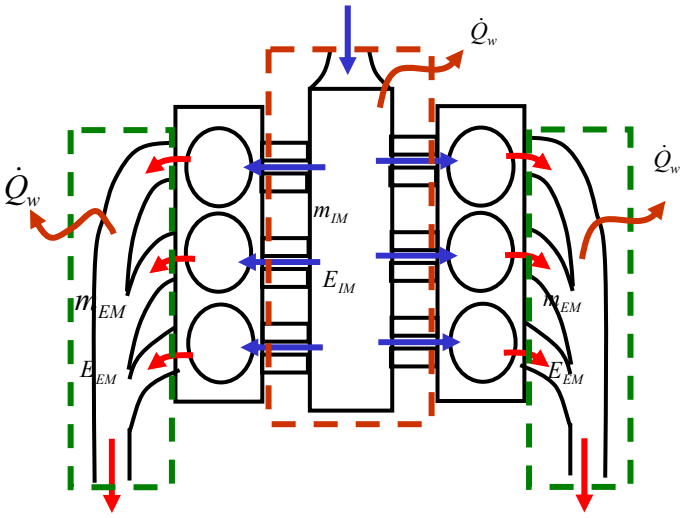

Figure 2. Intake/Exhaust manifold model

Mass and energy conservation equations are used to obtain differential equations for the temperature and pressure of the thermodynamic system. Conservation equations for the fuel mass are also used to develop differential equations for the change of fuel fraction in the system.

Conservation of mass

$$\dot{m}_a = \sum_j \dot{m}_{a,j} \tag{4}$$

$$\dot{m}_f = \sum_j \dot{m}_{f,j} \tag{5}$$

Conservation of energy

$$\dot{E} = \sum_j \dot{m}_j h_j - \dot{Q}_w - \dot{W} \tag{6}$$

$$\dot{E} = \frac{d}{dt}(mh) - \frac{d}{dt}(pV) \tag{7}$$

$$m\dot{h} = \sum_j \dot{m}_j h_j - \dot{Q}_w + \dot{p}V - \dot{m}h \tag{8}$$

Fuel fraction

$$F = \frac{m_f}{m_a + m_f} \tag{9}$$

$$\dot{F} = \frac{1}{m}\sum_j \dot{m}_j (F_j - F) \tag{10}$$

Once the governing equations are set up in the FORTRAN code, they are integrated and solved in MATLAB SIMULINK.

Heat transfer from the gas to the wall is modeled as a turbulent forced convection in circular tubes (Figure 3).

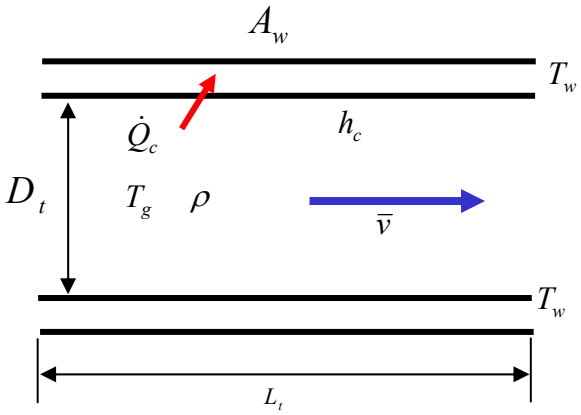

Figure 3. Heat transfer in intake/exhaust manifold

The heat transfer coefficient is derived from an experimental correlation that relates Nusselt, Reynolds and Prandtl numbers [47];

$$\dot{Q}_c = h_c A_w (T_g - T_w) \tag{11}$$

$$Nu = a\,\mathrm{Re}^b\,\mathrm{Pr}^c \tag{12}$$

The constant, *a* accounts for entrance effects, pipe bends etc., and exponents *b* and *c* are adjusted to fit experimental data.

The pressure drop is calculated using the friction factors and friction coefficients for the geometry of the passage. For straight sections,

$$\Delta p = 4f\frac{L}{D}\frac{\rho\bar{v}^2}{2} \tag{13}$$

$$f = \frac{0.046}{\mathrm{Re}^{0.2}} \qquad \text{with} \qquad \mathrm{Re} = \frac{\rho\bar{v}D}{\mu} \tag{14}$$

where *L* and *D* are length and diameter of the passage respectively, ρ is bulk density, $\bar{v}$ is average gas velocity. For bends, enlargement and contractions, friction coefficient, K_f is used, and representative values are reported by Primus *et al.* [52].

$$\Delta p = K_f\frac{\rho\bar{v}^2}{2} \tag{15}$$

2.2.4. In-cylinder process

Gas properties are calculated assuming ideal gas behavior. At low temperatures (below 1000 K), the cylinder contents are treated as a homogeneous mixture of non-reacting ideal gases. At high temperatures (above 1000 K), the properties of the cylinder contents are calculated with allowance for chemical dissociation by assuming that the burned gases are in equilibrium, using an approximate calculation method based on hydrocarbon-air combustion.

The compression process is defined so as to include the ignition delay period, i.e., the time interval between the start of the injection process and the ignition point. The

total length of the ignition delay is related to the mean cylinder gas temperature and pressure during the delay period by an empirical Arrhenius expression [47]. Combustion is modeled as a uniformly distributed heat release process. The rate of heat release is assumed to be proportional to the rate of fuel burning, which is modeled empirically. Since the Diesel combustion process is comprised of a pre-mixed and a diffusion-controlled combustion mechanism, Watson's fuel burning rate correlation, consisting of the sum of two algebraic functions, one for each combustion mechanism is used. The fraction of the total fuel injected that is burnt by either mechanism depends on the length of the ignition delay period and the engine load and speed.

Heat transfer is included in all the engine processes. Convective heat transfer is modeled using correlations based on the Nusselt number for the turbulent flow in pipes. The characteristic velocity and length scales required to evaluate the Reynolds number in the correlation are obtained from a mean and turbulent kinetic energy model [47], hence any changes in the flow field inside the cylinder directly affect the heat transfer process. Radiative heat transfer is added during combustion. The steady-state inside wall surface temperatures of the piston, cylinder head, and liner can be either specified or calculated from a specification of the component wall structure.

The rate of change of pressure in the cylinder is a function of volume, temperature, equivalence ratio, and mass change rate. And the rate of change of temperature is a function of mass, volume, equivalence ratio, enthalpy flux, and heat transfer rate.

$$\dot{p} = \frac{\rho}{\partial\rho/\partial p}\left(-\frac{\dot{V}}{V} - \frac{1}{\rho}\frac{\partial\rho}{\partial T}\dot{T} - \frac{1}{\rho}\frac{\partial\rho}{\partial\phi}\dot{\phi} + \frac{\dot{m}}{m}\right) \tag{16}$$

$$\dot{T} = \frac{B}{A}\left[\frac{\dot{m}}{m}\left(1-\frac{h}{B}\right)-\frac{\dot{V}}{V}-\frac{C}{B}\dot{\phi}+\frac{1}{Bm}\left(\sum_j \dot{m}_j h_j - \dot{Q}_w\right)\right] \tag{17}$$

$$\text{where} \quad A = c_p + \frac{\partial\rho/\partial T}{\partial\rho/\partial p}\left(\frac{1}{\rho}-c_T\right) \tag{18}$$

$$B = \frac{1}{\partial\rho/\partial p}\left(1-\rho c_T\right) \tag{19}$$

$$C = c_\phi + \frac{\partial\rho/\partial\phi}{\partial\rho/\partial p}\left(\frac{1}{\rho}-c_T\right) \tag{20}$$

These equations do not need an explicit heat release rate expression. However, they are implicitly linked by burned fuel fraction, *F*, which appears in the equivalence ratio equation.

$$\phi = \frac{m_f/m_a}{\left(m_f/m_a\right)_s} \tag{21}$$

$$\dot{\phi} = \frac{1}{\left(m_f/m_a\right)_s}\frac{\dot{F}}{\left(1-F\right)^2} \tag{22}$$

2.2.5. Valve flow

A quasi-one-dimensional, steady, adiabatic, inviscid flow model is used to calculate mass flow rate through the intake and exhaust valves during the gas exchange process.

$$\dot{m}_v = \frac{A_{v,eff}\,p_1}{\sqrt{RT_1}}\gamma^{\frac{1}{2}}\left(\frac{p_2}{p_1}\right)^{\frac{1}{\gamma}}\left\{\frac{2}{\gamma-1}\left[1-\left(\frac{p_2}{p_1}\right)^{\frac{\gamma-1}{\gamma}}\right]\right\}^{\frac{1}{2}} \quad \text{for} \quad \frac{p_2}{p_1} \le \left(\frac{2}{\gamma+1}\right)^{\frac{\gamma}{\gamma-1}} \tag{23}$$

$$\dot{m}_v = \frac{A_{v,eff}\,p_1}{\sqrt{RT_1}}\gamma^{\frac{1}{2}}\sqrt{\left(\frac{2}{\gamma+1}\right)^{\frac{\gamma+1}{\gamma-1}}} \quad \text{for} \quad \frac{p_2}{p_1} > \left(\frac{2}{\gamma+1}\right)^{\frac{\gamma}{\gamma-1}} \tag{24}$$

The effective area, $A_{v,eff}$, is product of discharge coefficient and valve opening area, both of which vary with valve lift. Intake and exhaust valve effective flow areas are shown in Figure 4. Thermodynamic properties such as specific heat ratio and gas constant are obtained from upstream of the restriction.

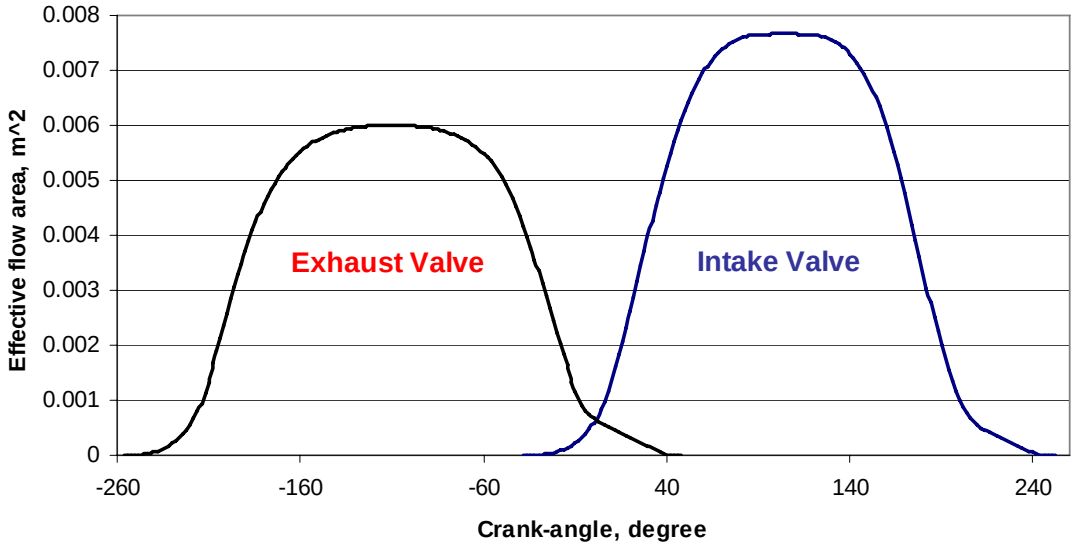

Figure 4. Valve effective flow area

The intake and exhaust manifolds are treated as plenums with known pressures at each computational time step. The temperature and average equivalence ratio of intake and exhaust charges are also known. When reverse flow into the intake manifold occurs, perfect and instantaneous mixing between the back-flowing charge and the intake charge is assumed.

2.2.6. Fuel injection control

The fuel injection control module, developed from the data provided by International [55], takes driver command, engine speed and intake manifold pressure as inputs and provides the amount of fuel injected per cycle and injection timing as outputs. The fuel control logic used in this study is fine-tuned for each boosting system for

optimal performance. The correction of the amount of fuel based on the boost pressure or density in the intake manifold is especially important during full load acceleration, when turbo lag may cause the engine to operate with much low boost pressures than normally experienced under corresponding steady-state conditions. An idle speed control module governs the fuel flow rate to prevent engine from stalling at low load and low speed condition.

2.2.7. Vehicle system model

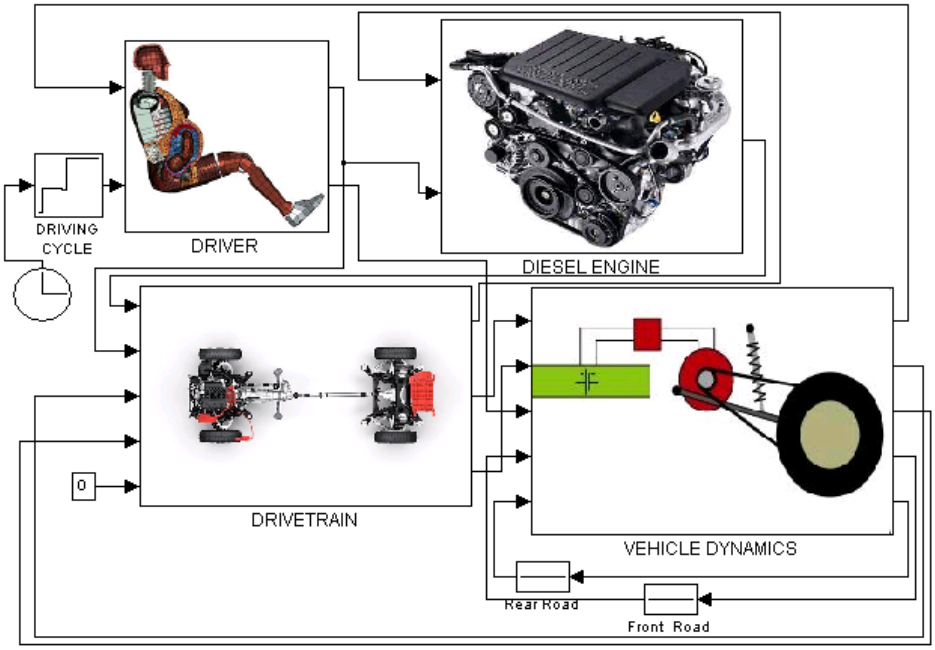

Figure 5. Vehicle system model

The vehicle system model used in the study is a Diesel-powered 4 x 4 truck with a 4-speed automatic transmission. The engine system is linked to the vehicle system through torque converter, whose output shaft is then coupled to the transmission. The power from the engine is then transferred to transfer case, front and rear differentials and finally to the driven wheels via drive shafts. The complete vehicle system is structured to directly resemble the layout of the physical system, and implemented in MATLAB

SIMULINK environment as shown in Figure 5. The driveline and vehicle dynamics model are modeled in 20SIM, a bond graph modeling language, and converted to C code [55]. It is then implemented in SIMULINK environment via S-functions.

Links between main modules represent physical parameters that define the interaction between the components such shaft torque and angular velocity. The driver module allows the feed-forward simulation to follow a prescribed vehicle speed schedule by providing the acceleration and brake signal based on the specified speed setting and the current vehicle speed.

VEHICLE DYNAMICS - The vehicle dynamics model is a pitch-plane model that describes its dynamic behavior in the longitudinal and heave directions. It includes wheels and tires, axles, suspension and chassis of the vehicle. The vehicle dynamics parameters are obtained from the manufacturer. The specifications for the vehicle are summarized in Table 2.

Table 2. Vehicle Specification

Sprung Mass	4672 kg
Unsprung Mass - Front	220 kg
Unsprung Mass - Rear	220 kg
Drag Coefficient	0.7
Rolling Resistance - Front	36 N
Rolling Resistance - Rear	42 M
Wheel Inertia	16 $kg \cdot m^2$

DRIVELINE - The torque converter model is a quasi-steady model based on experimental data available from the transmission supplier. The 4-speed automatic transmission is modeled as a non-power-conserving transformer that incorporates gear inefficiencies for different gears. Experimental data are used in determining input and

output inertias, stiffness and damping rates for transmission, propeller shafts, transfer case, differentials and drive shafts. The shift logic consists of two sets of shift schedules, one for up shifts and the other for downshifts. It takes vehicle speed and rack position as inputs and provides gear selection as an output.

2.3. Engine Model Calibration

The engine model is calibrated with experimental data obtained from a 6.0 *l* V8 Diesel engine with single-stage variable geometry turbine as it has the same cylinder geometry, valve timing and maximum speed as the downsized V6 engine. The V6 engine model is constructed virtually from the physical specification of the V8 engine except the number of cylinders. The specification of the engine is summarized in Table 3. A set of cylinder pressure data obtained from the V8 engine in different speed and load conditions are used to calibrate the engine model.

Table 3. Engine Specification

Engine Type	Diesel, 4-Stroke
Displacement	6.0 *l* V8
Bore	95 mm
Stroke	105 mm
Connecting Rod Length	176 mm
Compression Ratio	18.0
Maximum Speed	3300 rpm
Intake Valve Opening	-38^{o}
Intake Valve Closing	252 ^{o}
Exhaust Valve Opening	464 ^{o}
Exhaust Valve Closing	768o

Table 4 shows the speed and load conditions where the cylinder pressure data are obtained. The engine model is modified with intake and exhaust plenum instead of the manifold and turbomachinery model, and the intake and exhaust plenum conditions are specified at the start of the simulation using the data from the V8 engine, and remains

constant throughout the simulation. The cylinder pressure data obtained from the simulation model is then compared with the experimental data from V8 engine, and the simulation model is calibrated to match the experimental data.

Table 4. Data used for Engine Calibration

Case	BMEP bar	Torque Nm	Speed rpm	T_{int} ^{o}C	T_{exh} ^{o}C	T_{inj} $^{o}BTDC$
1	7.01	334.3	1200	34.0	411.5	-4.2
2	11.06	527.5	1200	35.5	528.7	-3.7
3	7.04	337.3	1800	32.1	407.2	-1.3
4	10.94	522.4	1800	37.2	482.4	-4.7
Case	P_{int} kPa	P_{exh} kPa	$\dot{m}_{air}$ g/s	$\dot{m}_{fuel}$ g/s	P_{amb} kPa	T_{amb} ^{o}C
1	139.0	188.2	77.1	2.75	98.9	30.8
2	162.1	219.6	90.7	4.20	98.9	35.2
3	152.2	176.6	127.3	4.04	98.9	36.8
4	198.1	228.2	169.2	6.11	98.9	36.3

The parameters adjusted in the engine model are:

1. The convective heat transfer coefficient
2. The temperatures at cylinder wall, head and piston top
3. The burn duration.

Figure 6 shows the simulation results after the calibration along with the experimental data from the V8 engine. The criterion for maximum permissible error at the peak pressure is set to less than 5 % for all four cases. The burn duration has the most pronounced effect on the shape of the pressure trace during the combustion phase, and the convective heat transfer coefficient is adjusted to match the pressure trace at the exhaust phase. The temperature conditions on combustion chamber boundaries have effect on pressure trace on intake phase as they affect the mass flow rate into the cylinder. As shown in Figure 6, the simulation results satisfy the criteria in all four cases.

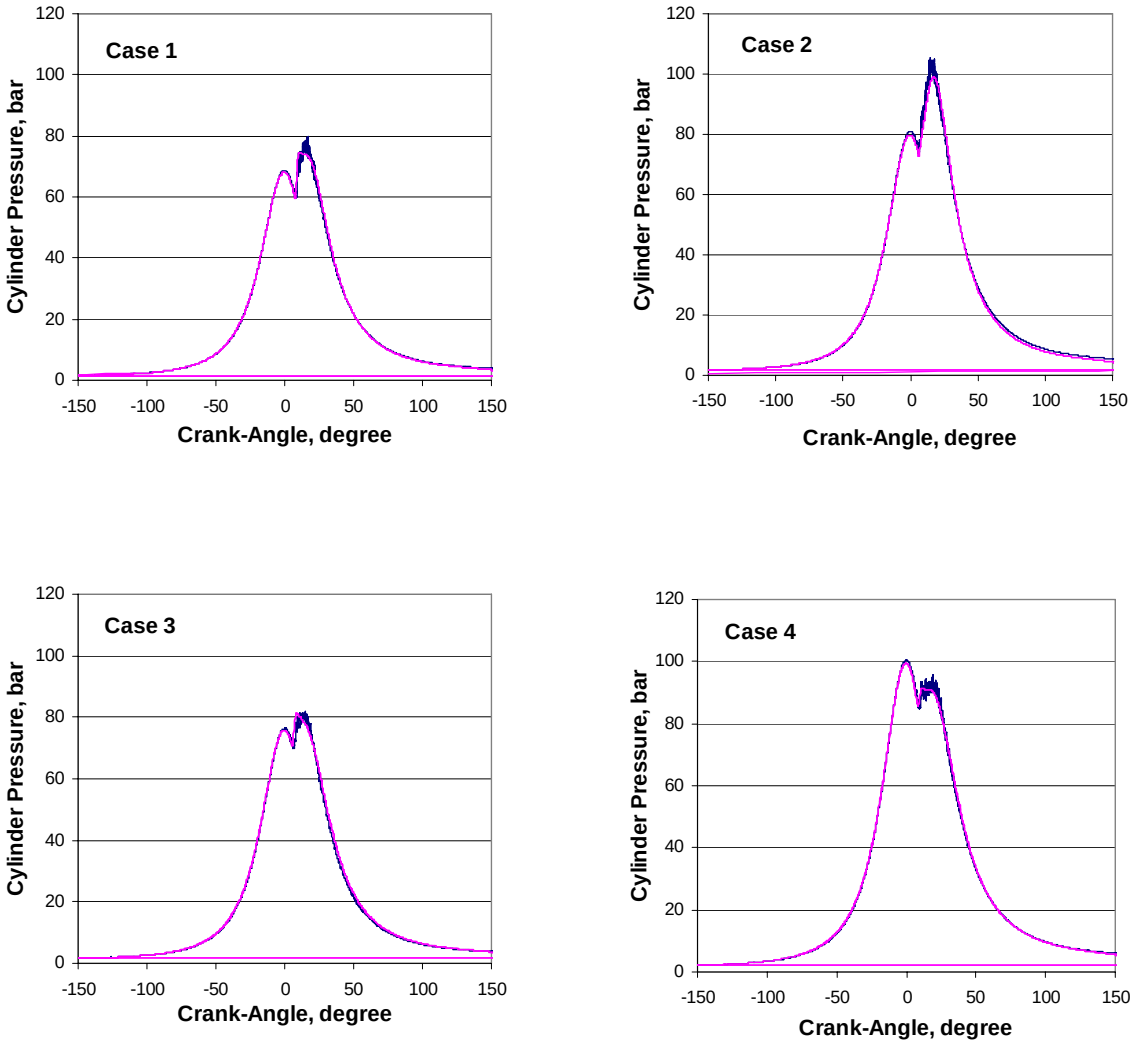

Figure 6. Pressure traces

CHAPTER 3. DUAL-STAGE TURBOCHARGER MATCHING

3.1. Matching procedure

Turbocharger matching in general is to optimize the selection of compressor and turbine combination in order to satisfy the required boosting characteristics for the specified range of engine operating conditions. Ideally, the compressor efficiency should be at its maximum in the main operating range of the engine at full load. The distance to the surge line should be sufficiently large as well.

The matching process hinges upon a thermodynamic cycle analysis with known properties of working fluid to obtain necessary information about the turbocharger operation such as pressure ratio, speed, efficiency, and mass flow rate. For the single-stage turbocharger, it is straightforward to determine pressure and temperature condition after the compression with the assumed value of compressor efficiency and known inlet conditions (P_1 and T_1). In the typical thermodynamic engine system simulation, the manifold pressure and instantaneous turbocharger speed will be predicted at each integration step, and the compressor (or turbine) mass flow rates and efficiencies will be determined from the turbomachinery performance maps. For the dual-stage turbocharger, however, p_2 and T_2 are unknown, since the pressure ratio across the low pressure compressor is unknown even though the overall pressure ratio is known. Therefore, it is necessary to make assumptions on pressure ratios across each compressor while keeping the overall pressure ratio constant in order to carry out the rest of the analysis. Once the

pressure ratios for each stage are fixed, the rest of the cycle analysis can be done and pressure and temperature conditions at inlets and outlets of turbochargers can be calculated. The pressure and temperature conditions obtained for turbocharger inlets and outlets are used to calculate the pressure ratio and corrected mass flow rate for each turbomachinery.

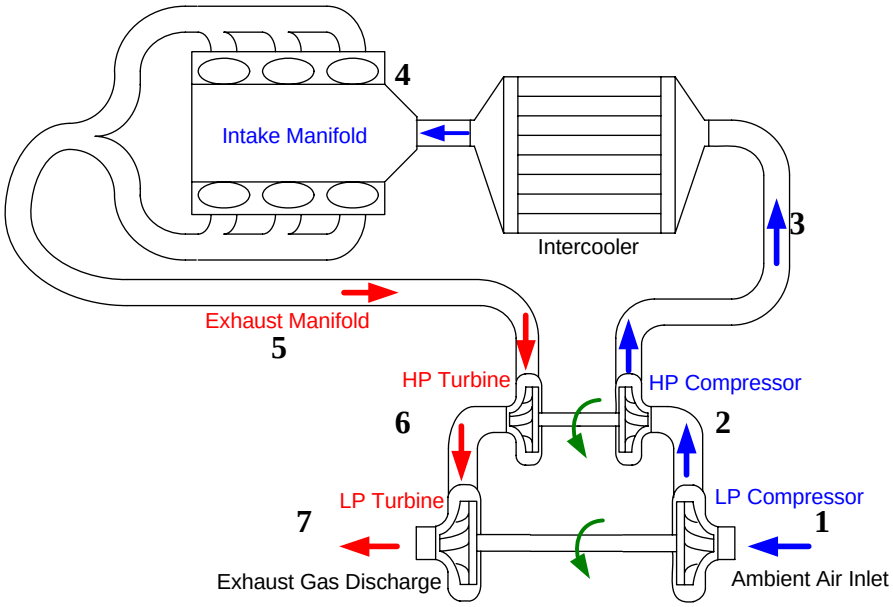

Figure 7. Dual-Stage turbocharger configuration

As for the determining pressure ratios for each stage, there is a rough guideline given by Watson and Janota [38], which states that the overall efficiency of the dual-stage turbocharging system is optimal if the work is divided evenly between each stage. This means that the pressure ratios across each stage have to be roughly equal for the turbochargers to operate efficiently. However, the efficiency is virtually not sensitive to ratios in the range of 1.4 to 1.7, thus, in many cases, the guideline is not sufficient to find the optimal pressure ratio for each stage.

For this reason, we propose to parameterize the “ratio of pressure ratios”, the high pressure compressor pressure ratio over the low pressure compressor pressure ratio, and

determine the optimal combination in a systematic way. Known conditions are engine speed (N_e), pressure and temperature of the ambient air (P_1, T_1, P_7), engine displacement (V_d) and overall pressure ratio across compressors (P_4/P_1 or P_4). In order to carry out the calculations from state 1 through 7 and determine thermodynamic properties of each stage, assumptions must be made on the pressure ratios at each stage (P_2/P_1, P_3/P_2), volumetric efficiency of the engine at the designed operating condition, turbomachinery efficiencies and temperature at the exhaust manifold (T_5). Thus the procedure requires iterative calculations illustrated in the Flow Chart shown in Figure 8.

In order to expedite the matching procedure, a Microsoft Excel program with empirical correlation that calculates thermodynamic properties of the fuel-air mixture is developed, using the same assumptions as [47]. The program takes temperature, pressure and fuel fraction of the mixture as inputs and thermodynamic properties of the gas, such as specific heat ratio, density, gas constant and enthalpy, as outputs. The equations used in the following procedure, i.e., Eqs. 25 through 47 are also included in the program. As we describe individual steps in detail, the flow chart shown in Figure 8 will be helpful in following the flow of the complete procedure.

Step 1. From State 1 to 2

Pressure and temperature at the low pressure compressor inlet are all known. In order to carry out the calculation, the low pressure compressor outlet conditions must be known. But they are unknown because the pressure ratio across the low pressure compressor has not been determined yet. At this stage, known conditions include the overall pressure rise across the two compressors (P_3/P_1), engine speed, compressor inlet conditions (P_1, T_1) and exhaust back pressure (P_7).

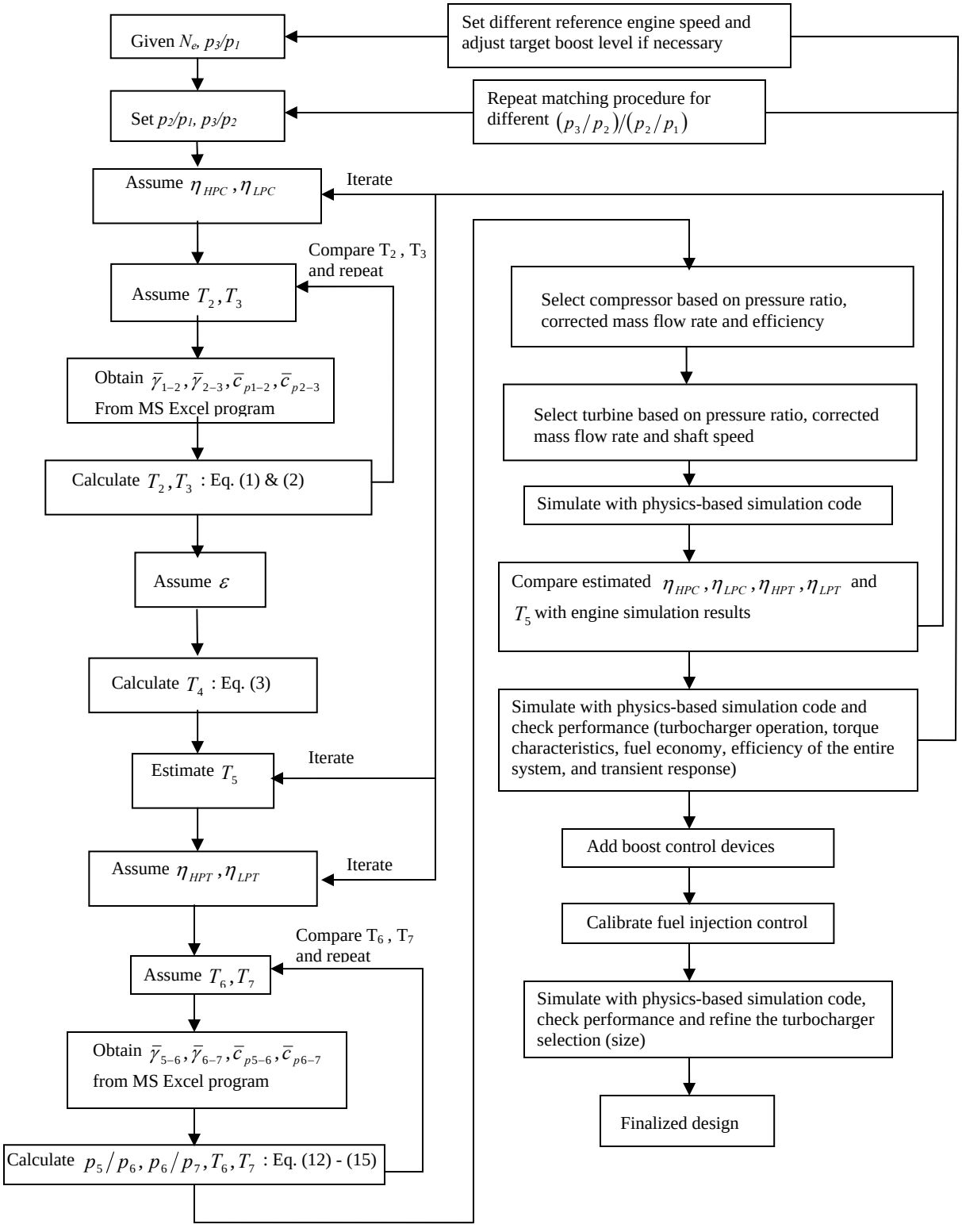

Figure 8. Dual-stage turbocharger matching flow chart

For a single-stage turbocharger matching, compressor inlet condition and overall pressure ratio would be sufficient to complete the analysis. However, with the dual-stage turbocharger, the individual pressure ratios of the two compressors have to be assumed first while keeping the overall pressure ratio at a predetermined value. A systematical method to do this is parameterizing the ratio of each pressure ratio, and check the effect of each variation. Now with P_2/P_1 fixed, T_2 can be calculated once appropriate value for compressor efficiency is assumed as shown in Eq. 25.

$$T_2 = T_1 + \frac{T_1}{\eta_{LPC}}\left[\left(\frac{p_2}{p_1}\right)^{(\bar{\gamma}_{1-2}-1)/\bar{\gamma}_{1-2}} - 1\right] \tag{25}$$

However, the specific heat ratio at the average temperature between the compressor inlet and outlet temperatures, $(T_1+T_2)/2$, is still unknown on the right side of the Eq. 25, since the compressor outlet temperature, T_2, is not known yet. Thus, the compressor outlet temperature needs to be estimated to obtain the specific heat ratio using the Excel program, and then compared with the temperature calculated from Eq. 25. This step is repeated until the difference between the estimated and calculated temperatures becomes small enough.

The estimated compressor efficiency, however, cannot be checked until the engine simulation results become available in Step 9. The engine simulation requires selection of the compressors and turbines at the end of Step 8.

Step 2. From State 2 to 3

This step is similar to Step 1. Assumptions are made for the high pressure compressor efficiency and outlet temperature. The estimated compressor outlet temperature is used to obtain gas properties using the Excel program, and then compared

with T_3 from Eq. 26. This step is repeated until both temperatures are sufficiently close. Again, the estimated compressor efficiency cannot be compared with the simulation result until Step 9.

$$T_3 = T_2 + \frac{T_2}{\eta_{HPC}}\left[\left(\frac{p_3}{p_2}\right)^{(\bar{\gamma}_{2-3}-1)/\bar{\gamma}_{2-3}} - 1\right] \tag{26}$$

Step 3. From State 3 to 4

Pressure drop across intercooler can be either assumed at a reasonable value or ignored without significantly affecting the outcome of the matching in the initial matching stage. However, it is fully accounted for in the engine simulation as the simulation code is capable of capturing the phenomenon. The simulation result confirms that the pressure drop in the intercooler is insignificant compared to the uncertainties introduced by other assumptions made in this stage such as turbomachinery efficiency, temperatures at various locations, and heat transfer effect.

The intercooler effectiveness must be assumed in order to calculate temperature at the intake manifold (T_4).

$$T_4 = T_3(1-\varepsilon) + \varepsilon T_{cool} \tag{27}$$

Step 4. From State 4 to 5

Assuming a realistic air-fuel ratio at a designed engine operating condition, the temperature rise across the engine can be estimated from previous engine simulation results. Although the exhaust manifold temperature does not vary significantly between one iteration to another, as the variation in relative turbocharger size is usually small, it is necessary to compare the estimated temperature with the engine simulation result in Step 9. If the difference is not negligible, the exhaust manifold temperature is adjusted and the

entire procedure is repeated in an iterative manner. The pressure at the exhaust manifold is determined after the overall expansion ratio calculated from the compressor-turbine power balance equations – refer to Steps 5 and 6.

Step 5. From State 5 to 6

Expansion ratio for the high pressure turbine can be calculated from energy balance equation between compressor and turbine. First, the temperature at the turbine outlet is assumed in order to obtain necessary thermodynamic properties of the gas. It is also necessary to assume the compressor and turbine efficiencies and mechanical efficiency of the turbocharger. The compressor and turbine efficiencies are compared with the engine simulation results in Step 9.

The power required to drive the high pressure compressor is expressed as

$$\dot{W}_{HPC} = \frac{1}{\eta_{HPC}} \dot{m}_a \bar{c}_{p2-3} \left(T_3 - T_2 \right) \tag{28}$$

or

$$\dot{W}_{HPC} = \frac{1}{\eta_{HPC}} \dot{m}_a \bar{c}_{p2-3} T_2 \left(\frac{T_3}{T_2} - 1 \right) \tag{29}$$

For isentropic process,

$$\frac{T_3}{T_2} = \left(\frac{p_3}{p_2} \right)^{(\bar{\gamma}_{2-3}-1)/\bar{\gamma}_{2-3}} \tag{30}$$

Substituting this into Eq. 29,

$$\dot{W}_{HPC} = \frac{1}{\eta_{HPC}} \dot{m}_a \bar{c}_{p2-3} T_2 \left[\left(\frac{p_3}{p_3} \right)^{(\bar{\gamma}_{2-3}-1)/\bar{\gamma}_{2-3}} - 1 \right] \tag{31}$$

The power developed by high pressure turbine is

$$\dot{W}_{HPT} = \eta_{HPT}\left(\dot{m}_a + \dot{m}_f\right)\bar{c}_{p5-6}\left(T_5 - T_6\right) \tag{32}$$

or

$$\dot{W}_{HPT} = \eta_{HPT}\left(\dot{m}_a + \dot{m}_f\right)\bar{c}_{p5-6}T_5\left[1-\left(\frac{p_6}{p_5}\right)^{(\bar{\gamma}_{5-6}-1)/\bar{\gamma}_{5-6}}\right] \tag{33}$$

The power balance for the compressor-turbine assembly is

$$\dot{W}_{HPC} = \eta_{mech}\dot{W}_{HPT} \tag{34}$$

or

$$\frac{1}{\eta_{HPC}}\dot{m}_a\bar{c}_{p2-3}T_2\left[\left(\frac{p_3}{p_3}\right)^{(\bar{\gamma}_{2-3}-1)/\bar{\gamma}_{2-3}} - 1\right]_t = \eta_{mech}\eta_{HPT}\left(\dot{m}_a + \dot{m}_f\right)\bar{c}_{p5-6}T_5\left[1-\left(\frac{p_6}{p_5}\right)^{(\bar{\gamma}_{5-6}-1)/\bar{\gamma}_{5-6}}\right] \tag{35}$$

Therefore,

$$\frac{p_5}{p_6} = \left[1-\frac{\left[\left(p_3/p_2\right)^{(\bar{\gamma}_{2-3}-1)/\bar{\gamma}_{2-3}} - 1\right]T_2\bar{c}_{p2-3}}{\left(1+\dot{m}_f/\dot{m}_a\right)T_5\bar{c}_{p5-6}\eta_{HPC}\eta_{HPT}\eta_{mech}}\right]^{\bar{\gamma}_{5-6}/(1-\bar{\gamma}_{5-6})} \tag{36}$$

The temperature at the high pressure turbine outlet is determined from the expansion ratio. The estimated turbine outlet temperature is then compared with the value obtained from Eq.37, and this step is repeated if necessary.

$$T_6 = T_5 - T_5\eta_{HPT}\left[1-\left(\frac{p_6}{p_5}\right)^{(\bar{\gamma}_{5-6}-1)/\bar{\gamma}_{5-6}}\right] \tag{37}$$

Step 6. From State 6 to 7

Expansion ratio and turbine outlet temperature for low pressure turbine are calculated similarly with the estimated values of turbocharger efficiencies and turbine outlet temperature. The estimated turbocharger efficiencies are compared with the engine simulation results in Step 9. The estimated turbine outlet temperature is compared with the value obtained from Eq. 39, and this step is repeated if necessary.

$$\frac{p_6}{p_7} = \left[1 - \frac{\left[(p_2/p_1)^{(\bar{\gamma}_{1-2}-1)/\bar{\gamma}_{1-2}} - 1 \right] T_1 \bar{c}_{p1-2}}{(1+\dot{m}_f/\dot{m}_a) T_6 \bar{c}_{p6-7} \eta_{LPC} \eta_{LPT} \eta_{mech}} \right]^{\bar{\gamma}_{6-7}/(1-\bar{\gamma}_{6-7})} \tag{38}$$

$$T_7 = T_6 - T_6 \eta_{LPT} \left[1 - \left(\frac{p_7}{p_6} \right)^{(\bar{\gamma}_{6-7}-1)/\bar{\gamma}_{6-7}} \right] \tag{39}$$

With expansion ratios obtained for each stage, the exhaust manifold pressure is calculated from p_7.

$$p_5 = \frac{p_5}{p_6} \frac{p_6}{p_7} p_7 \tag{40}$$

Step 7. Compressor Selection

Mass flow rate of the air entering the engine is calculated from displacement volume, estimated volumetric efficiency, and rotational speed of the engine and density of air in the intake manifold,

$$\dot{m}_a = \frac{N_e}{2} \rho V_d \eta_{vol} \tag{41}$$

The corrected mass flow rate for compressors is calculated from compressor inlet conditions,

$$\dot{m}_{corr\_HPC} = \dot{m}_a \frac{\sqrt{T_2/T_{amb}}}{p_2/p_1} \tag{42}$$

and,

$$\dot{m}_{corr\_LPC} = \dot{m}_a \frac{\sqrt{T_1/T_{amb}}}{p_1/p_1} \tag{43}$$

With the corrected mass flow rates and the pressure ratios for each stage, compressors can be selected for each stage by positioning the operating points on the most efficient region of the compressor maps made available by the turbomachinery scaling routine. With the scaling routine, a single compressor map can generate infinitely many maps by changing the scaling factor. Thus the compressor selection is no longer limited by the availability from the turbocharger manufacturer. Compressors that perform most efficiently at the mass flow rate determined from Eq. 42 and 43, and pressure ratios determined by the ratio of the pressure ratios are selected from compressor maps.

Step 8. Turbine Selection

The mass flow rate of fuel is obtained from air-fuel ratio, since

$$\dot{m}_f = \frac{1}{A/F}\dot{m}_a \tag{44}$$

The total mass flow rate through the turbine is

$$\dot{m}_e = \dot{m}_a + \dot{m}_f \tag{45}$$

The corrected mass flow rate for turbines is calculated from the turbine inlet conditions

$$\dot{m}_{corr\_HPT} = \dot{m}_e \frac{\sqrt{T_5/T_{amb}}}{p_5/p_7} \tag{46}$$

$$\dot{m}_{corr\_LPT} = \dot{m}_e \frac{\sqrt{T_6/T_{amb}}}{p_6/p_7} \tag{47}$$

With the corrected mass flow rates, the expansion ratios, and the shaft speeds determined from compressor selection, turbines are selected from the turbine maps made available by the turbomachinery scaling routine.

Step 9. Iteration

In this step, the estimated exhaust manifold temperature, T_5, and the estimated turbomachinery efficiencies, η_{LPC}, η_{LPT}, η_{HPC}, η_{HPT}, are compared with the results from the physics-based engine simulation code as the initial matching procedure is completed and the compressors and turbines are selected. The matching procedure is repeated with the updated values.

Once the simulation results and the assumed values are in reasonable agreement, the matching is completed for that 'ratio of pressure ratios' (or pressure ratio parameter) parameterized at the beginning of the matching. Then, the turbocharger operations at various engine operating conditions are evaluated for sufficient surge margin, choking and the overall efficiency. The engine torque characteristics and transient response of the system are also evaluated.

Once the evaluation is completed for one ratio of pressure ratios, the entire matching procedure is repeated for another ratio in order to find the optimal value for the given target manifold boost, e.g. the procedure is repeated for $(P_3/P_2)/(P_2/P_1)$ = 0.8, 1.0, 1.2, etc. Once the evaluation for different ratios of pressure ratios is completed, a decision can be made about the best ratio for the engine operating condition chosen for a reference point. A logical choice for a reference operating point is the mid-speed and high load, essentially a point at which the optimal turbocharger efficiency is desired at the target boost level (P_3/P_1).

The final step then depends on the system architecture. If no additional device is used for boost control, the turbochargers selected for the reference operating point are checked for sufficient surge margin at low engine speed and sufficient flow capacity at high engine speed using the physics-based engine system simulation.

If boost pressure control devices are used, a follow up study using the engine system simulation is necessary to further adjust the turbocharger selection. This is explained in the next sub-section and illustrated in the Flow Chart.

Step 10. Adding Boost Control Devices

It is often necessary to control the boost level in order to prevent the cylinder pressure from exceeding its designed limit. This is of particular interest in high-speed engines for passenger cars and trucks. A bypass valve or a wastegate must be added to the system to keep the maximum cylinder pressure at a safe level. Several parameters are involved in designing such devices. Valve diameter, spring rate and pre-load pressure are among the parameters to be determined depending on preset valve activation point (intake manifold boost). The final design is chosen after iterations using the results from the physics-based engine simulation code. With the addition of these boost control devices, it is likely to find a certain degree of deviation from the performance without such devices. Therefore, it is necessary to refine the turbocharger selection (sizing) at this stage and iterate on the final design. The fuel injection calibration should be addressed in parallel, as the boost level changes after the addition of a bypass valve or a wastegate.

Step 11. Checking Critical Operating Conditions and Final Iteration

The efficiency of the entire system, fuel economy, torque characteristics and transient response of the engine must be carefully investigated to confirm that the targets

are met. After the system is evaluated over a full range of steady-state conditions, the transient response should be investigated as well. An example is discussed in the following section. This completes the Flow Chart shown in Figure 8.

3.2. Turbomachinery scaling

The scaling routine is based on non-dimensional representation of compressor and turbine characteristics. The functional relationships between non-dimensional variables [38] are

$$\frac{\dot{m}\sqrt{RT_{01}}}{p_{01}D^2}, \eta, \frac{\Delta T_0}{T_{01}} = f\left(\frac{ND}{\sqrt{RT_{01}}}, \frac{p_{02}}{p_{01}}, \frac{\dot{m}}{\mu D}, \gamma\right) \tag{48}$$

Since turbochargers operate on a specific gas (air for the compressor, exhaust gas for the turbine), the values of R and γ are specified. Hence the non-dimensional groups become

$$\frac{\dot{m}\sqrt{RT_{01}}}{p_{01}D^2}, \eta, \frac{\Delta T_0}{T_{01}} = f\left(\frac{ND}{\sqrt{RT_{01}}}, \frac{p_{02}}{p_{01}}, \frac{\dot{m}}{\mu D}\right) \tag{49}$$

The Reynolds number of the gas has little effect on the performance of the machine, and can usually be ignored. Hence

$$\frac{\dot{m}\sqrt{RT_{01}}}{p_{01}D^2}, \eta, \frac{\Delta T_0}{T_{01}} = f\left(\frac{ND}{\sqrt{RT_{01}}}, \frac{p_{02}}{p_{01}}\right) \tag{50}$$

Since the turbomachineries to be scaled operates on the same pressure ratio, the non-dimensional groups become

$$\frac{\dot{m}\sqrt{RT_{01}}}{p_{01}D^2}, \eta, \frac{\Delta T_0}{T_{01}} = f\left(\frac{ND}{\sqrt{RT_{01}}}\right) \tag{51}$$

The same impeller/blade tip speed should be maintained among the family of turbomachinery as the impellers/blades have the same tensile strength and durability since they are manufactured with the same material.

$$N_1 D_1 = N_2 D_2 \tag{52}$$

Assuming the similar geometry, the functional relationship becomes,

$$\frac{\dot{m}_1}{D_1^2} = \frac{\dot{m}_2}{D_2^2} \tag{53}$$

and

$$\eta_1 = \eta_2 \tag{54}$$

Even though, the efficiency varies with the size of the turbomachinery in reality, the variation is usually not very significant if the geometry is similar.

By defining a scaling factor,

$$\alpha = \frac{\dot{m}_2}{\dot{m}_1} \tag{55}$$

the diameter and shaft speed can be expressed as

$$\frac{D_1}{D_2} = \frac{N_2}{N_1} = \sqrt{\frac{1}{\alpha}} \tag{56}$$

With Eqs. 55 and 56, the compressor/turbine map can be scaled based on either the mass flow rate (scaling factor) or the diameter. For example, once the scaling factor is determined, the shaft speed can be scaled by Eq. 56, while the efficiency and the pressure ratio remain unchanged.

CHAPTER 4. BOOST CONTROL OPTIONS

4.1. Introduction

Boost control options considered in the study are a bypass valve placed across the high pressure turbine, and a wastegate placed across the low pressure turbine. Although there are more complicated boost control options available for a dual-stage turbocharging system, these two basic configurations are selected as they provide the fundamental understanding for building more complex systems.

The automated matching procedure is performed for a reference operating point first, with valves inactive. Then, steps 10 and 11 are pursued with a systematic simulation work using a thermodynamic engine system simulation. The position of operating points on compressor maps are studied to ensure efficient and safe operation (no surge, no over-speeding) in the complete range. This guided the final adjustments of high pressure and low pressure turbocharger and lead to performance predictions discussed in the last part of this section. The bypass valve placed across high pressure turbine limits the amount of power available for high pressure compressor while the wastegate placed across low pressure turbine limits the power available for low pressure compressor. They prevent the cylinder pressure from exceeding its mechanical limit by regulating intake manifold boost. The cylinder pressure limit is set to 180 bar.

While both configurations provide effective means to control the manifold boost, each configuration has its own advantages and tradeoffs compared to each other. In this

study, the effectiveness of each configuration is weighed up against each other to provide a guideline for developing more complicated system with both the bypass valve and the wastegate are utilized with various control methods.

Another boost control option considered in the study is not a device but a different engine cycle with early intake valve closure (EIVC). In spark ignition engine applications, EIVC is often used for load control instead of the throttle valve at part load and light load conditions. The inherent pumping loss associated with the throttling process is eliminated by controlling the engine load with EIVC.

In Diesel engine applications, the EIVC can be used as a mean to regulate the turbocharger operation by controlling the air flow to the combustion chamber, thus eliminating the bypass valve, and lower the peak cylinder pressure at the same time. Since considerable portion of the compression is carried out in the compressor and the charge is cooled afterward by intercooler before it enters the cylinder, the final temperature of the charge reached after the compression stroke will be lower than that of the charge compressed only in the cylinder. The air is cooled as it expands after the intake valve is closed until the piston reaches the BDC. The overall thermal efficiency of the engine is also improved as the available energy in the exhaust gas is better utilized.

4.1.1. Dual-stage turbocharger with wastegate

The wastegate configuration is shown in Figure 9. A wastegate is placed across the low pressure turbine in this configuration to limit the available power to the low pressure compressor. With this configuration, a relatively small low pressure turbocharger can be used compared to the bypass valve configuration. The scaling factors found in the matching are 0.72 and 1.29 for the high pressure compressor and low

pressure compressor, respectively. Compared to the scaling factors found for the bypass valve configuration, 0.58 and 1.72, the compressors are relatively similar in size and both are utilized evenly throughout the entire operating range.

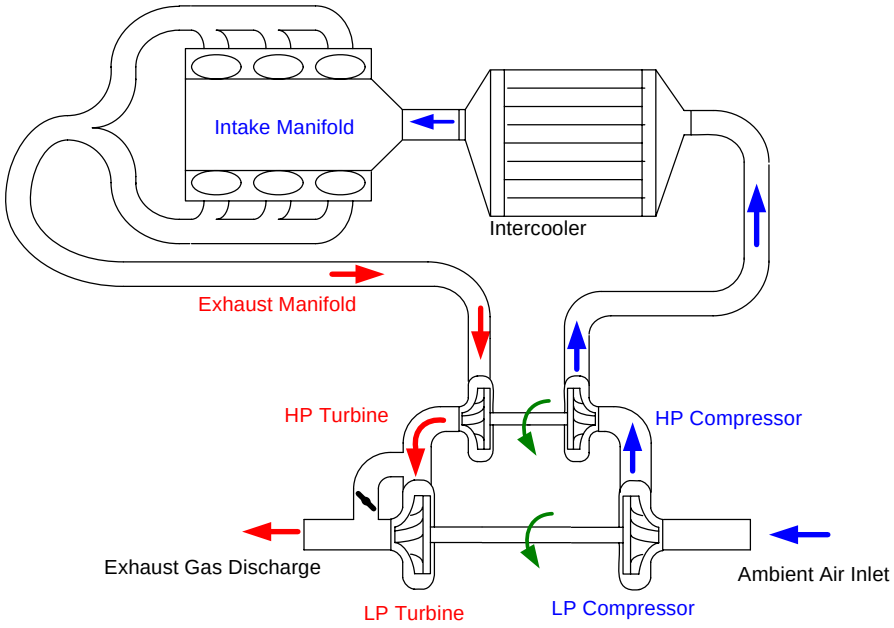

Figure 9. Dual-stage turbocharger with wastegate

4.1.2. Dual-stage turbocharger with bypass valve

The bypass valve configuration is shown in Figure 10. A bypass valve is placed across the high pressure turbine in this configuration, and a smaller high pressure turbocharger is used compared to the wastegate configuration (scaling factor = 0.58). As a result, the high pressure turbocharger reaches its efficient operating region even at a moderate engine speed. And at higher engine speed, the bypass valve limits the amount of air that passes through the high pressure turbine keeping the compressor from boosting excessively.

The low pressure compressor used in this configuration, however, is larger than that used in wastegate configuration. At low load low speed conditions, it is less efficient than that used in wastegate configuration due to its larger size. Nonetheless, the matching

method has produced a uniquely balanced dual-stage system with good efficiency and sufficient margin from either the surge line or the choke limit.

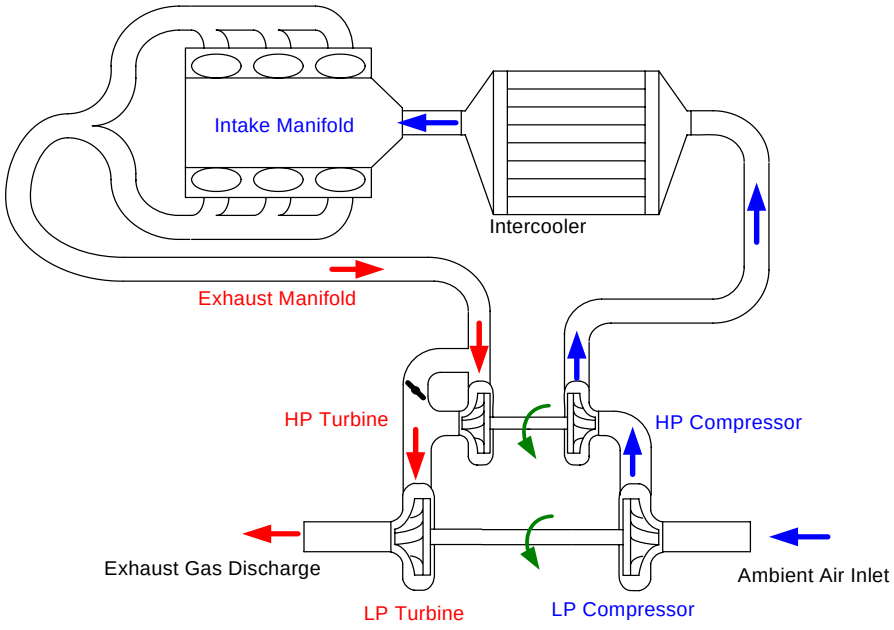

Figure 10. Dual-stage turbocharger with bypass valve

4.1.3. Early Intake Valve Closure (EIVC) cycle

The early intake valve closure (EIVC) strategy is often used in spark ignition engines in order to improve fuel economy at part load conditions. Tuttle [56, 57] showed that both the early and late intake valve closure (EIVC and LIVC) strategy can improve the part load efficiency by eliminating or reducing pumping loss caused by throttling process in spark ignition engines. By varying the position at which the intake valve is closed to control the mass of charge inducted per cycle, the engine load can be controlled without the throttling process in spark ignition engines. A number of studies [58-63] have explored the potential of these strategies in improving part load fuel economy in spark ignition engines. Also, while the effective compression ratio reduces with both the LIVC and EIVC strategy, the expansion ratio does not change, giving a thermodynamic benefit.

In Diesel engine applications, these strategies have been used to reduce NO_x emissions [45, 64], and to improve fuel economy [65].

With the LIVC strategy, air is drawn into the cylinder close to atmospheric pressure for the entire induction stroke. The intake valve remains open during the beginning of the compression stroke however, allowing some of the trapped air to flow back out into the intake manifold. Once the intake valve has closed, the air remaining in the cylinder is compressed in the conventional way.

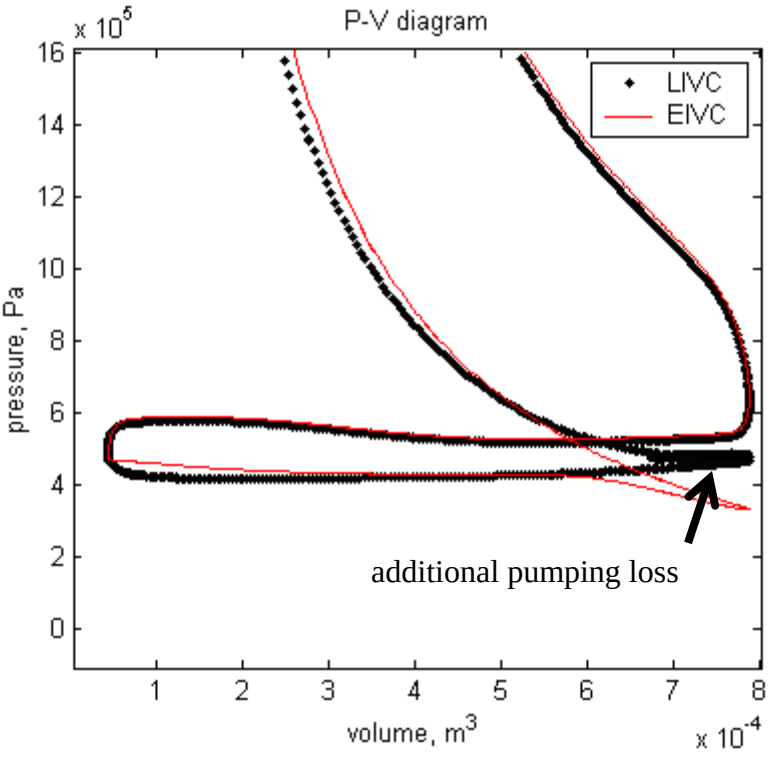

Figure 11. EIVC vs. LIVC

On the other hand, with the EIVC strategy, the intake valve closes part of the way through the induction stroke to prevent any further air from entering the cylinder, thus restricting the trapped air mass. Once the intake valve has closed, the pressure inside the cylinder will fall as the piston moves towards BDC, but the work done on the piston to expand the air will mainly be recovered at the beginning of the compression stroke. Once

the intake valve is closed, the air within the cylinder will act like a gas spring, allowing this work recovery.

P-V diagram of the EIVC and LIVC cycles with the same trapped air mass are shown in Figure 11. It illustrates the principle of the EIVC and LIVC strategies, and shows that there is additional pumping loss associated with the portion of air that is drawn into the cylinder and expelled back into the intake manifold at the beginning of the compression stroke when the LIVC cycle is used. This also affects the air-fuel mixture of next cycle as the fresh charge is mixed with residual gas inside the cylinder and then blown back into the intake port.

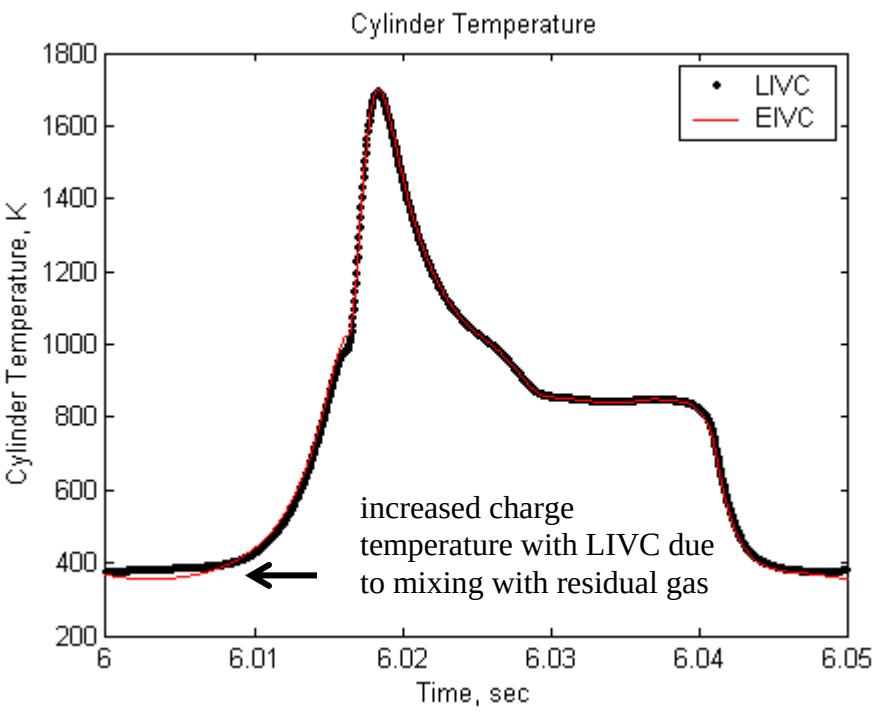

Figure 12. Cylinder temperature

Another issue associated with this phenomenon is the heat transfer to the intake manifold resulting in increased charge temperature compared to the EIVC cycle as shown in Figure 12, which, in part, negates the reason the LIVC is used. The cylinder

temperature plot is also obtained with the same trapped air mass for both EIVC and LIVC cycles. Besides the benefits of throttle-less operation in SI engines, the LIVC is often used to reduce charge temperature to avoid knock, but the increased charge temperature due to the charge expelled from the cylinder, which is mixed with hot residual gas, creates problem in this regard. In addition, the LIVC strategy is limited in the range of throttle-less operation as the intake valve closure can occur significantly after the ideal ignition timing for very light loads. Thus, there exists a conflict between ideal ignition timing and the ideal intake valve closing timing to reduce the load.

However, the LIVC strategy offers benefits over the EIVC strategy such as lower cost and better mixing and turbulence that promotes better combustion compared to the EIVC. With the EIVC cycle, the intake valve needs to resist the adverse pressure when the intake valve is closed before the bottom dead center, which requires substantial change in valve train design, whereas only minimal modification is required with the LIVC cycle. In addition, Tuttle [56, 57] has shown that the EIVC can reduce turbulence and mixing to levels lower than those experienced over a complete un-throttled induction stroke, and the subsequent entrainment and combustion processes are slowed down.

However, with the EIVC strategy, deactivating one intake valve at part load can increase turbulence at reduced air flow. GM has employed such technique in production engines with conventional valve train. The adverse effect of the EIVC on combustion can also be countered by using asymmetric valve profiles. Wilson *et al.* [66] investigated the effect of such valve profiles on combustion in a fully variable valve train research engine. The same method is used in Honda VTEC-E engines.

The EIVC strategy offers throttle-less operation throughout the engine speed and load range because there is in principle no limit to the reduction of trapped air mass that can be achieved by early closing of the intake valve. This is the strategy used in the Valvetronic, a variable EIVC system, by BMW. GM has also tried the EIVC strategy, which uses the variable intake valve closing and intake valve lift control to un-throttle the engine at part-load and light-load operating conditions.

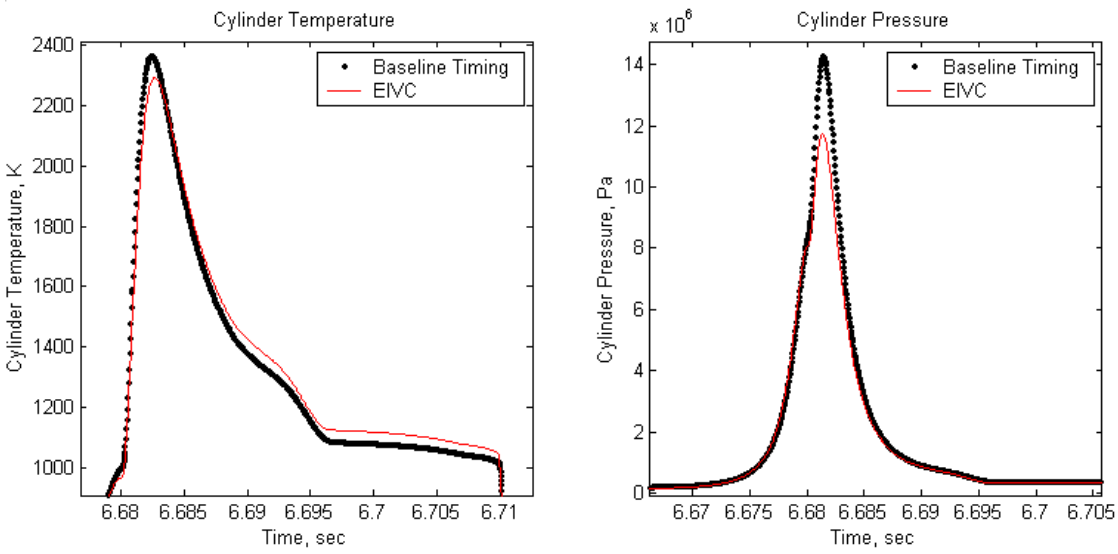

Figure 13. Peak cylinder temperature and pressure

The EIVC also offers reduction of peak temperature and pressure in the cylinder compared to the conventional valve timing through its charge cooling effect as shown in Figure 13. The trapped air mass and the amount of fuel injected are same for both the baseline timing and EIVC, but since considerable portion of the compression is carried out in the compressor and the charge is cooled afterward by intercooler, the final temperature of the charge reached after the compression stroke will be lower than it would have been if the charge was compressed entirely inside the cylinder alone. This results in lower peak cylinder pressure and temperature during the combustion process. In

Diesel engine applications, it can reduce NO_x emissions and raise the boost considerably more than normal level as the peak cylinder pressure is reduced during the combustion.

Additionally, with the lower peak cylinder pressure through EIVC, the injection timing can be further advanced compared to the conventional valve timing, which leads to better overall system efficiency. The overall thermal efficiency of the engine is also improved as the expansion stroke is longer than the effective compression stroke.

In this study, the EIVC is employed to regulate the dual-stage turbocharger operation by controlling the trapped air charge in the combustion chamber, which allows the turbocharger to operate without the bypass valve resulting in better system efficiency thanks to better utilization of the exhaust energy. With the EIVC, the bypass valve is eliminated and the boost is controlled by varying the IVC timing at medium to high engine speed.

A preliminary study was performed in order to determine the optimal intake valve closing timing at 2000 rpm where the bypass valve typically begins to open with conventional valve timing. Initially, the performance of the engine with the baseline valve timing was simulated at full load at 2000 rpm, and a series of runs was conducted to determine optimum intake valve closing timing by comparing the BSFC at a specified intake manifold pressure.

The intake manifold conditions are specified at the start of the simulation and remain constant throughout the simulation. In order to eliminate the effect of turbomachinery matching on overall efficiency of the engine system, the intake manifold is treated as a plenum, and the exhaust manifold is modified to an open system with specified pressure. The exhaust manifold temperature is determined by the mass and

energy equations as the exhaust gas from the engine flows into and out of the exhaust manifold.

The exhaust pressure is determined by a specified turbomachinery efficiency model. Instead of using the physics-based turbomachinery model, a simpler model with constant isentropic efficiency is used to determine the exhaust pressure that satisfies the turbomachinery power balance based on mass flow rate from the physics-based engine system model. With the specified turbomachinery efficiency and intake manifold condition, the effect from the turbomachinery matching is eliminated.

At the start of the calculations, initial estimates are made for the exhaust manifold temperature and volumetric efficiency of the engine as these are inputs to the specified turbomachinery efficiency model that determines the exhaust manifold pressure. Then the physics-based simulation with the intake plenum and modified exhaust manifold model is used to update the estimated exhaust manifold temperature and volumetric efficiency of the engine until the convergence is achieved.

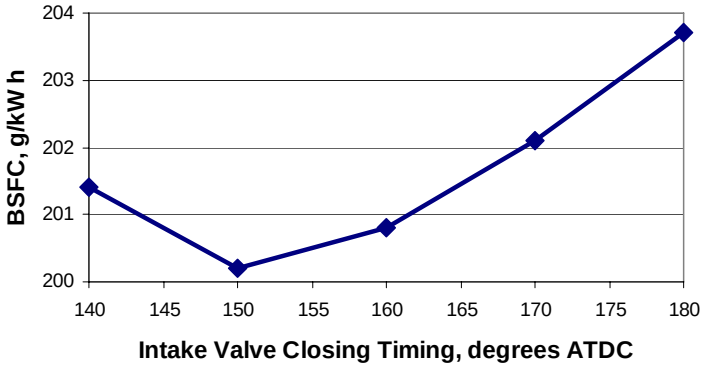

Figure 14. BSFC with varying intake valve closing timing

In order to eliminate the effect of air-fuel equivalence ratio on BSFC, it is kept constant by adjusting the fuel injection as the air flow to the engine varies with intake valve closing timing. The compression ratio is also adjusted to produce the same peak

cylinder pressure as the baseline intake valve timing in order to take full advantage of the EIVC. As shown in Figure 14, the optimal intake valve closing timing is found at 150^{o} ATDC at 2000 rpm as the engine operates most efficiently with this IVC timing.

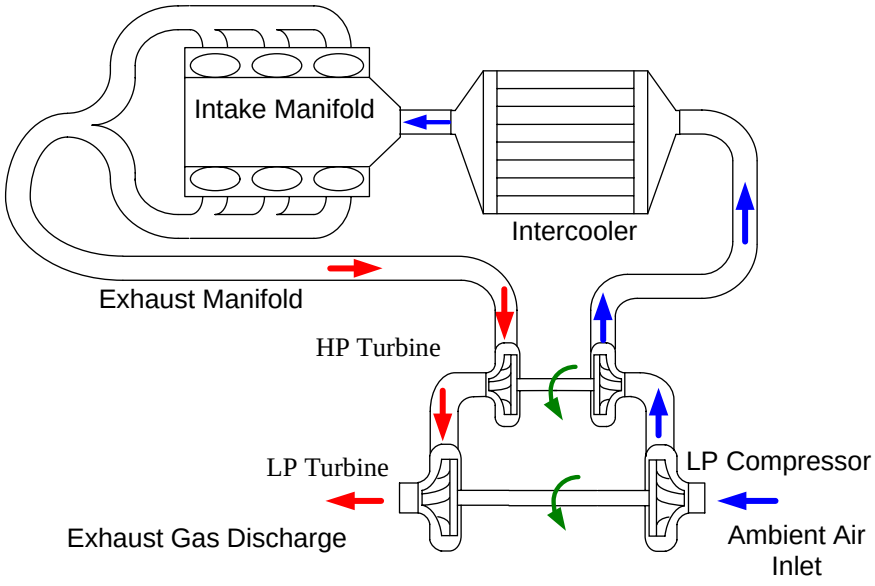

Figure 15. Dual-stage turbocharging system without bypass valve utilizing EIVC

The system configuration is shown in Figure 15. The intake valve closing timing switches from baseline timing (252^{o} ATDC) to 150^{o} ATDC at 2000rpm and the optimal scaling factors found for EIVC configuration after careful turbocharger matching are 0.53 and 1.25 for HP compressor and LP compressor respectively, both of which are smaller than either the HP compressor of the bypass valve configuration or LP compressor of the wastegate configuration.

4.2. Simulation results

4.2.1. The effect of the ratio of each stage pressure ratios

The ratio of pressure ratio on the high pressure stage to that of the low pressure stage is parameterized and the optimal value is determined after running the physics-based engine system simulation with different values of the ratios.

The parameterized ratio of pressure ratios, along with ambient conditions and the overall pressure ratio, is an input to the Excel program that is developed to assist the turbocharger selection process. With outputs from the Excel program, the turbocharger map that produces the target boost pressure with the optimal ratio between the HP stage and LP stage is selected from the scaled turbocharger maps.

Compressor operating points at full load condition are shown in Figure 16. Each dot represents the engine speed as indicated in Figure 16 (a), and the rest of the plots follow the convention. The target boost in this case is 2 bar at 1500rpm, and the ratio of pressure ratios is also calculated at 1500rpm (the second dots from the lower left corner) since the performance of the downsized engine at low engine speed is more critical in engine downsizing than at high engine speed. The results shown in the Figure 16 are obtained from the physics-based engine system simulation before any boost control devices are added. Thus the boost reached at high engine speed is excessive and the peak cylinder pressure exceeds the 180 bar limit. As the ratio of the pressure ratio increases, i.e. the contribution from the HP compressor to the overall boost increases, the relative size of the HP compressor decreases and the pressure ratio at the HP stage increases.

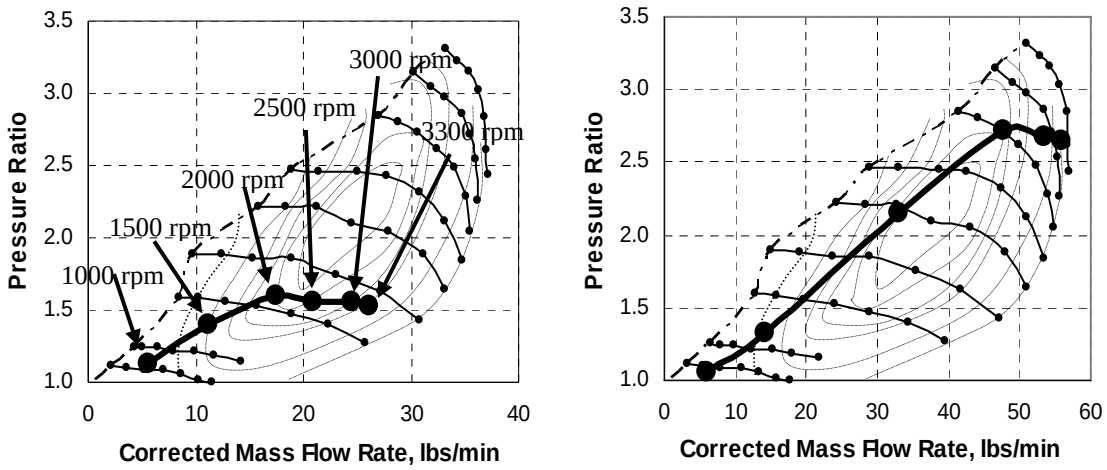

(a) $(p_3/p_2)/(p_2/p_1)=1.0$

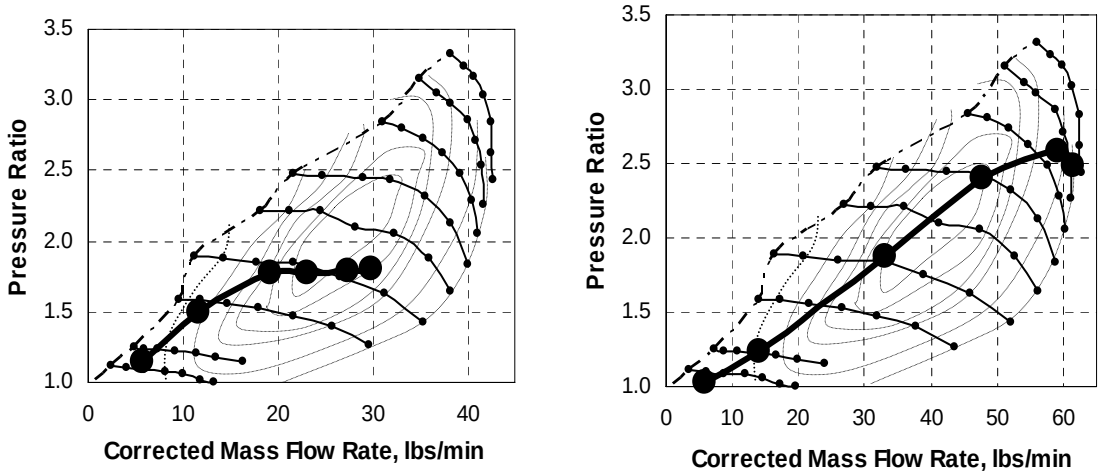

(b) $(p_3/p_2)/(p_2/p_1)=1.2$

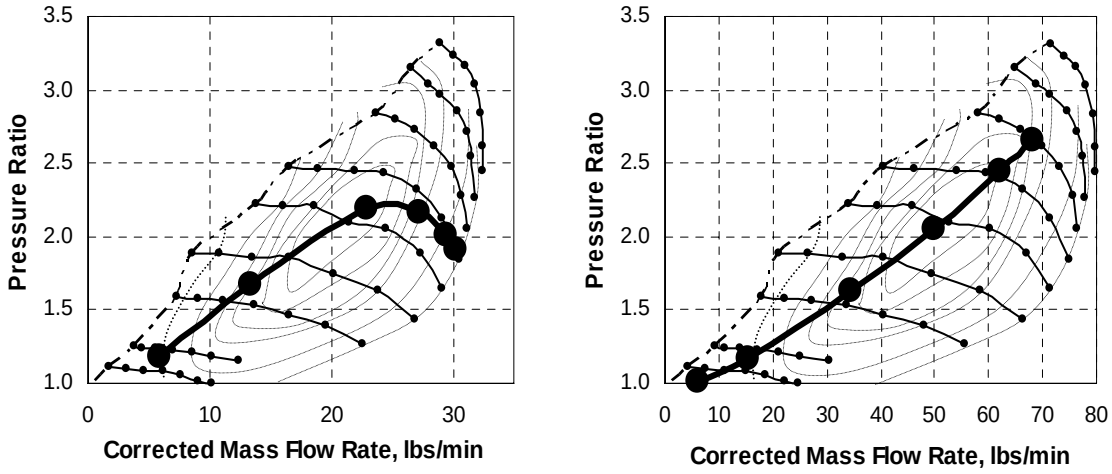

(c) $(p_3/p_2)/(p_2/p_1)=1.4$

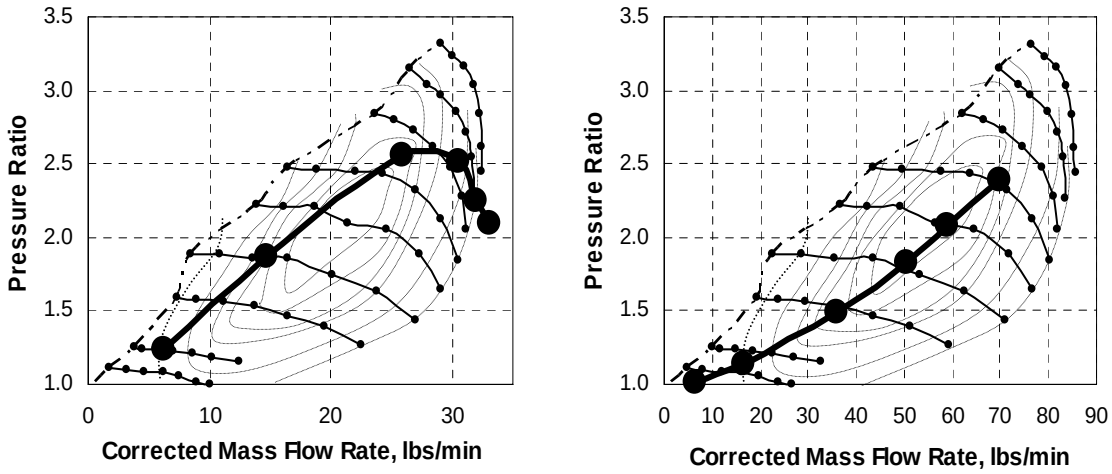

(d) $(p_3/p_2)/(p_2/p_1)$=1.6

Figure 16. Effect of ratios of each stage pressure ratios on compressor performance

This is reflected in the brake torque produced by the engine and fuel consumption as shown in Figure 17. With higher ratio of HP stage contribution, i.e. smaller HP turbocharger, the engine produces more torque at lower engine speed, and less torque at higher engine speeds as the turbocharger efficiency of the HP turbocharger is reduced substantially mainly due to its limited flow capacity. The brake specific fuel consumption (BSFC) also suffers from the reduced turbocharger efficiency at higher engine speeds.

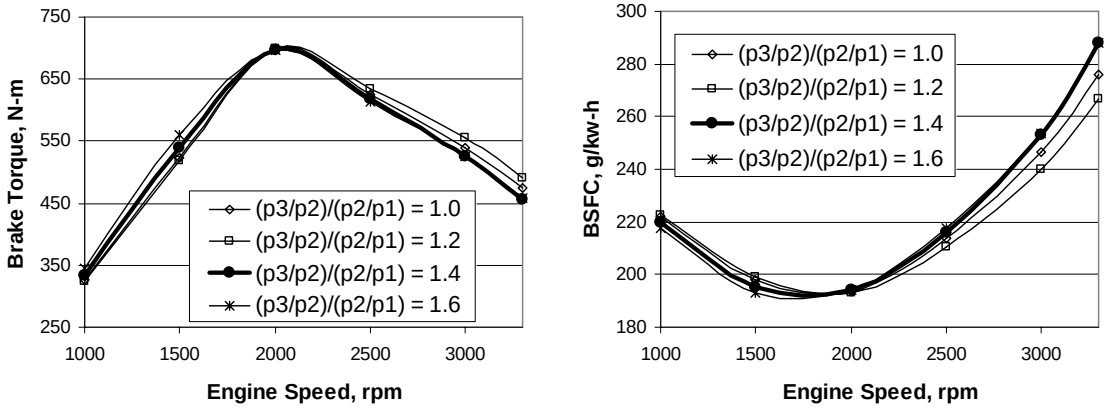

Figure 17. Effect of ratios of each stage pressure ratios on brake torque and BSFC

On the other hand, with lower ratio of HP contribution, the HP compressor is relatively larger and has sufficient flow capacity even at higher engine speeds, but the LP

compressor is smaller and efficiency suffers at higher engine speeds. The effect of using larger HP compressor is shown in less torque produced and higher specific fuel consumption at low engine speeds. The optimal value is selected depending on the priorities of the engine system design. For this study, enhancing the low end torque of the engine is the main factor in determining the ratio and the ratio of 1.4 is found to be optimal as the results show acceptable low end torque without excessive reduction in turbocharger efficiency at high engine speed.

4.2.2. Fuel injection rate and timing

In order to properly compare characteristics of different boost control options considered in the study, it is necessary to adjust the fuel injection parameters such as the injection rate and timing for each system as the performance of the system is strongly affected by them. The individual fuel injection timing map for each system is carefully tuned based on the simulation results obtained for each system at different engine speeds and loads.

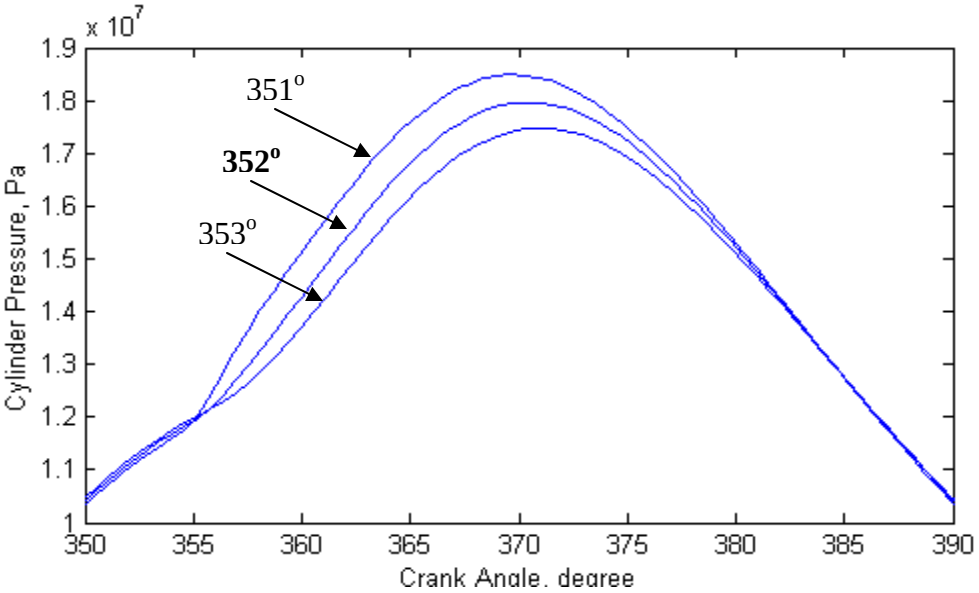

Figure 18. Cylinder pressure at 2000 rpm full load condition

The injection timing is tuned to achieve maximum brake torque at a given speed and load unless the peak cylinder pressure exceeds the limit of 180 bar. An example from the dual-stage system with wastegate at 2000 rpm full load condition is shown in Figure 18. In this particular example, 352^{o} is selected as optimum injection timing since the cylinder pressure exceeds the limit if the injection timing is advanced further.

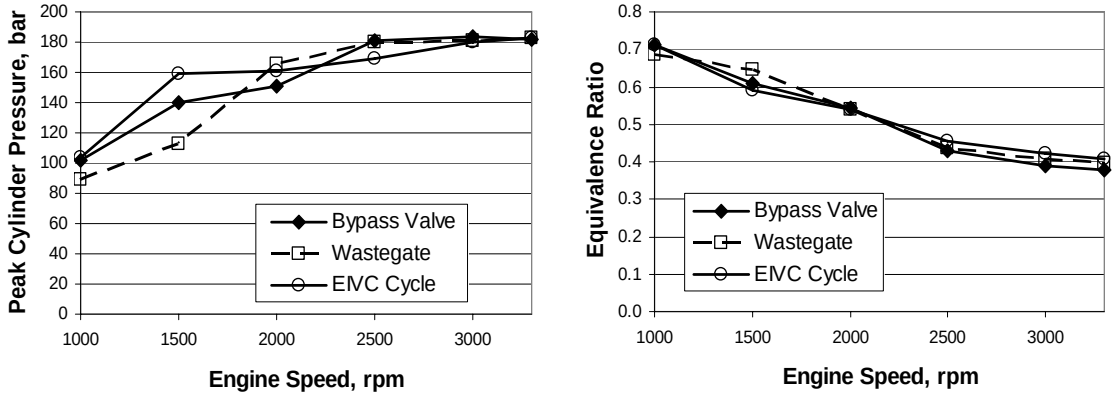

Figure 19. Peak cylinder pressure and equivalence ratio

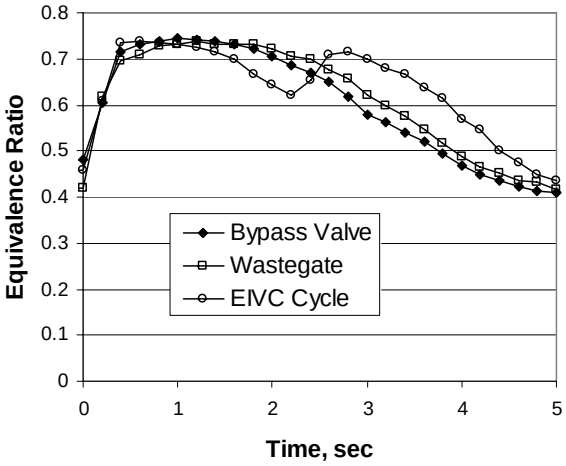

Figure 20. Fuel-air equivalence ratios under full load acceleration

The fuel injection rate at low engine speed is regulated not to produce excessive smoke emission both in steady-state and transient operations as shown in fuel-air equivalence ratio plots in Figure 19 and Figure 20. At high engine speed, the fuel injection rate is adjusted for optimal fuel economy. Fuel injection rate and timing maps

for wastegate, bypass valve and EIVC configurations are shown in Figure 21, Figure 22, and Figure 23, respectively.

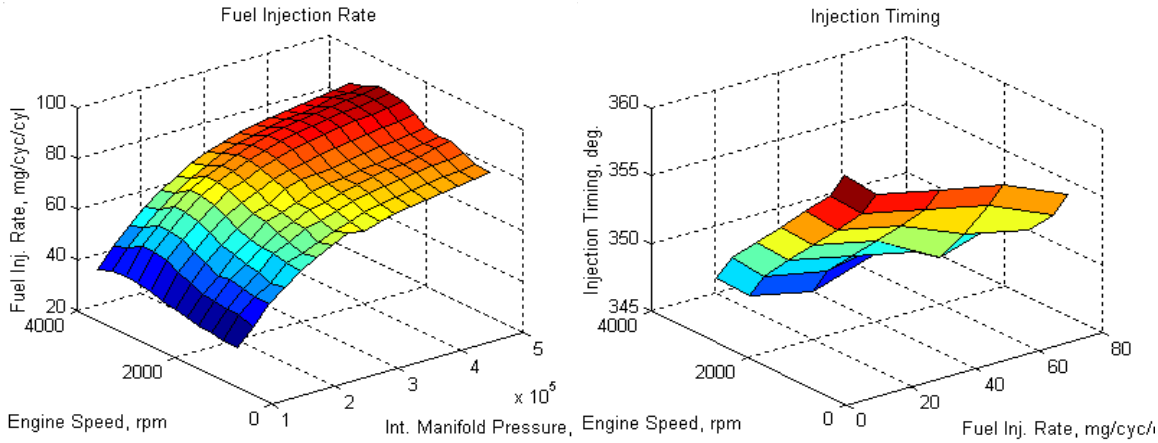

Figure 21. Fuel injection rate and timing for wastegate configuration

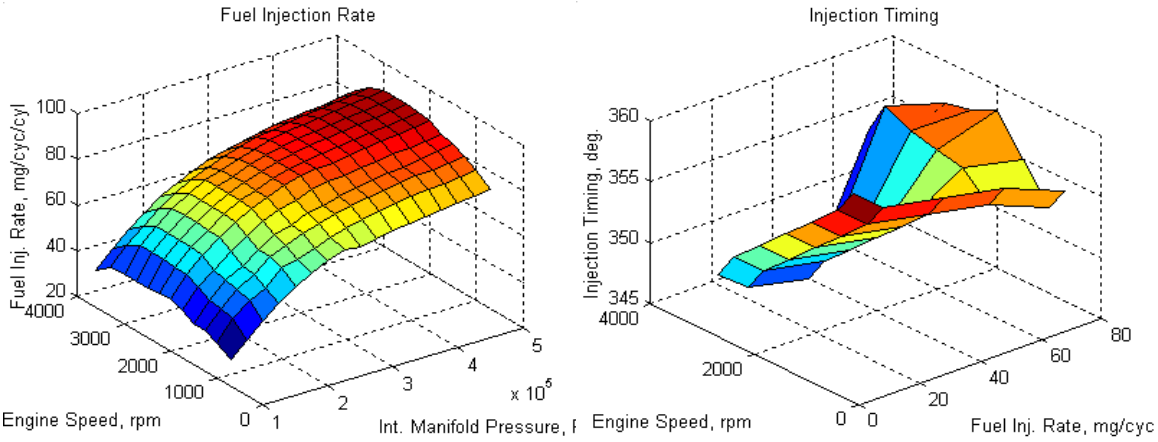

Figure 22. Fuel injection rate and timing for bypass valve configuration

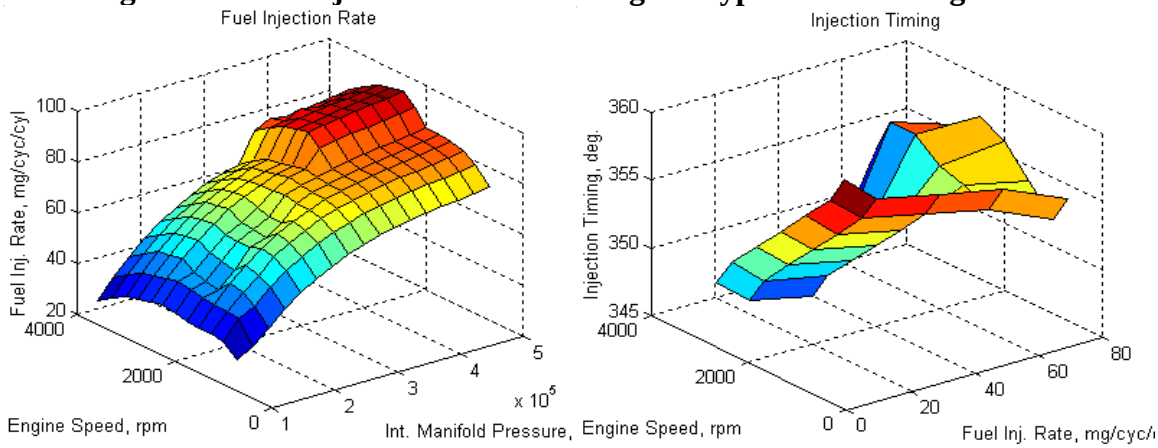

Figure 23. Fuel injection rate and timing for bypass valve configuration

4.2.3. Steady state results

Operating points on compressor maps for the wastegate, bypass valve and EIVC configurations are shown in Figure 24, Figure 25, and Figure 26**,** respectively. The operating points on the compressor map indicate good turbocharger matching showing efficient operation at all speed and load conditions, and sufficient margin from both the surge line and the choke limit.

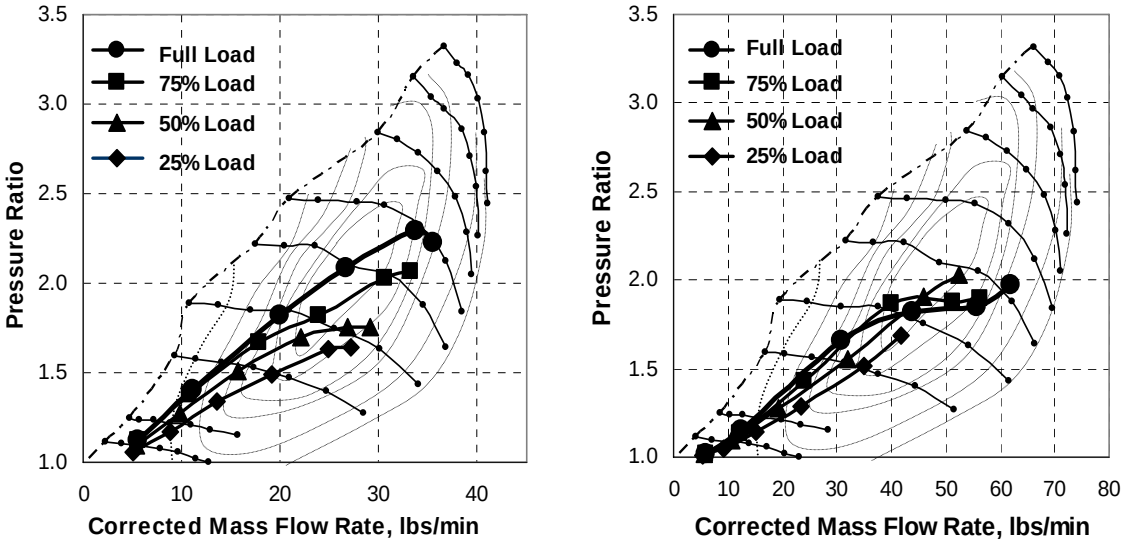

(a) HP compressor **(b)** LP compressor

Figure 24. Operating points of wastegate configuration

The wastegate opens up at a preset intake manifold pressure, and the results are shown in the low pressure compressor map in Figure 24. The operating lines level out as the intake manifold pressure reaches the preset limit, and as the load increases the wastegate opens up earlier in the engine speed. Overall, the final dual-stage system is well balanced between two stages and operating points stay within the efficient operating region.

With the bypass valve placed across the high pressure (HP) turbine, the effect of bypass valve is shown in the HP compressor map as shown in Figure 25. The operating

point on the HP compressor map indicates that the bypass valve is actuated at higher engine speed on HP turbine while the pressure ratio on the LP compressor map continues to increase. The operating points on both compressor maps show efficient operations of both HP and LP compressors at medium to high engine speeds.

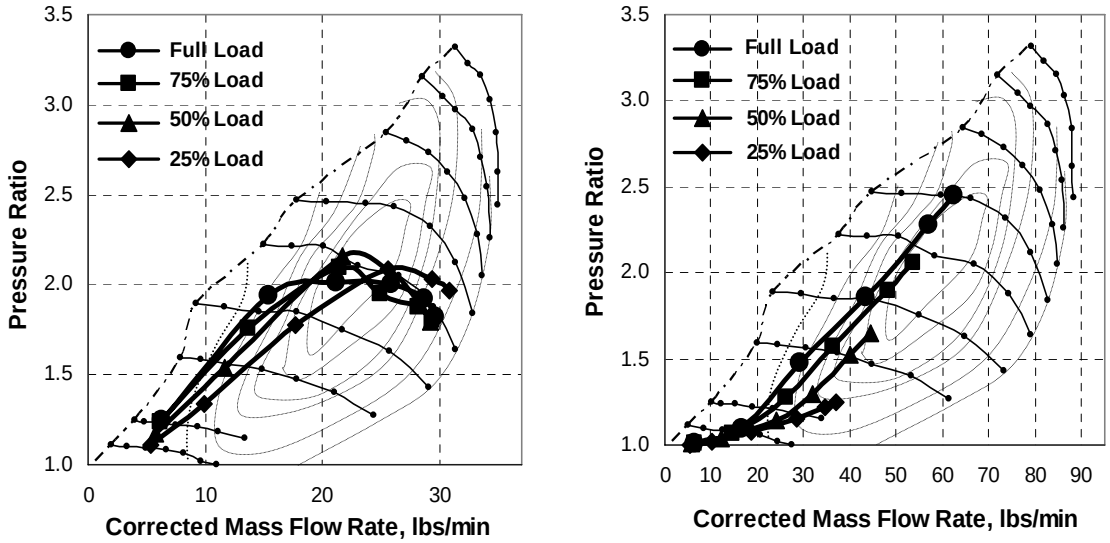

(a) HP compressor **(b)** LP compressor

Figure 25. Operating points of bypass valve configuration

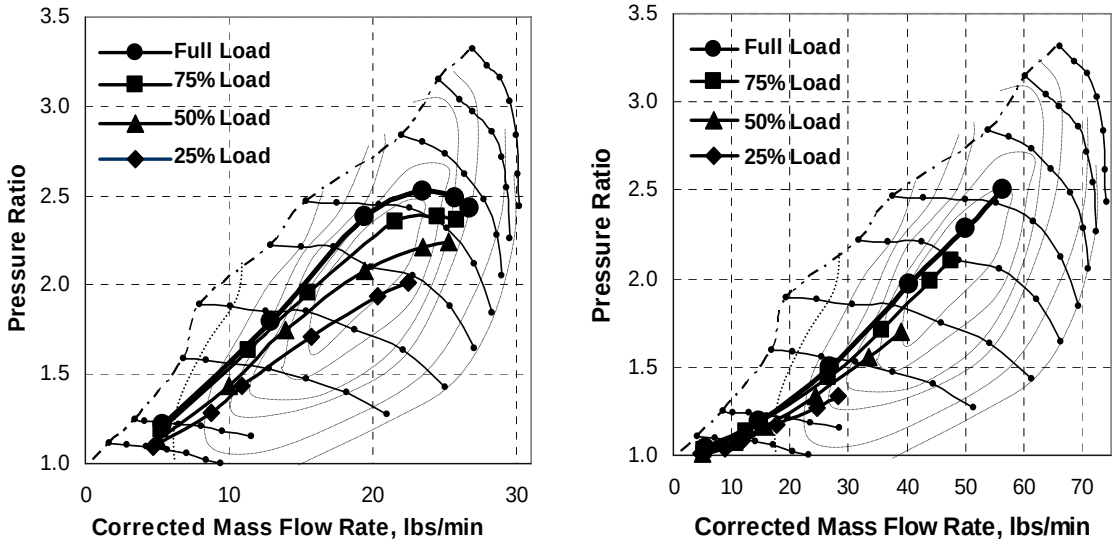

(a) HP compressor **(b)** LP compressor

Figure 26. Operating points of EIVC cycle engine

The operating points of the EIVC cycle engine without bypass valve are shown in Figure 26. Compared to either the bypass valve or the wastegate configuration, both the HP and LP compressors are operating at higher pressure ratios, resulting in higher overall pressure ratio due to their smaller sizes. The EIVC cycle allows higher intake pressure as the peak cylinder pressure is lowered due to reduced effective compression ratio. Smaller turbochargers are used in both HP and LP stages even without the bypass valve since the EIVC allows significantly higher intake manifold pressure without exceeding the cylinder pressure limit.

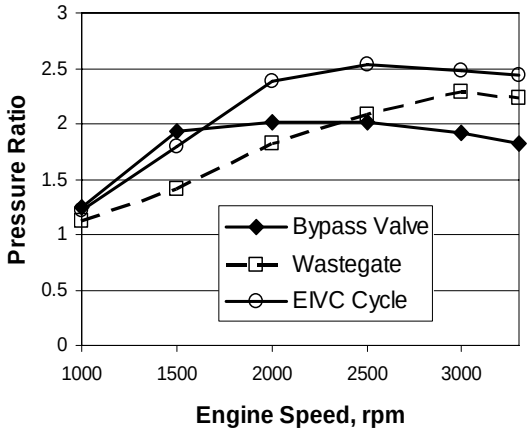

(a) HP compressor

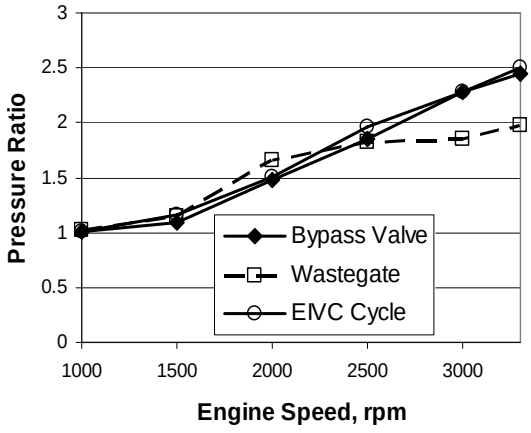

(b) LP compressor

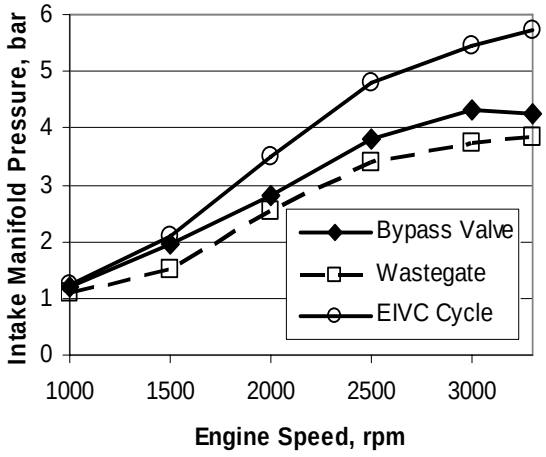

(c) Intake manifold pressure

Figure 27. Steady-state full load boosting characteristics

In Figure 27**,** boosting characteristics of different configurations are shown. With wastegate configuration, compression is done evenly between both stages. On the other hand, with bypass valve configuration, most of the boosting is accomplished by high pressure compressor at low speed operation while the low pressure compressor slowly takes over as the engine speed increases. With EIVC controlling the boost instead of bypass valve or wastegate, both the high pressure and low pressure compressors are allowed to boost higher than the other configurations. The reason that higher boost is allowed with EIVC is that the exhaust enthalpy is lower since more exhaust energy is utilized by the engine before the exhaust gas reaches the turbine due to longer exhaust stroke.

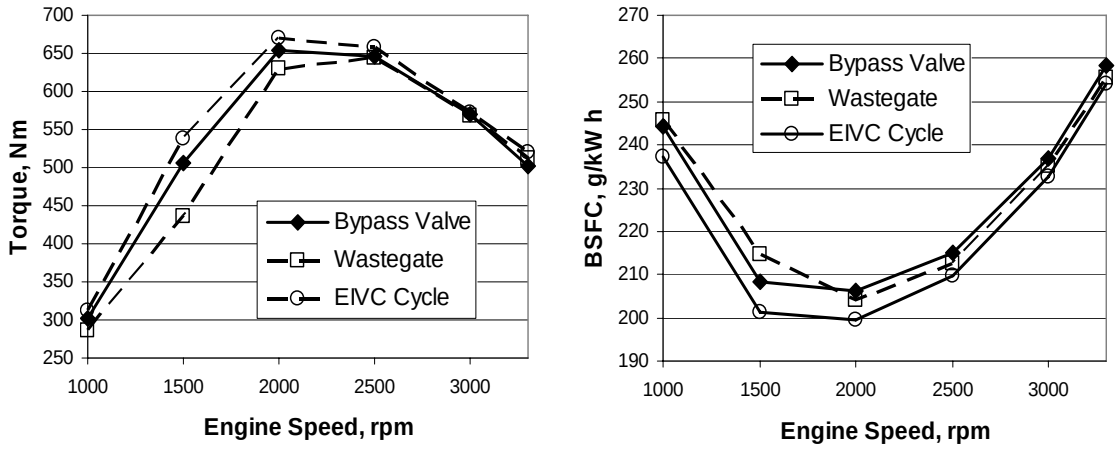

Figure 28. Torque and BSFC

Brake torque and brake specific fuel consumption (BSFC) of the dual-stage systems are compared in Figure 28. The low end torque is much improved with the bypass and EIVC configuration compared to the wastegate configuration while all three systems produce relatively similar torque at high engine speed. The difference in low end torque mainly comes from the use of smaller high pressure turbocharger with bypass valve configuration and even smaller turbocharger with EIVC. The EIVC allows smaller

turbocharger at the low pressure stage than that used with bypass valve, and the smaller low pressure turbocharger allows even smaller turbocharger at the high pressure stage as the low pressure turbocharger operates on higher pressure ratio at high engine speed, which prevents the high pressure turbocharger from choking at high engine speed.

The brake specific fuel consumption (BSFC) of the EIVC shows sizeable improvement from both the bypass valve and wastegate configuration since more exhaust energy is utilized by the engine due to longer effective exhaust stroke and the boosting system utilizes the exhaust energy more efficiently. Comparing the bypass valve and wastegate configurations, the bypass valve configuration has advantage in fuel consumption at low engine speed as the boosting system is more efficient with smaller high pressure turbocharger. On the other hand, the wastegate configuration shows improved fuel economy at high engine speed, as the boosting system operates more efficiently at high engine speed due to larger low pressure turbocharger and the smaller turbocharger in the bypass valve configuration does not operate efficiently at high engine speed.

4.2.4. Transient results

In order to study the transient characteristics of the three different boosting configurations, the engine system model is integrated with the vehicle dynamics model described in chapter 2, and then series of full load acceleration tests are performed with prescribed driving schedule. Initially the virtual vehicle is at rest with the engine idling and the full load acceleration command is given to the driver module until the vehicle reaches the speed of 70 mph in order to measure the time that takes for the vehicle to reach 60 mph from standstill. Then the vehicle is decelerated to 30 mph and maintains

that speed for 10 seconds, and another full load acceleration command is given to the driver module until the vehicle reaches 60 mph in order to measure 30 to 50 mph acceleration time, which often represents the vehicle passing performance. The results are shown in Figure 29 and Figure 30.

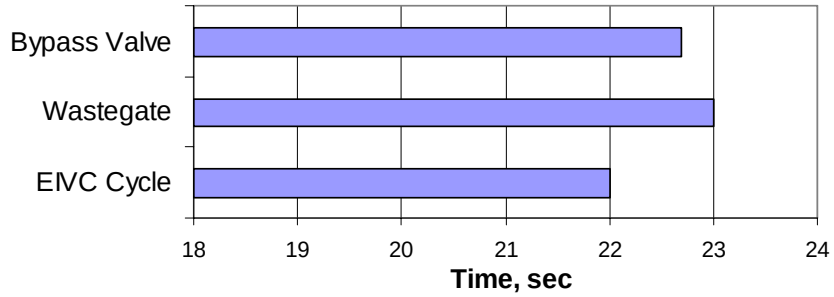

Figure 29. Vehicle launch performance (0 to 60 mph full load acceleration)

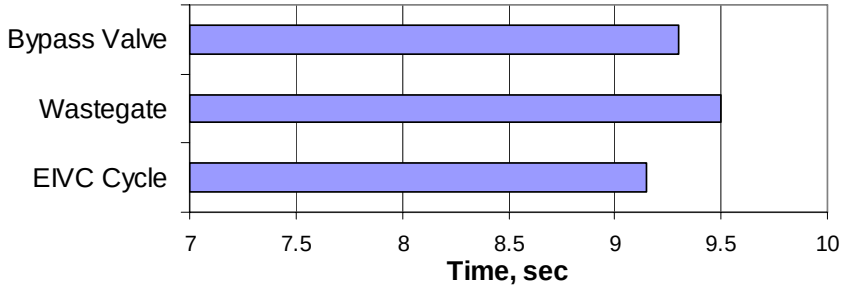

Figure 30. Vehicle passing performance (30 to 50 mph full load acceleration)

In both tests, the boosting system with EIVC clearly out-accelerates the systems with either bypass valve or the wastegate, while the gap is narrowed to some extent in 30 to 50 mph. The faster 0 to 60 mph time of the EIVC configuration is mainly attributed to the improved torque in the high engine speed range as the engine speed remains in that range for the most part of the test period once the engine speed passes low speed range. However, the difference becomes smaller in passing performance test as the EIVC configuration takes more time to build up boost in this highly transient condition since the available exhaust energy is less than systems with conventional valve timing. This is evident in Figure 31 and Figure 32.

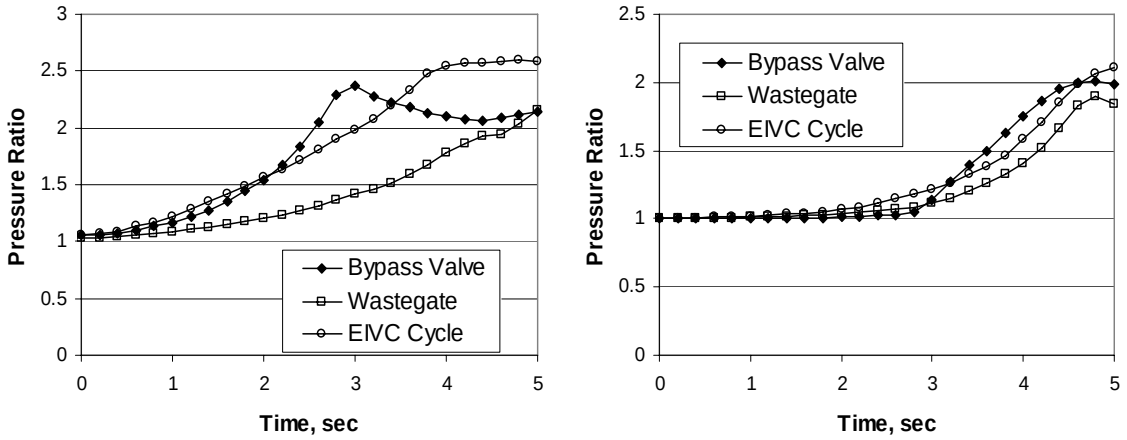

(a) HP compressor **(b)** LP compressor

Figure 31. Transient boosting characteristics under full load acceleration

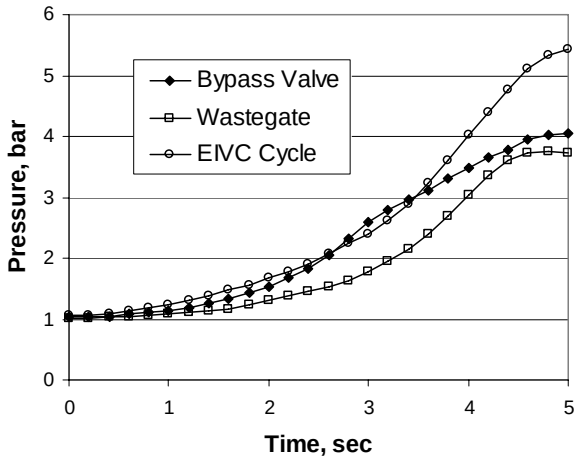

Figure 32. Intake manifold pressure under full load acceleration

Even with smaller size turbochargers in both HP and LP stages, EIVC configuration clearly takes more time to build up boost in the transient condition compared to bypass valve configuration, which even with slightly larger HP turbocharger and much larger LP turbocharger builds boost faster at the beginning of the acceleration as shown in Figure 31. Compared to the wastegate configuration, however, the EIVC configuration is quicker mainly due to much larger difference in turbocharger sizes even with disadvantage in available exhaust energy. It is also clearly shown that at the early stage of the acceleration, the larger low pressure turbocharger does not contribute much

to the overall boost for both configurations and the relative difference in size is not as important as the high pressure turbocharger size.

4.3. Summary

In this chapter, three different boost control options are compared in terms of engine performance and fuel consumption. The dual-stage turbocharger matching method described in chapter 3 is applied to optimize the turbocharger selections for each boost control options, and the fuel injection rates and timings are also optimized for the performance and fuel economy improvements using the engine simulation model described in chapter 2. The results demonstrate very good utilization of both high pressure and low pressure turbochargers in terms of turbomachinery efficiency and engine torque characteristics.

The boost control options considered in this chapter include three basic configurations; a wastegate across the LP turbine, a bypass valve across HP turbine and a system utilizing EIVC. Between the exhaust bypassing mechanisms investigated in the study, the bypass valve across the HP stage provides better low end torque and transient responses mainly due to the use of smaller turbocharger in the HP stage where the aforementioned performances are critically affected. The bypass configuration has shown slightly worse performance and fuel economy at high engine speed than the wastegate configuration as the smaller turbocharger chokes with increased air flow. However, the bypass valve configuration is preferable since the performance at low engine speed and in transient condition is more critical in order to allow aggressive engine downsizing.

Overall the system with EIVC proved to be the best among the options in terms of the engine performance both in steady state and transient operating conditions and fuel

economy improvement. The EIVC cycle has inherent advantage over the conventional valve timing in terms of thermal efficiency as the effective exhaust stroke is longer than the intake stroke utilizing more exhaust energy. It is also proven to be very effective and efficient in controlling boost in a dual-stage turbocharging system as it allows the boosting system to operate without exhaust gas bypassing mechanism, which is possible because the exhaust enthalpy is lower with longer effective exhaust stroke and the peak cylinder pressure is reduced due to charge cooling effect allowing much higher boost without exceeding the mechanical limits of the engine block.

CHAPTER 5. HYBRID DUAL-STAGE BOOSTING SYSTEMS

5.1. Introduction

A hybrid dual-stage boosting system is a boosting system that consists of a number of different types of air charging devices connected in a series configuration. Such devices include exhaust-driven turbochargers, mechanically driven superchargers, and electrically driven superchargers. Although it is preferable to use exhaust driven turbochargers whenever possible if the ultimate efficiency is the main interest of building a dual-stage boosting system, they do not always provide sufficient boost over the entire operating range of an engine. Especially in the low speed range, the downsized engine with dual-stage turbocharging system does not deliver the same level of performance of the baseline engine with larger displacement as shown in Figure 33.

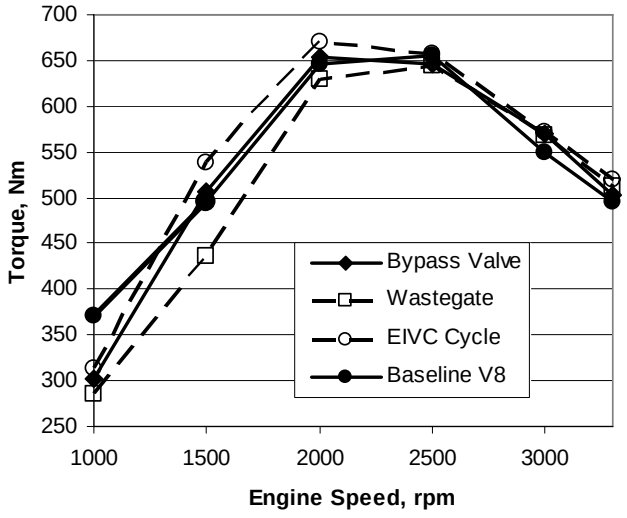

Figure 33. Torque from downsized engine with dual-stage turbocharger compared to torque from baseline V8 engine

While the torque produced at mid to high engine speed is comparable or even exceeds the torque produced by the baseline V8 engine, the torque produced in the lower rpm range is noticeably lower than that of the baseline engine. This is where the hybridization of the dual-stage boosting system is desirable even though the fuel economy must be sacrificed to some extent in favor of performance. For example, a mechanically driven supercharger connected in series with an exhaust driven turbocharger can provide strong boost even at low engine speed taking advantage of its direct connection to the output shaft of the engine. The combined effect of the boosting system is more consistent boost over the entire operating range of the engine at the cost of slightly less overall efficiency.

Electrically driven superchargers are even better in this regard since they are completely decoupled from the engine and have the freedom to spin at any rate regardless of the engine operating condition. With this feature, the hybrid boosting system can become an effective method not only to increase torque at low engine speed, but also to reduce smoke by ensuring sufficient air volume. However, the electric motor and power supply system are the limiting factors [67, 68]. The battery and the generator cannot supply sufficient power for the electric compressor to maintain air flow as the engine displacement volume increases.

In general, the hybridization of the boosting system results in fewer compromises in the boosting system matching. With the hybrid components enhancing the low speed performance, the turbocharger needs to perform efficiently only within the high speed range, which in turn improves the overall efficiency of the system.

The drawbacks of these types of hybrid systems include higher cost, complexity of the boosting system matching, and compatibility with the EGR system. With the hybrid dual-stage boosting system, the exhaust manifold pressure is often lower than the intake manifold pressure as there is only one turbine at the exhaust side but there are two compressors in intake side. Therefore, it is necessary to route the EGR feed line into upstream of the compressors. This may lead to the component fouling and the reduction of the component durability due to the particulate contents and the corrosive compounds in the exhaust gas [69].

In this chapter, the performance of the downsized V6 engine with several different types of hybrid dual-stage boosting systems is compared with that of the baseline V8 engine with single-stage turbocharging system. The main focus is to enhance the low end torque and reduce the boosting system lag often associated with heavy downsizing. The performance of the hybrid systems are also compared with the performance of the dual-stage turbocharging system with EIVC as it offers the best performance among the turbocharger-only dual-stage systems compared in chapter 4.

5.2. Hybrid dual-stage boosting systems

5.2.1. Hybrid dual-stage boosting system with screw type supercharger

The hybrid dual-stage boosting system with a screw type supercharger is illustrated in Figure 34. In this configuration, the turbocharger at the high pressure stage is replaced by a mechanically driven screw type supercharger. It draws power through mechanical connection to the crankshaft, and its rotational speed is directly proportional to the rotational speed of the engine. Thus it is relatively easier to design and predict its boosting characteristics than a turbocharger. However, superchargers are inherently less

efficient since they consume more power than turbochargers [70]. The screw type supercharger was selected for the hybrid boosting system component since its efficiency is superior to the other common type of superchargers such as roots type supercharger.

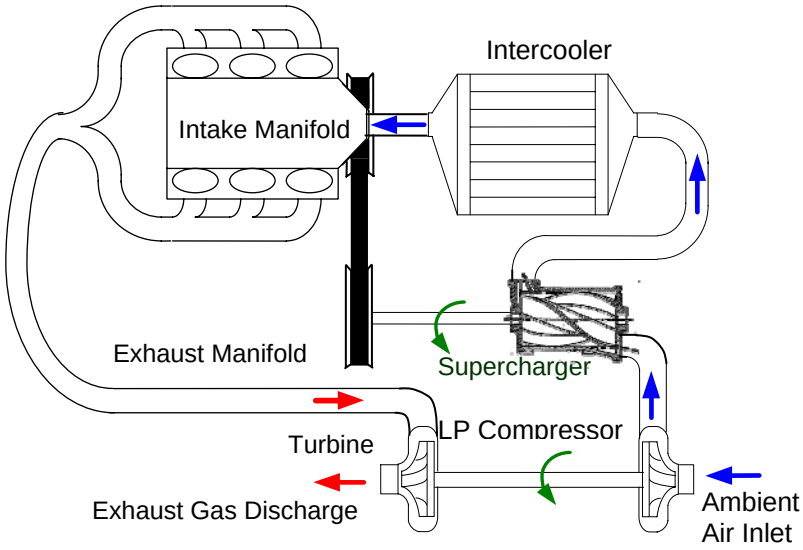

Figure 34. Hybrid dual-stage boosting system with mechanically driven screw type supercharger

Before the design of the hybrid boosting system with supercharger was finalized, the supercharger was placed in the LP stage instead of HP stage as in the final design in an attempt to enhance the LP stage performance as the LP stage was considered to be the bottle neck of the overall boosting performance. However, the performance of the dual-stage boosting system was severely hindered by the presence of another displacement type device at the entry point of the air flow to the system since the HP turbocharger didn't do anything but redistributing the pressure ratios between the LP stage and the HP stage while the overall pressure ratio of the boosting system is unaffected. The boosting system essentially acted as a single-stage system since the air flow is entirely dictated by the screw type supercharger at the LP stage and the benefit of the dual-stage boosting

diminished as the down stream pressure has negligible effect on the mass flow rate of the screw type supercharger. Therefore, the screw type supercharger had to be moved to the HP stage as in the final design.

5.2.2. Hybrid dual-stage boosting system with electrically driven supercharger

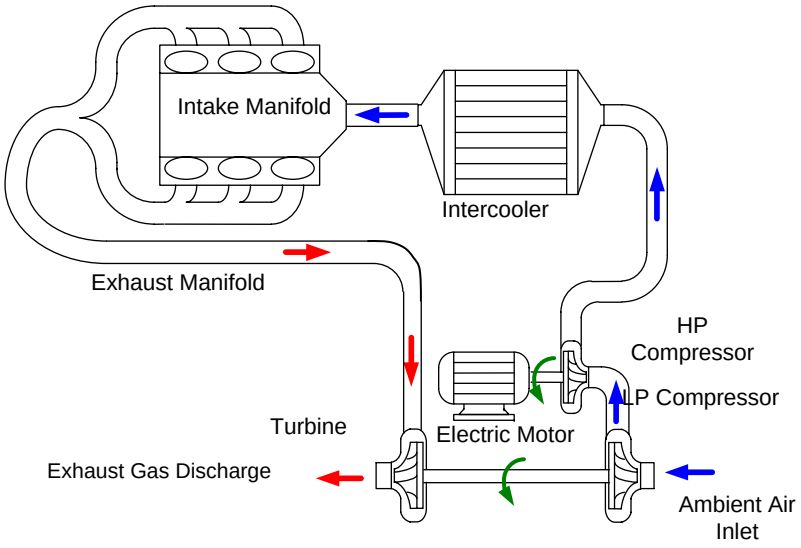

Figure 35. Hybrid dual-stage boosting system with electrically driven supercharger

In this hybrid boosting system, the turbocharger at the high pressure stage is replaced by an electrically driven supercharger as shown in Figure 35. A centrifugal compressor is used in the electrically driven supercharger since it is very compact in size and has very low rotational inertia. However, even with much less rotational inertia compared to other types of superchargers, substantial portion of the power must be wasted in just overcoming the inertia of the compressor when the vehicle is accelerated in a short period of time as the centrifugal type supercharger requires very high speed (in excess of 100,000 rpm in many cases) to achieve desired boost. Therefore, the placement of the electrically driven supercharger at the HP stage is more advantageous as this configuration allows smaller compressor with less rotational inertia. Another reason that

this configuration is more efficient than the configuration with the electrical supercharger at the LP stage is that the overall boosting performance is more sensitive to the changes in the HP stage.

The electric motor used for the supercharger has maximum power output of 8 kW. Considering the CCA (cold cranking ampere) ratings of the automotive batteries typically range from 500 A to 1200 A, the maximum power output of the motor is certainly near the upper limit of the electrical current handling of the system, but feasible without switching to a higher voltage system.

5.2.3. Hybrid dual-stage boosting system with variable geometry turbine

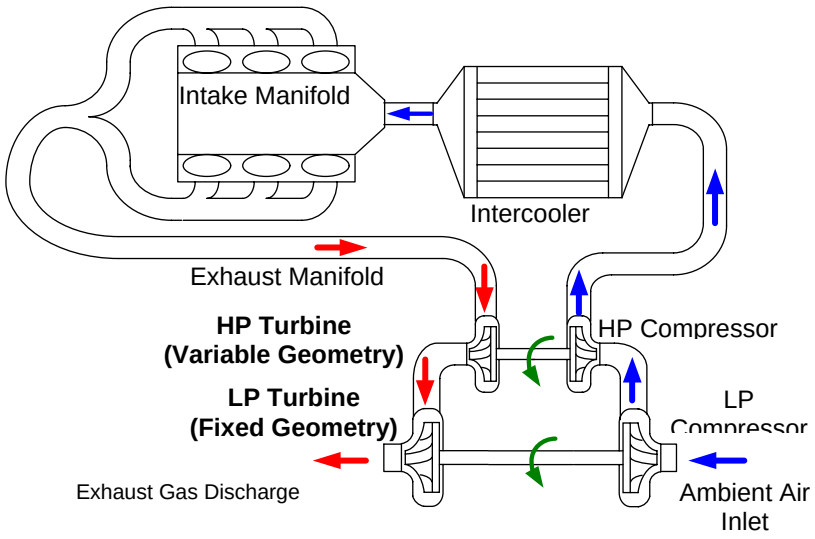

Figure 36. Dual-stage turbocharger with VGT at the high pressure stage

In a conventional dual-stage turbocharging system with fixed geometry turbines at both high and low pressure stage, it is desirable to have a small high pressure turbocharger in order to improve system transient response to sudden changes in speed and load. However, the small high pressure turbocharger restricts the gas flow at higher engine speed, and typically part of the gas flow must be bypassed to prevent choking and

over-boosting. However, by replacing one of the fixed geometry turbines with the variable geometry turbine (VGT), which typically has larger flowing capacity when the inlet vanes are fully opened, the bypass valve can be effectively eliminated as the boost can be controlled by adjusting the vane position of the VGT.

In this hybrid configuration, the fixed geometry turbine at the high pressure stage is replaced by VGT as shown in Figure 36. Initial study showed that it is more effective to replace the high pressure turbine with the VGT than to replace the low pressure turbine as the performance of the system is more sensitive to the changes in the high pressure stage. In addition, as the exhaust gas is no longer bypassed, the size of the low pressure turbine can be reduced, further improving boosting characteristics.

5.3. Fuel injection rate and timing

Fuel injection rates and timings adjusted with the similar procedure taken in the previous chapter. First the fuel injection rate is adjusted keeping the equivalence ratio low enough to avoid excessive smoke emission at low engine speed and transient condition, and efficient combustion at high engine speed. Then, MBT timings are established at different engine speed and load conditions using the engine simulation code and the timings are retarded where the peak cylinder limit is exceeded. The peak cylinder pressure, and the equivalence ratio in steady state and transient conditions are shown in Figure 37 and Figure 38.

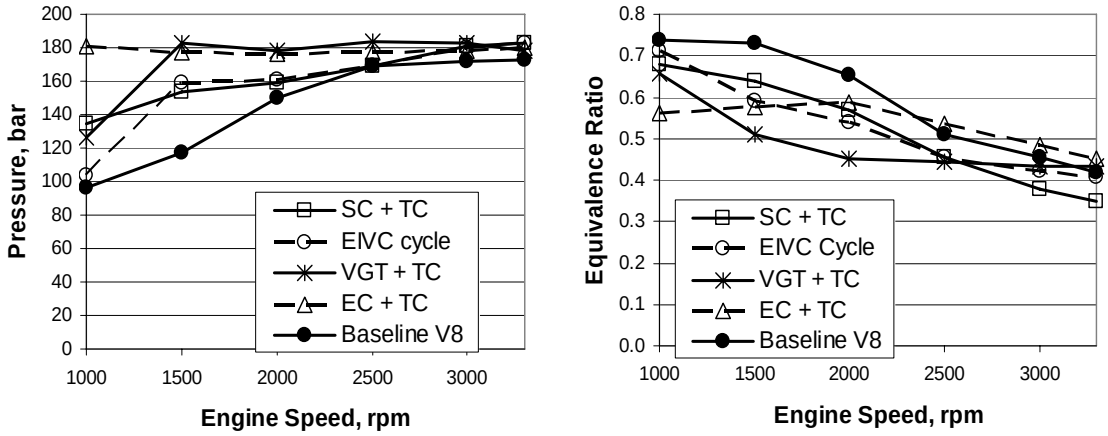

Figure 37. Peak cylinder pressure and equivalence ratio under steady-state full load condition

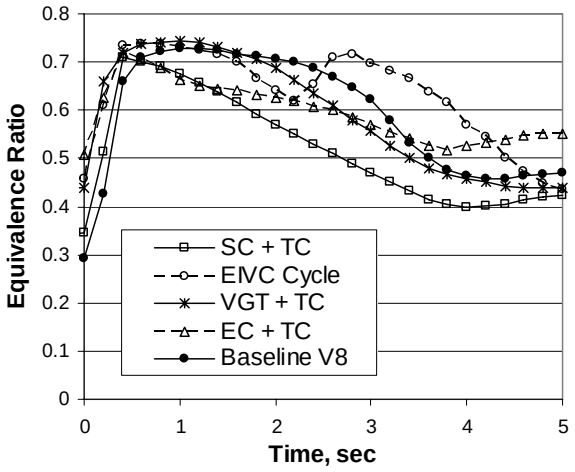

Figure 38. Fuel-air equivalence ratios under full load acceleration

Since the boost level reached by the hybrid boosting systems with an electric compressor and a VGT is substantially higher than that reached by other systems at low engine speed, the fuel injection rates and timings are already limited by the peak cylinder pressure even at the very low engine speed as shown in Figure 37. For other boosting systems, on the other hand, the fuel injection rates and timings are affected by the peak cylinder pressure only at high engine speed. The fuel injection rates and timings for different boosting systems are shown in Figure 39 through Figure 42.

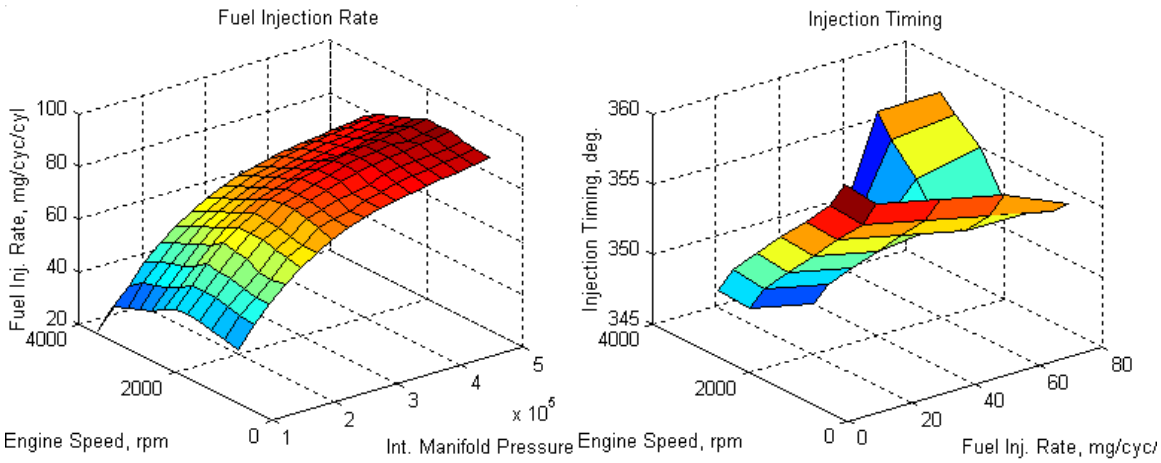

Figure 39. Fuel injection rate and timing for SC+TC configuration

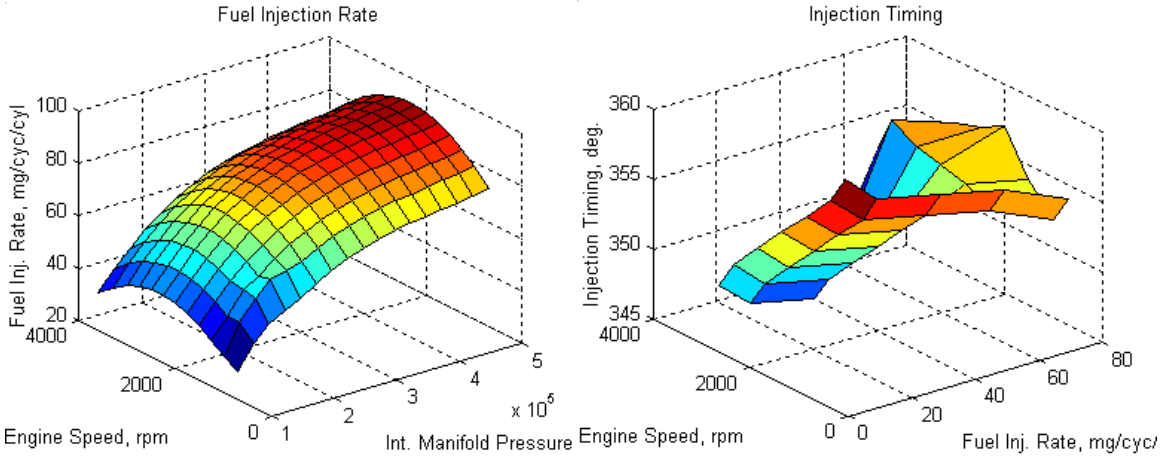

Figure 40. Fuel injection rate and timing for VGT+TC configuration

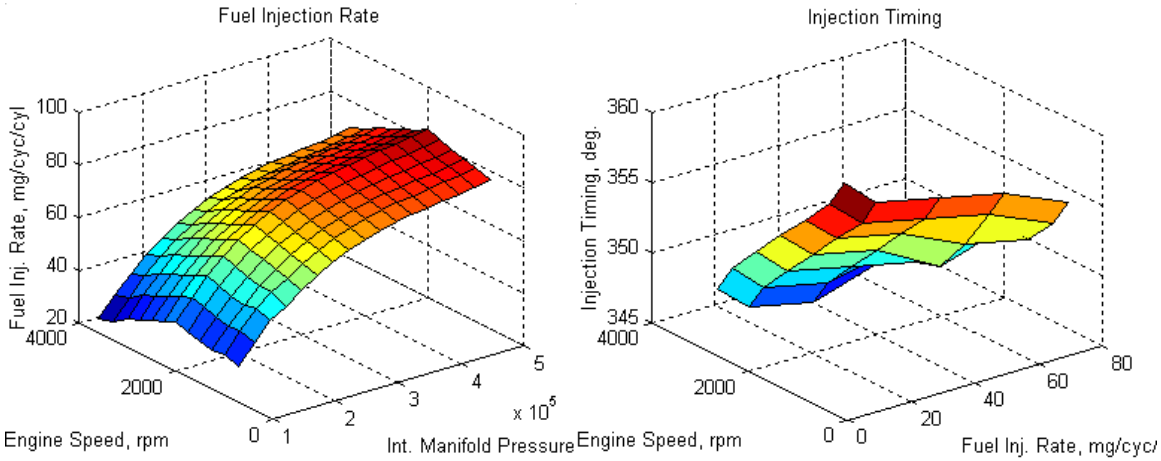

Figure 41. Fuel injection rate and timing for EC+TC configuration

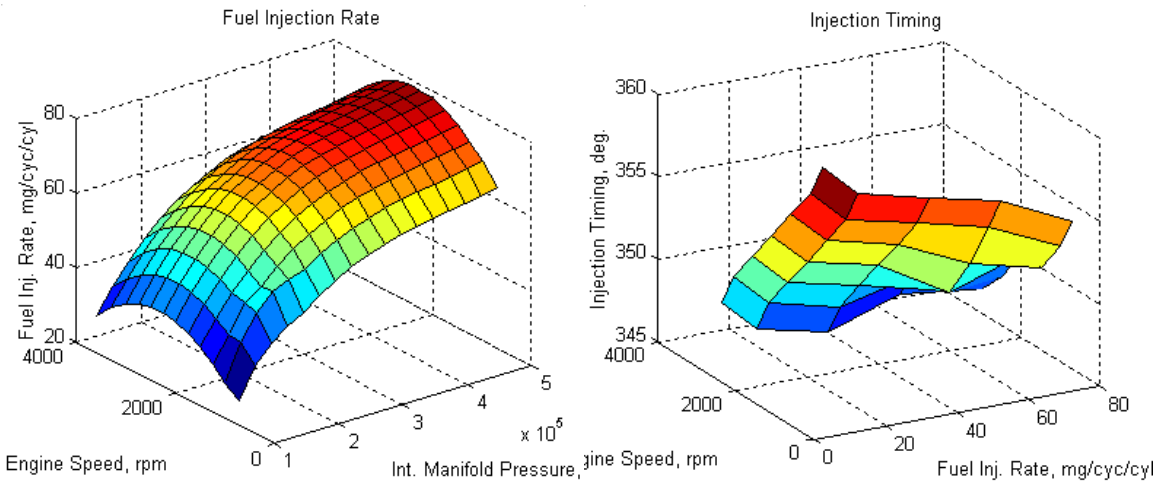

Figure 42. Fuel injection rate and timing for baseline V8 engine

5.4. Steady state simulation results

HYBRID BOOSTING SYSTEM WITH SCREW TYPE SUPERCHARGER – By replacing the turbocharger at the high pressure stage with a screw type supercharger, the low end torque is improved substantially at the cost of slight fuel economy penalty as shown in Figure 43.

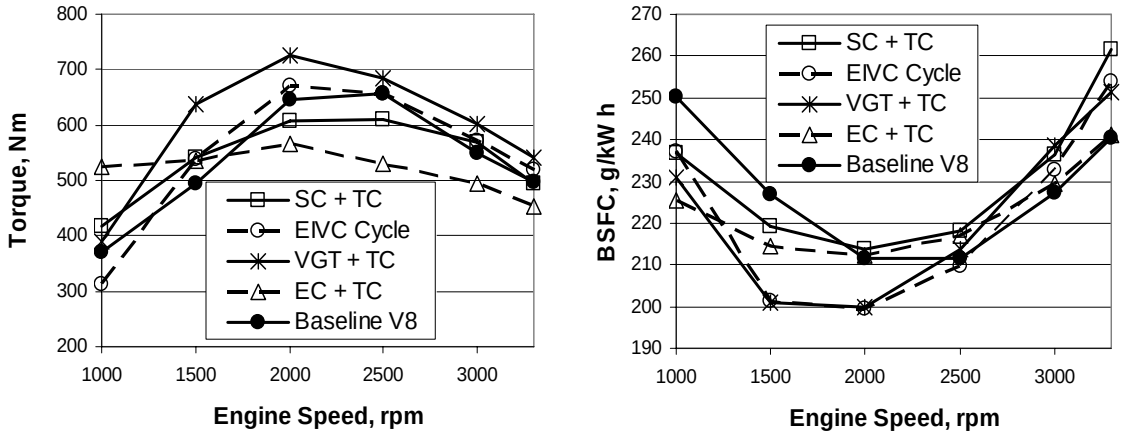

Figure 43. Brake torque and BSFC under steady-state full load condition

The boost is very strong even from the very low engine speed due to the excellent boosting characteristics of the screw type supercharger at the HP stage as shown in Figure 44. Thus the engine with this hybrid boosting system produces excellent low end

torque which even exceeds the low torque of the baseline V8 engine. The shape of the torque curve in general is relatively even throughout the entire engine speed compred to the other systems due to the linear boosting characteristics shown in Figure 44. However, the BSFC is relatively high since the supercharger draws power from the engine output shaft. The boost from the supercharger is nearly constant thought the operating range of the engine, while the boost from the turbocharger at the low pressure stage increases steadily as shown in Figure 44.

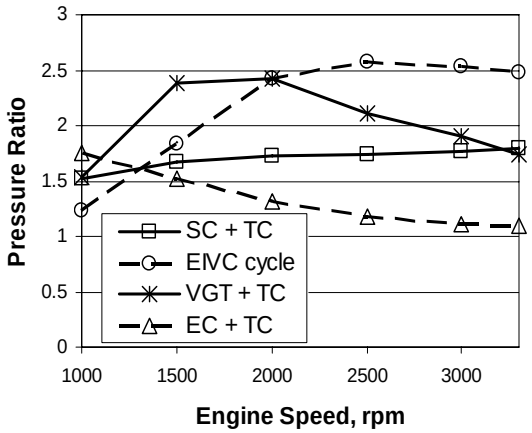

(a) HP compressor

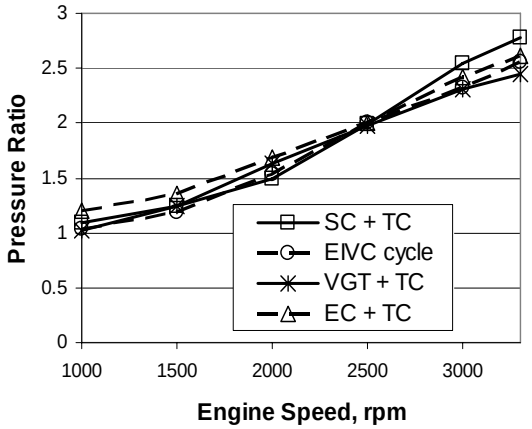

(b) LP compressor

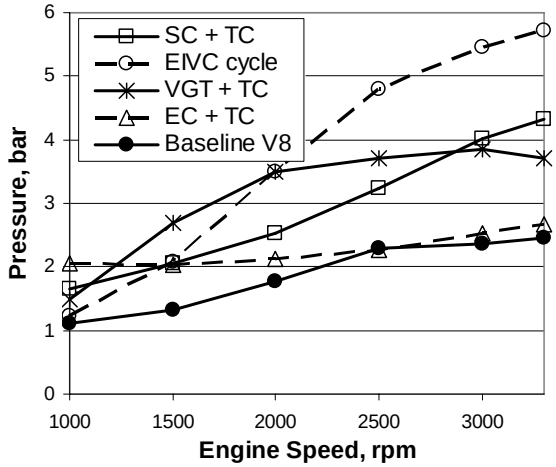

(c) Intake manifold pressure

Figure 44. Steady-state full load boosting characteristics

DUAL-STAGE TURBOCHARGER WITH VGT - The low end torque is improved due to higher boost realized by variable geometry turbine. The torque is already limited by peak cylinder pressure even at 1500 rpm as shown in Figure 37. The torque produced with this hybrid boosting system is superior to the other hybrid systems and the baseline V8 engine as well for the entire engine operating range with substantial margin. At higher engine speed, the boost is controlled by opening up the inlet vane. As a result, the boost from the high pressure turbocharger decreases as the engine speed increases while the boost from the low pressure turbocharger increases steadily as shown in Figure 44.

The VGT allows the use of larger turbocharger at the high pressure stage without sacrificing the performance at low engine speed, which in turn allows smaller low pressure turbocharger since the exhaust gas does not need to be bypassed even at high engine speed. With the fixed geometry turbine, the exhaust gas needs to be bypassed at high engine speed due to its limited flow capacity, dumping much of the exhaust energy unused at the high pressure stage. Therefore, the turbine at the low pressure stage must be large enough to cope with the increased expansion ratio.

With the larger swallowing capacity of the high pressure turbine with VGT, the efficiency of the turbocharger is higher, and results in better overall efficiency as the exhaust energy is evenly utilized in both high and low pressure stages even at high engine speed. Bypass valve is unnecessary since the swallowing capacity of both the high pressure and the low pressure turbocharger are sufficiently large even at high engine speed.

HYBRID BOOSTING SYSTEM WITH ELECTRICALLY DRIVEN SUPER-CHARGER – The torque is very strong at low engine speed exceeding the low end torque of the baseline V8 engine, as the electric motor can be operated at its full capacity even from the idle speed as shown in Figure 43 and Figure 44. The effectiveness of the electric compressor is clearly shown in low engine speed, but the boost tapers off rapidly as the 8 kW electric motor becomes limiting at higher engine speed. The power required to compress the incoming air at medium to high engine speed becomes much larger than the electric motor can provide and the boosting system effectively becomes a single-stage system at these speeds. Therefore, the compression ratio of the engine dose not need to be lowered as the boost pressure at high engine speed where the peak cylinder pressure reaches its maximum is sufficiently low. The higher compression ratio (18.0) partially compensates for the performance deficiency with this boosting system.

5.5. Transient simulation results

Similar to the procedures taken in the previous chapter, the engine system model is integrated with the vehicle dynamics model described and then series of full load acceleration tests are performed with prescribed driving schedule. The results shown in Figure 45 and Figure 46 are obtained by running a full load acceleration from 0 to 60 mph, and 30 to 50 mph with the engine systems integrated with the vehicle dynamics model. The results shown in Figure 47 and Figure 48 represent the boosting characteristics of the hybrid boosting systems for the first 5 seconds into the full load acceleration.

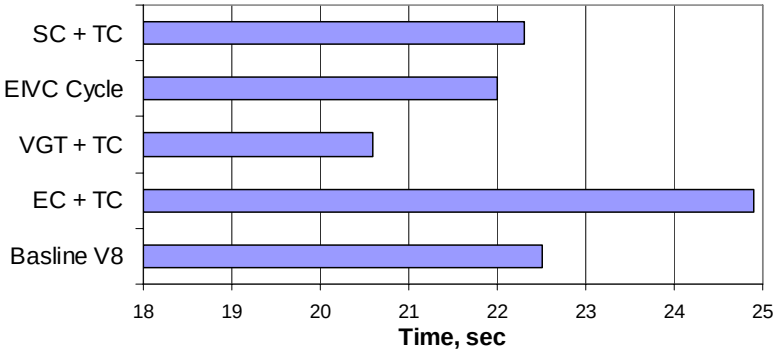

Figure 45. Vehicle launch performance (0 to 60 mph full load acceleration)

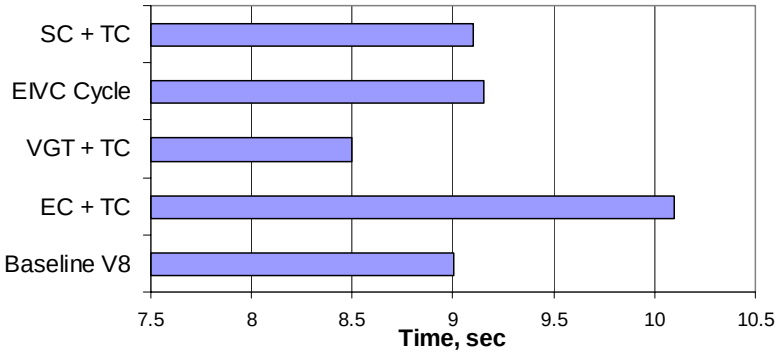

Figure 46. Vehicle passing performance (30 to 50 mph full load acceleration)

HYBRID BOOSTING SYSTEM WITH SCREW TYPE SUPERCHARGER – The transient response characteristics of the system are substantially improved due to the instant boost availability of the mechanically driven supercharger at the HP stage combined with very linear boosting characteristics of the screw type compressor as shown in Figure 47. The boost from the screw type supercharger at the high pressure stage is very strong from the beginning and nearly constant throughout the acceleration. This is reflected in the 0 to 60 mph vehicle launch performance as the second fastest system among the three hybrid boosting systems compared in the study (Figure 45). It is even faster to the 60 mph than the baseline V8 engine due to its slight advantage in high end and low end torque as shown in Figure 43. However, it is slightly slower from 30 to 50 mph than the baseline V8 engine due the torque deficit in mid engine speed.

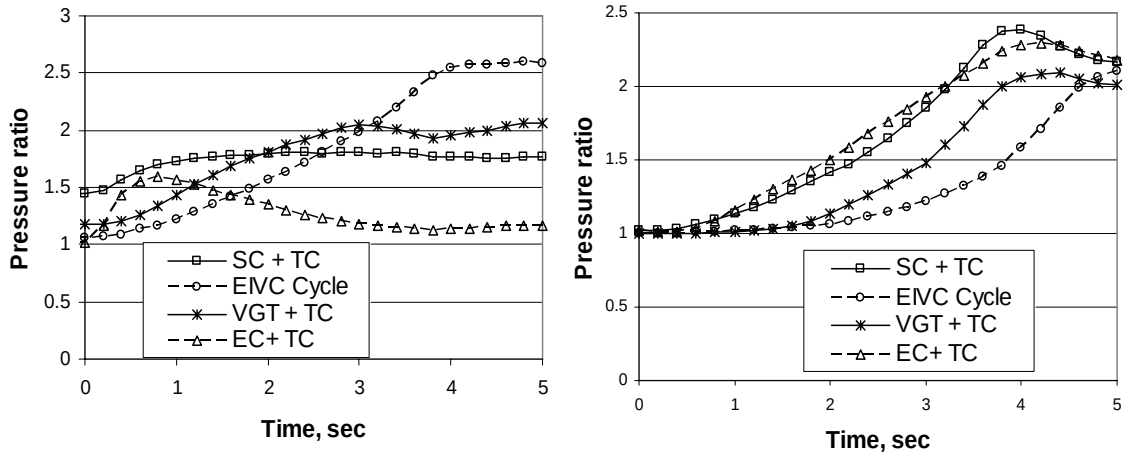

(a) HP compressor **(b)** LP compressor

Figure 47. Transient boosting characteristics under full load acceleration

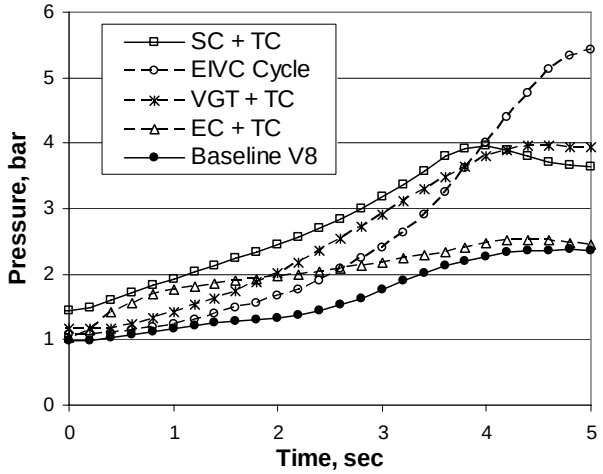

Figure 48. Intake manifold pressure under full load acceleration

In terms of boosting characteristics, the supercharger at the HP stage clearly shows advantage over the other hybrid systems in both steady state and transient operating conditions (Figure 47 and Figure 48) even though the overall vehicle launch performance is somewhat behind the hybrid system with VGT.

DUAL-STAGE TURBOCHARGER WITH VGT – This is the fastest system in both acceleration categories with good transient response with the VGT at the high pressure stage. Even though the initial boosting characteristics of the hybrid boosting system with supercharger seems better in 0 to 60 mph launch performance, it is quickly

caught up by vastly superior torque of the hybrid boosting system with VGT once the initial transient phase is over.

HYBRID BOOSTING SYSTEM WITH ELECTRICALLY DRIVEN SUPERCHARGER - The limitation of the available power from the electrical system is more evident in transient conditions since the electric motor must overcome not only the load required for compression but also the inertia of the compressor. The boost from the electric compressor at the high pressure stage diminishes very quickly as the electric motor reaches its maximum power as shown in Figure 47. From that point on, the hybrid boosting system is essentially a single-stage boosting system as the electric compressor does not provide meaning boost for the remainder of the acceleration.

5.6. Fuel economy

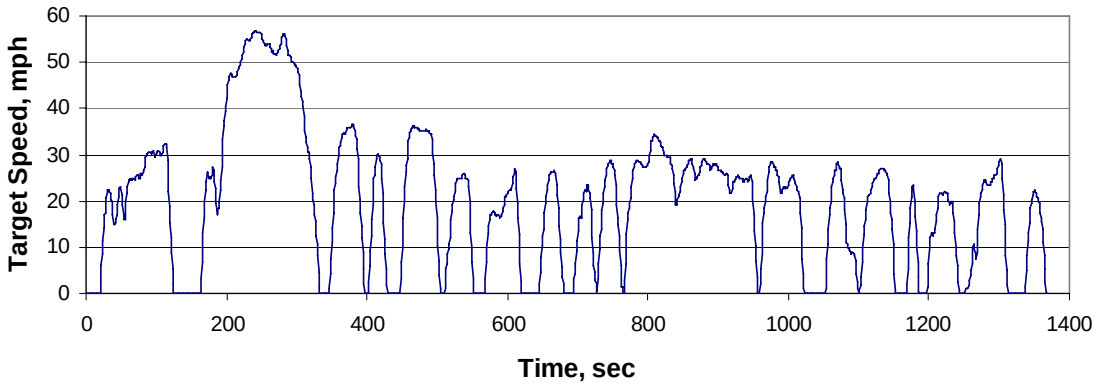

Figure 49. U.S. FTP-72 cycle

The driving cycle used for fuel economy measurement is the U.S. FTP-72 (Federal Test Procedure) cycle shown in Figure 49. In order to measure the fuel consumption and evaluate the engine system behavior, the engine system model integrated with the vehicle dynamics model is driven through the driving cycle which

simulates an urban route of 7.5 miles with frequent stops. The maximum speed is 56.7 mph and the average speed is 19.6 mph.

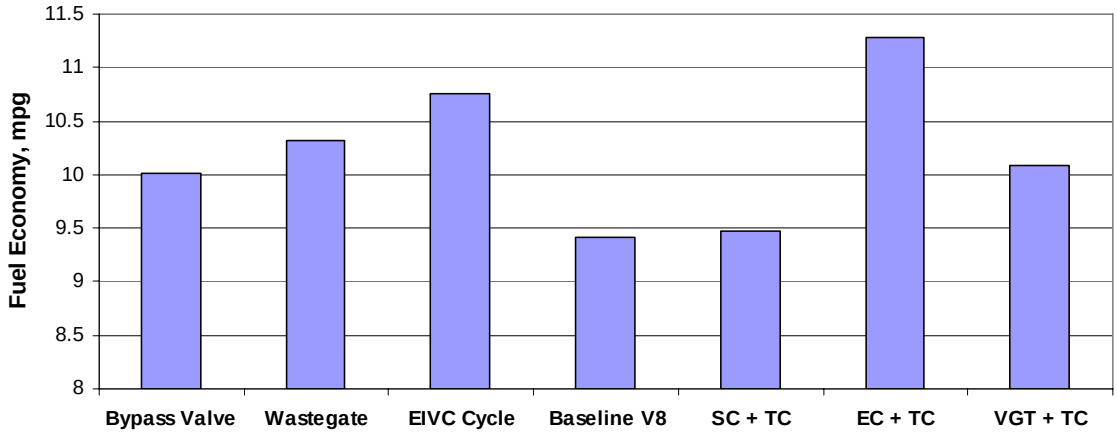

Figure 50. Fuel economy through FTP-72 cycle

As summarized in Figure 50, all the downsized V6 engines with dual-stage boosting systems show improved fuel economy over the baseline V8 engine due to reduced displacement volume. This signifies that the goal of engine downsizing with advanced dual-stage boosting system is achieved without too much compromise in performance except for the hybrid boosting system with electric compressor.

Table 5. Fuel-air equivalence ratio when the electric compressor is turned off

Load (%)	700 rpm	1000 rpm	1500 rpm	2000 rpm	2500 rpm	3000 rpm	3300 rpm
100						0.58	0.51
90					0.72		
80					0.68		
70			0.77	0.74			
60	0.73	0.70	0.67	0.65			
50	0.61	0.59					

However, the hybrid boosting system with electric compressor offers the highest fuel economy improvement over the baseline V8 engine since the electric compressor operates only when the fuel-air equivalence ratio exceeds the limit of 0.7 as shown in Table 5. The shaded area in the table shows the engine speed and load condition where

the fuel-air equivalence ratio exceeds the limit if the electric compressor is turned off. This resulted in reduced fuel consumption as the electric compressor operates only in the high load, low speed conditions, and it is reflected in the broadened BSFC contours in the medium to high speed engine operation region as shown in Figure 51 (f).

The driving cycle used in the study puts emphasis on low speed, part load performance of the engine system as shown in engine visiting point plots in Figure 51. Since the engine visiting points are mostly clustered in low to medium speed medium load region, the fuel economy in this region is the most important factor in reducing the fuel consumption during the driving cycle.

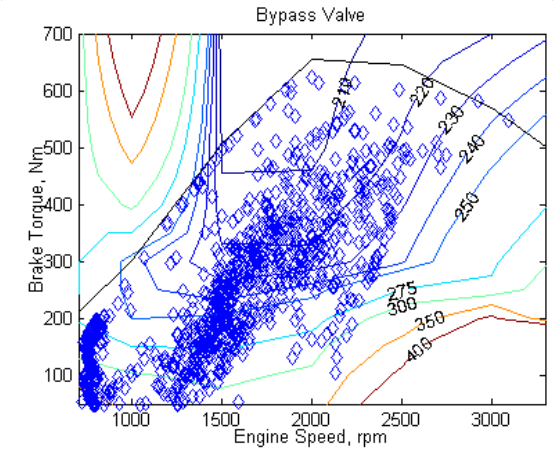

(a) Bypass Valve

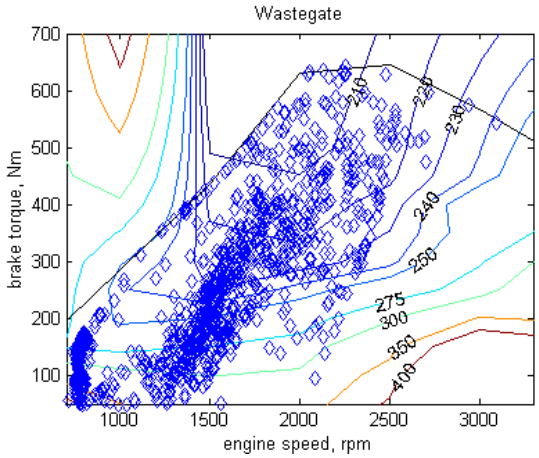

(b) Wastegate

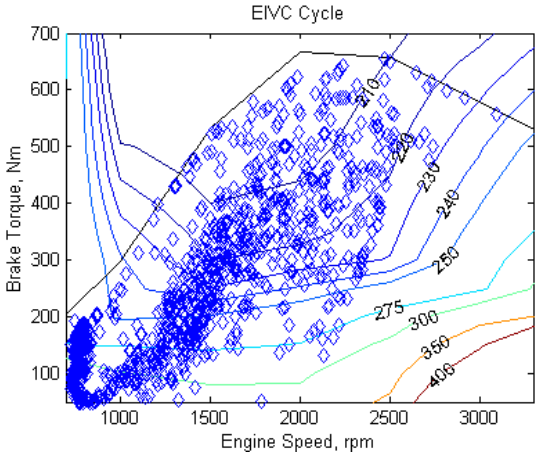

(c) EIVC cycle

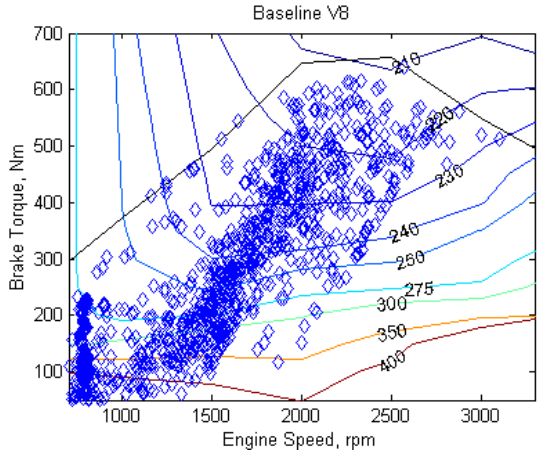

(d) Baseline V8

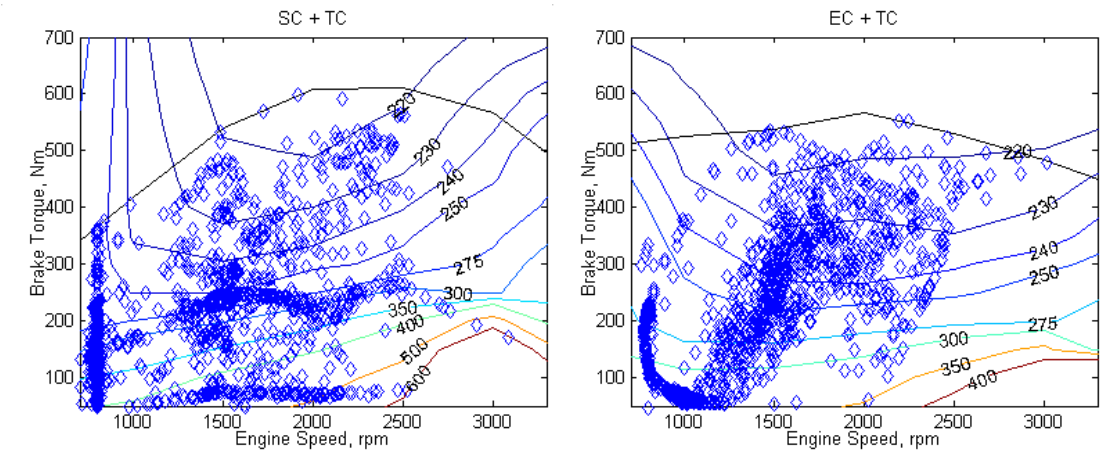

(e) SC + TC

(f) EC + TC

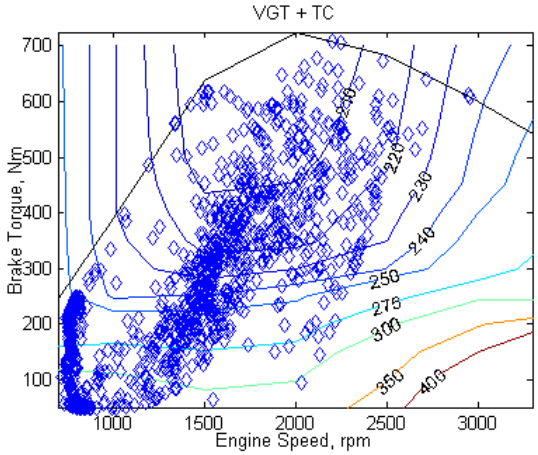

(g) VGT + TC

Figure 51. Engine visiting points during FTP-72 drivng cycle simulation

Compared to the baseline V8 engine, the dual-stage boosting systems in general moves the efficient region toward the low speed region by taking advantage of the dual-stage boosting system, and it is reflected in the reduced fuel consumption as the engine operates in this region more frequently. Bypass valve, wastegate and EIVC cycle systems are good examples. The dual-stage turbocharging systems are optimized for the low speed engine operation, and the fuel economies are significantly improved over the baseline V8 engine and more so with the EIVC cycle as the thermal efficiency of the engine with improved and the exhaust energy is utilized more efficiently. The hybrid system with VGT also shows reduced fuel consumption due to the same benefit as the

other dual-stage turbocharging systems with significantly improved performance as well. The fuel economy benefit from the hybrid system with supercharger is not as significant as the other dual-stage boosting systems as most visiting points are in the less efficient region.

Visiting points on compressor maps are shown in Figure 52. These plots show the utilization of the boosting systems while driving through the FTP-72 cycle. In general, the boosting systems are very well utilized showing most visiting points are clustered in the efficient region of the map, and show no sign of compressor surging or choking. Thus it can be concluded that the boosting systems are well matched to the downsized engine. The hybrid boosting system with electric compressor, however, shows distinctly different pattern as the pressure ratio and the mass flow rate through the electric compressor are inversely proportional because of the limited electrical power supply to the motor. Due to these characteristics, it requires more attention to avoid surging and choking. For example, it tends to surge when the electric motor spins at full capacity while there's not enough air flow to maintain the pressure ratio. However, using a smaller compressor to solve this problem often leads to choking problem. Thus, finding the right compressor requires more iteration. It seems advantageous to move the operating region toward the center of the map, where the efficiency and flow range improves, either by increasing the supplied electric power or by changing the physical characteristics of the compressor itself.

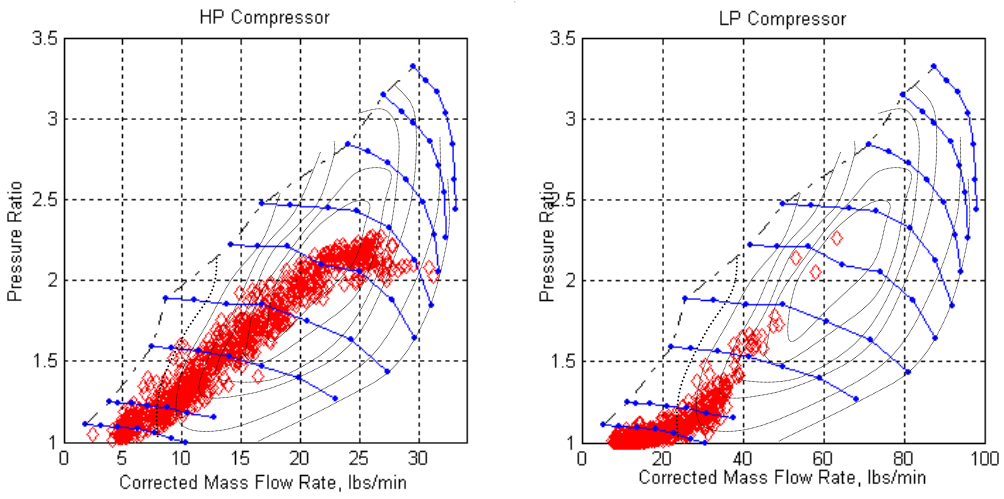

(a) Bypass Valve

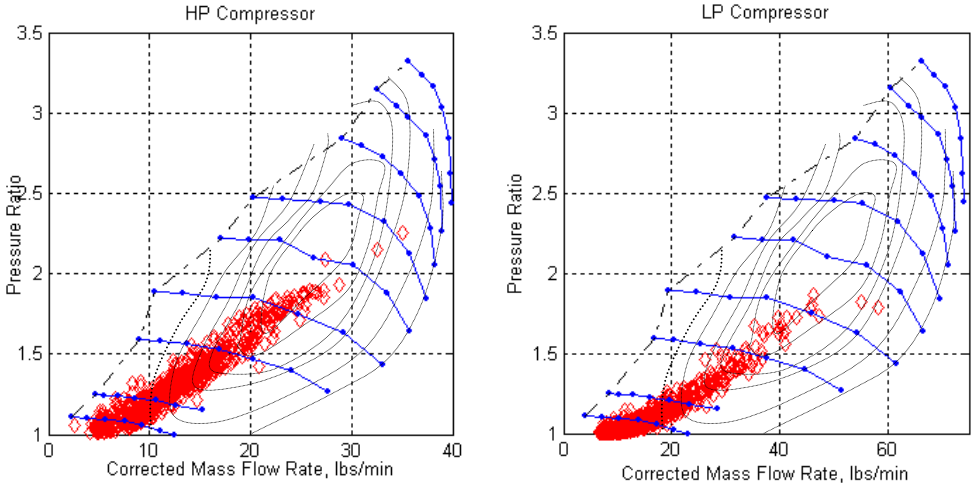

(b) Wastegate

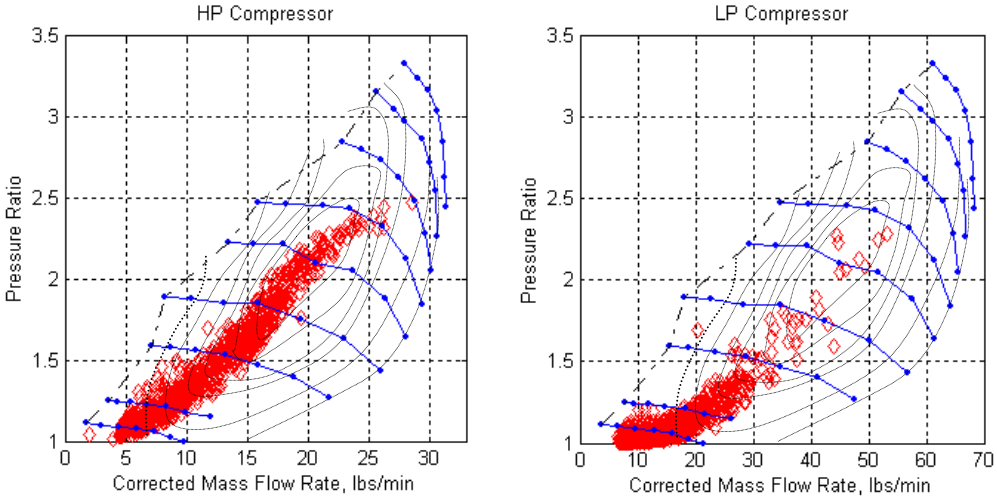

(c) EIVC cycle

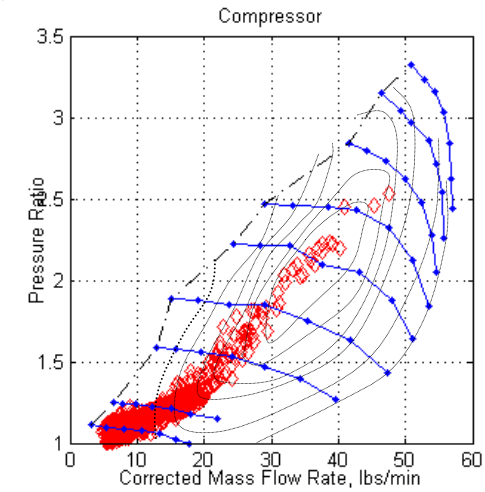

(d) Baseline V8

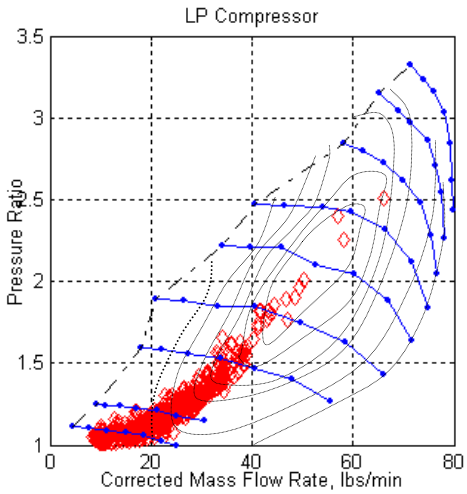

(e) SC + TC

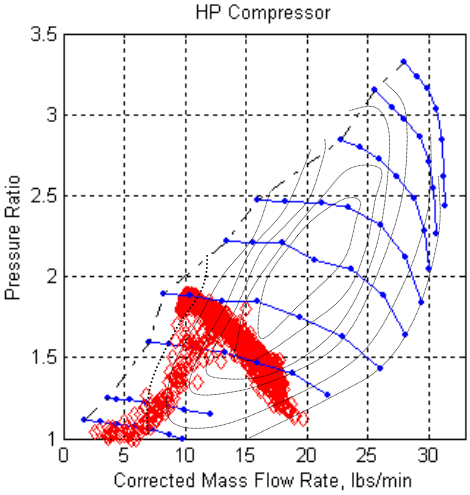

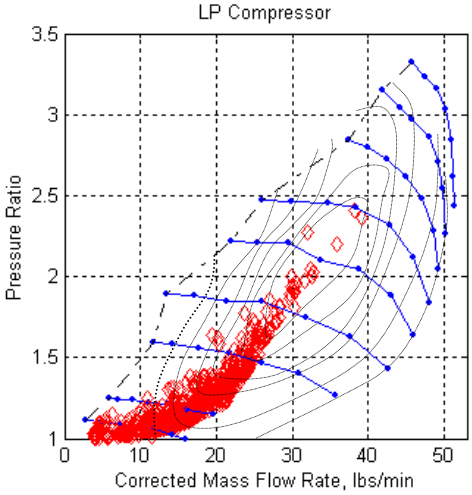

(f) EC + TC

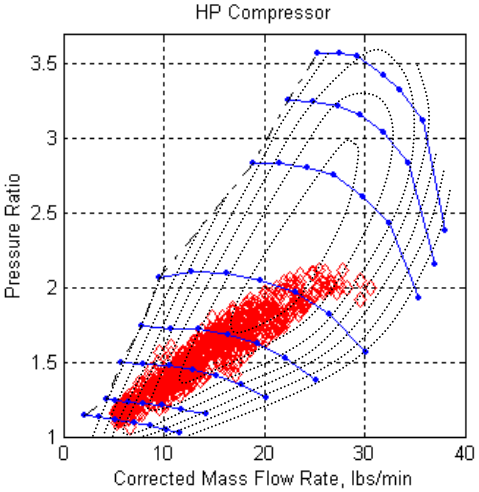

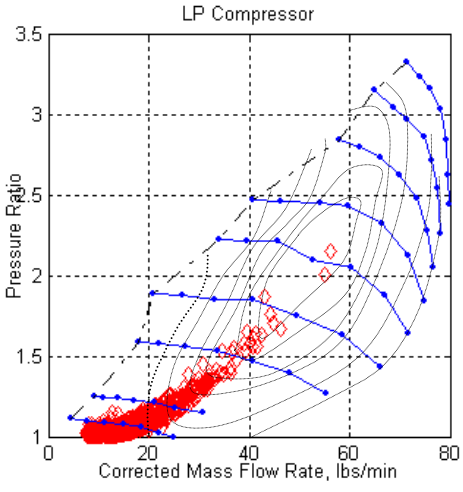

(g) VGT + TC

Figure 52. Visiting points on compressor map

5.7. Summary

When compared to the conventional dual-stage turbocharging system, the hybrid dual-stage boosting systems show improvements in low end torque under steady-state condition and in transient responses since the hybridization of the boosting system results in fewer compromises in the boosting system matching. The hybrid boosting system with the screw type supercharger shows significantly improved performance at low speed and in transient conditions, while sacrificing the fuel economy at low to mid engine speeds. In terms of transient boosting characteristics, this system offers unparalleled performance even though the vehicle launch performance figures are not as impressive as the hybrid boosting system with VGT.

The hybrid boosting system with VGT offers the best performance as well as substantial fuel savings over the baseline V8 engine. The hybrid system with the electrical compressor offers excellent low end torque under steady-state conditions where sufficient time for the electrical compressor to build up boost is available, but poor performance in transient conditions due to the limitation in electrical power supply. This system also offers the best fuel economy through the U.S. FTP-72 driving cycle as the system operates on a single-stage mode most of the time except when the extra boost from the electrical compressor is needed. Therefore, this hybrid boosting system is ideal for fuel economy improvement in a smaller displacement engine where the electrical power supply is no longer the limiting factor.

CHAPTER 6. SUMMARY AND CONCLUSION

The major technical achievements of this study are summarized below.

First, a systematic dual-stage turbocharger matching method has been developed using a turbomachinery scaling and iterative procedure utilizing a combination of turbocharger thermodynamic relations and a physics-based Diesel engine simulation code. Simulation based turbocharger matching can significantly reduce the cost and evaluation time and can be tailored to a specific application. Unlike the turbocharger matching methods presented in [9, 46], where the best match is selected from the available compressor-turbine combinations of the inventory, the method developed in this study involves finding the best match for a specific engine application. Hence, it can be used for initial development of a new dual-stage turbocharging system, as it does not rely on available turbomachinery maps, but rather utilizes the turbomachinery scaling routine to explore a broad design space.

Second, the matching method has been applied to a dual-stage turbocharging with three distinctly different boost control options to investigate the effect of different boosting control methods on engine performance and fuel economy. The effectiveness of the matching method is demonstrated by excellent utilization of both high pressure and low pressure turbochargers in terms of turbomachinery efficiency and engine torque characteristics.

The boost control options considered in the study include two differently configured exhaust bypassing mechanisms, and an EIVC strategy that regulates

turbocharger operation without the exhaust gas bypassing mechanism. Regulating turbocharger operation by EIVC cycle is a novel approach that provides more reliable and efficient alternative to the conventional bypassing mechanisms such as bypass valves and wastegates. The simulation results demonstrates the EIVC strategy is clearly a preferred boost control method as it provides not only better thermal efficiency but also the charge cooling effect to the intake charge that resulted in lower peak cylinder pressure during the combustion which allowed smaller turbocharger selection than the other boost control options considered without exceeding the mechanical limit of the engine block.

Third, in order to further enhance the low end torque and transient characteristics of the dual-stage boosting system, three different types of hybrid boosting systems were investigated and compared their benefits and trade-offs with the baseline V8 engine that is to be replaced by the downsized V6 with advanced turbocharging system. When compared to the dual-stage turbocharging system, the hybrid dual-stage boosting systems show improvements in low end torque under steady-state condition and in transient responses since the hybridization of the boosting system results in fewer compromises in the boosting system matching. In terms of performance compared to the baseline V8 engine both in steady state and in transient conditions, the downsized V6 engine with hybrid dual-stage boosting systems with either VGT or screw type supercharger exceed the performance of the V8 engine. The downsized engine also shows improved fuel economy compared to the V8 engine.

Fourth, the fuel economy of each system through the U.S. FTP-72 driving cycle is compared with the baseline V8. While the hybrid boosting system with electrical compressor offers the best fuel economy, the dual-stage turbocharging system with EIVC

cycle and the hybrid system with VGT offer the best overall balance between the performance and fuel economy, followed by the dual-stage turbocharging system with bypass valve. The hybrid system with screw type supercharger does not offer substantial fuel economy improvement nor the performance enhancement over the baseline V8 engine. However, it offers better control over fuel-air equivalence ratio than the baseline engine, benefiting from the excellent boosting characteristics of the screw type supercharger.

The assessment of the different types of hybrid dual-stage boosting systems presented in the study using physics-based engine simulation and the methodology used in the process provide valuable means to evaluate and develop a new boosting system that requires excellent low end torque and transient boosting characteristics as well as the fuel economy benefit from the downsized engine. It is also very economic compared to the experimental procedure that requires prototyping and testing of the new boosting system.

APPENDIX

Appendix A1. Engine specification

Bore	mm	95
Stroke	mm	105
Con-rod length	mm	176
Compression ratio		18
Firing order		1-2-7-3-4-5-6-8
Firing distance	deg.	90
valve numbers		4
Swirl number		1.8-1.9
Lower heating value	MJ/kg	42.5
Stoichiometric air-fuel ratio		14.5

Appendix A2. Turbocharger performance maps for the baseline V8 engine

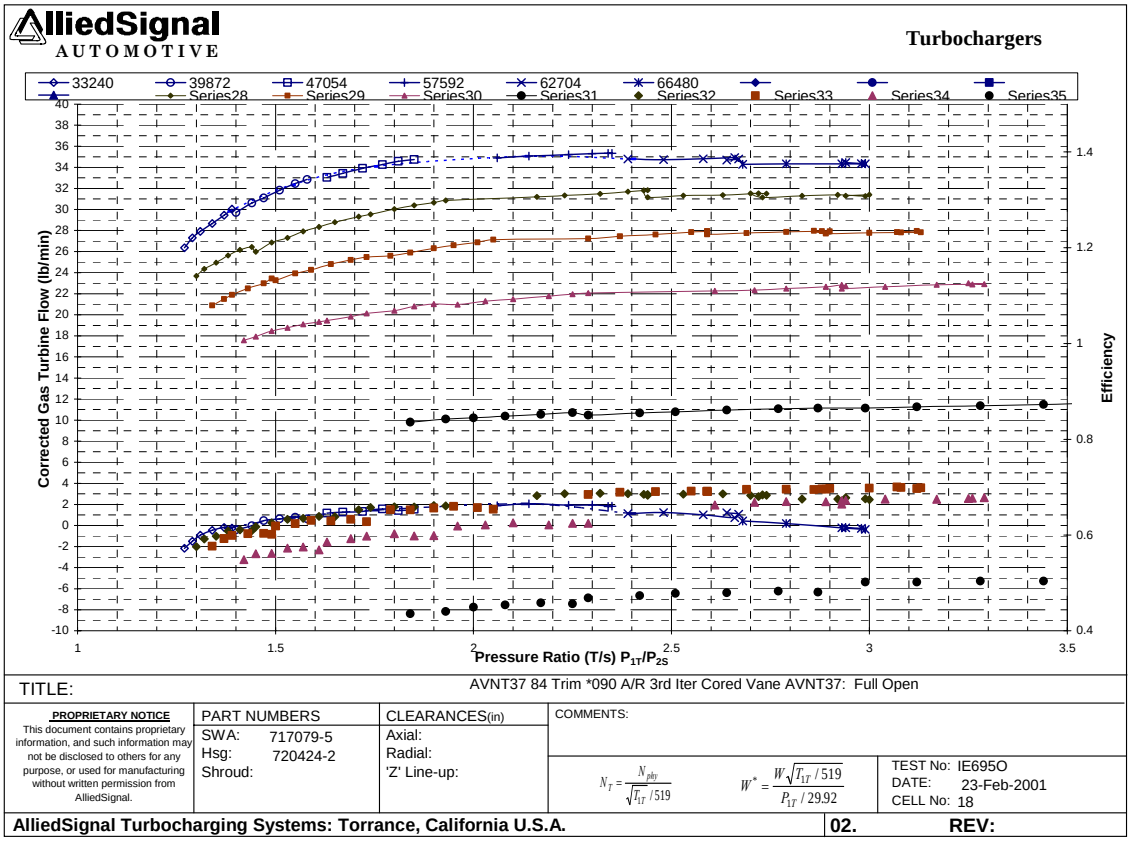

AlliedSignal AUTOMOTIVE

Turbochargers

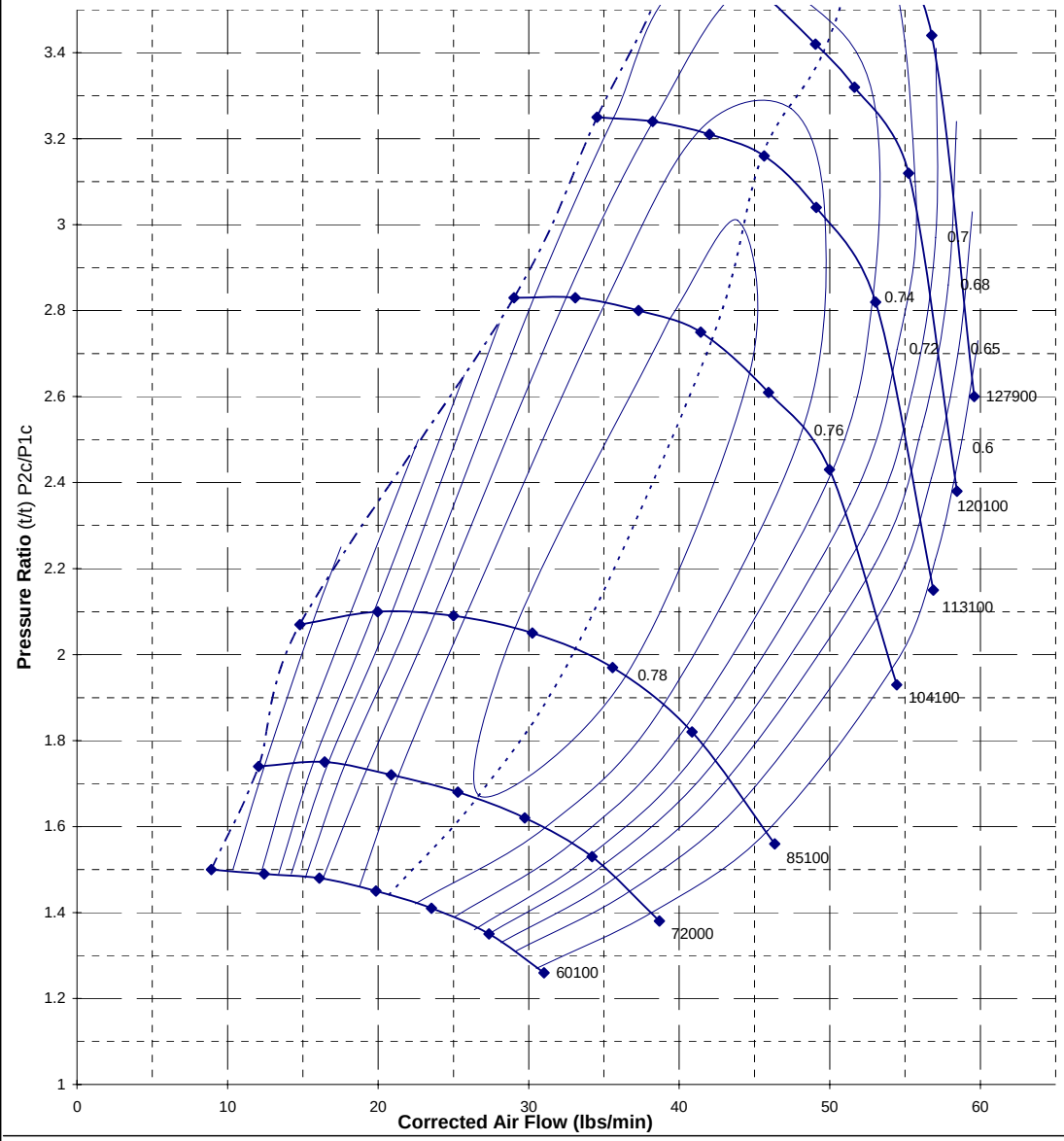

TITLE: GT37 52 Trim *058 A/R C117

PART NUMBERS	CLEARANCES(in)
Wheel: 722142-0006	Axial:
Hsg: 720404-0010	Radial:
B/plate: 712810-0003	'Z' Line-up:
EI = DE =	Diff exit width:

COMMENTS:

$N_c = \frac{N_{phy}}{\sqrt{T_{1c}/545}}$ $W^* = \frac{W\sqrt{T_{1c}/545}}{P_{1c}/28.4}$

TEST No: IE758O
DATE: 13-Apr-
CELL No: 18

AlliedSignal Turbocharging Systems: Torrance, California U.S.A. **01.** **REV:**

BIBLIOGRAPHY

1. Keppeler, S., Schulte, H., and Hermann Josef Ecker, H. J., “The Technical Ramifications of Downsizing HSDI Diesel Technology to the 300 cc Displacement Class,” SAE paper 981916.
2. Cantore, G., Mattarelli, E., and Fontanesi, S., “A New Concept of Supercharging Applied to High Speed DI Diesel Engines,” SAE paper 2001-01-2485.
3. Ecker, H. J., Schwaderlapp, M., and Gill, D. K., ” Downsizing of Diesel Engines: 3-Cylinder / 4-Cylinder,” SAE paper 2000-01-0990.
4. Guzzella, L., Wenger, U., and Martin, R., “IC-Engine Downsizing and Pressure-Wave Supercharging for Fuel Economy,” SAE paper 2000-01-1019.
5. Atkins, M. J., and Koch, C. R., “A Well-to-Wheel Comparison of Several Powertrain Technologies,” SAE paper 2003-01-0081.
6. Lecointe, B., and Monnier, G., “Downsizing a Gasoline Engine Using Turbocharging with Direct Injection,” SAE paper 2003-01-0542.
7. Stoffels, H., and Schroeer, M., “NVH Aspects of a Downsized Turbocharged Gasoline Powertrain with Direct Injection,” SAE paper 2003-01-1664.
8. Beatrice, C., Belardini P., Bertoli, C., Del Giacomo, N., and Migliaccio, M., “Downsizing of Common Rail D.I. Engines: Influence of Different Injection Strategies on Combustion Evolution,” SAE paper 2003-01-1784.
9. Saulnier, S., and Guilain, S., “Computational Study of Diesel Engine Downsizing Using Two-StageTurbocharging,” SAE paper 2004-01-0929.

10. Lake, T., Stokes, J., Murphy, R., Osborne, R., Schamel, A., “Turbocharging Concepts for Downsized DI Gasoline Engines,” SAE paper 2004-01-0036.
11. Toussaint, Y., “Achieving a Low CO_2 Emissions Hybrid Vehicle with a Well to Wheel Approach,” SAE paper 2000-01-3237.
12. Palumbo, A. J., “The "Space Bus" – Performance, Major Components, and Implications for Engineered Hybrid Drive Systems for Medium and Heavy Hybrid Vehicles,” SAE paper 1999-01-3725.
13. Hayes, R. R., Williams, A., Ireland, J., Walkowicz, K., and Black, S., “King County Metro – Allison Hybrid Electric Transit Bus Testing,” SAE paper 2006-01-3570.
14. Katrašnik, T., “Analysis of Fuel Consumption Reduction Due to Powertrain Hybrid-ization and Downsizing of ICE,” SAE paper 2006-01-3262.
15. Takada, Y., Ueki, S., and Saito, A., ” Study on Fuel Economy and Nox Emissions of Medium Duty Hybrid Truck in Real Traffic Conditions,” SAE paper 2004-01-1086.
16. Walters, J., Husted, H., and Rajashekara, K., “Comparative Study of Hybrid Powertrain Strategies,” SAE paper 2001-01-2501.
17. Polletta, D. F., Louckes, T., and Severinsky, A. J., “Fuel Economy and Performance Impact of Hybrid Drive Systems in Light Trucks, Vans & SUV's,” SAE paper 2001-01-2826.
18. Husted, H. L., “A Comparative Study of the Production Applications of Hybrid Electric Powertrains,” SAE paper 2003-01-2307.
19. Burke, A., “Saving Petroleum with Cost-Effective Hybrids,” SAE paper 2003-01-3279.

20. Tamai, G., Jeffers, M. A., Lo, C., Thurston, C., Tarnowsky, S., and Poulos, S., "Development of the Hybrid System for the Saturn VUE Hybrid," SAE paper 2006-01-1502.
21. Wu, B., Lin, C. C., Filipi, Z., Peng, H., and Assanis, D., "Optimization of Power Management Strategies for a Hydraulic Hybrid Medium Truck," Proceedings of the 2002 Advanced Vehicle Control Conference, Hiroshima, Japan, September 2002.
22. Lin, C. C., Filipi, Z., Louca, L., Peng, H., Assanis, D., Stein, J., "Modelling and control of a medium-duty hybrid electric truck," Heavy Vehicle Systems, Int. J. of Vehicle Design, Vol. 11, Nos. 3/4, 2004.
23. Attard, W., Watson, H. C., Konidaris, S., and Khan, M. A., "Comparing the Performance and Limitations of a Downsized Formula SAE Engine in Normally Aspirated, Supercharged and Turbocharged Modes," SAE paper 2006-32-0072.
24. Lefebvre, A., and Guilain, S., "Modelling and Measurement of the Transient Response of a Turbocharged SI Engine," SAE paper 2005-01-0691.
25. Watanabe, T., Koike, T., Furukawa, H., Ikeya, N., Sakakida, M., "Development of Turbocharger for Improving Passenger Car Acceleration," SAE paper 960018.
26. Kawaguchi, J., Adachi, K., Kono, S., and Kawakami, T., "Development of VFT (Variable Flow Turbocharger)," SAE paper 1999-01-1242.
27. Kattwinkel, T., Weiss, R., and Boeschlin, J. P., "Mechatronic Solution for Electronic Turbocharger," SAE paper 2003-01-0712.
28. Cantemi, C. G., "Twin Turbo Strategy Operation," SAE paper 2001-01-0666.
29. Tashima, S., Okmoto, H., Fujimoto, Y., and Nakao, M, " Sequential Twin Turbocharged Rotary Engine of the Latest RX-7," SAE paper 941030.

30. Choi, C., Kwon, S., and Cho, S., “Development of Fuel Consumption of Passenger Diesel Engine with 2 Stage Turbocharger,” SAE paper 2006-01-0021.
31. Serrano, J. R., Arnau, F. J., Dolz, V., Tiseira, A., Lejeune, M., and Auffret, N., “Analysis of the Capabilities of a Two-stage Turbocharging System to Fulfill the US2007 Anti-Pollution Directive for Heavy Duty Diesel Engines,” International Journal of Automotive Technology, Vol. 9, No. 3, pp. 277-288 (2008).
32. Bonello, M. J., Caldwell, D. M., Pigott, J. A., Prior, G. P., and Schag, T. M., “The Supercharged Northstar DOHC 4.4L V8 Engine for Cadillac,” SAE paper 2005-01-1854.
33. Pallotti, P., Torella, E., New, J., Criddle, M., andBrown, J., “Application of an Electric Boosting System to a Small, Four-Cylinder S.I. Engine,” SAE paper 2003-32-0039.
34. Ueda, N., Matsuda, N., Kamata, M., and Sakai, H., Kanesaka, H., ” Proposal of New Supercharging System for Heavy Duty Vehicular Diesel and Simulation Results of Transient Characteristics,” SAE paper 2001-01-0277.
35. George, S., Morris, G., Dixon, J., Pearce, D., and Heslop, G., “Optimal Boost Control for an Electrical Supercharging Application,” SAE paper 2004-01-0523.
36. Miyagi, Y., Takabe, S., Miyashita, K., and Ikeya, N., “Experimental study of New Lysholm Supercharger with a Simple Unloading System”, SAE Paper 960952.
37. Takabe, S., Ikeya, N., and Miyagi, Y., “Second Generation Lysholm Compressor,” SAE paper 980774.
38. Watson, N. and Janota, M.S., “Turbocharging the internal combustion engine,” Wiley-Interscience, 1982.

39. Johannes Andersen, Erik Karlsson and Anders Gawell, “Variable Turbine Geometry on SI Engines,” SAE paper 2006-01-0020.

40. Brace, C. J., Cox, A., Hawley, J. G., Vaughan, N. D., Wallace, F. W., Horrocks, R. W., and Bird, G. L., “Transient Investigation of Two Variable Geometry Turbo-chargers for Passenger Vehicle Diesel Engines,” SAE paper 1999-01-1241.

41. Arnold, S., Groskreutz, M., Shahed, S. M., and Slupski, K., “Advanced Variable Geometry Turbocharger for Diesel Engine Applications,” SAE paper 2002-01-0161

42. Filipi, Z., Wang, Y., and Assanis, D., “Efffect of Variable Geometry Turbine (VGT) on Diesel Engine and Vehicle System Transient Response”, SAE Paper 2001-01-1247, 2001.

43. Nelson, S. A., Filipi, Z. S., and Assanis, D. N., “The Use of Neural Nets for Matching Fixed or Variable Geometry Compressor with Diesel Engines,” Journal of Engineering for Gas Turbines and Power Vol. 125, April 2003, pp. 572-579.

44. Backlund O, Kee P R, Rydquist J E, Giselmo K, Sundin L, “Volvo’s MEP and PCP Engines: Combining Environmental Benefit with High Performance “, SAE Paper 910010.

45. Millo, F., Mallamo, F., and Mego, G.G., “The Potential of Dual Stage Turbocharging and Miller Cycle for HD Diesel Engines”, SAE Paper 2005-01-0221, 2005.

46. Benson, R. S., and Sventnicka, F. V., 1974, “Two-Stage Turbocharging of Diesel Engines: A Matching Procedure and an Experimental Investigation,” SAE Paper No. 740740.

47. Assanis, D.N., and Heywood, J.B., “Development and Use of a Computer Simulation of the Turbocompounded Diesel System for Engine Performance and Component Heat Transfer Studies”, SAE paper 860329.
48. Poola, R. R., Sekar, R., Assanis, D. N., and Cataldi, G. R., 1996, ‘‘Study of Oxygen-Enriched Combustion Air for Locomotive Diesel Engines,’’ ICE-Vol. 27-4, Proceedings of ASME-ICE Fall Technical Conference, Fairborn, OH.
49. Filipi, Z. S., Assanis, D. N., “A Nonlinear, Transient, Single-Cylinder Diesel Engine Simulation for Predictions of Instantaneous Engine Speed and Torque,” Journal of Engineering for Gas Turbines and Power, OCTOBER 2001, Vol. 123, pp. 951-959.
50. Anderson, J. D., “Fundamentals of Aerodynamics”, 2nd edition, 1991.
51. Heywood, J. B., “Internal Combustion Engine Fundamentals”, Mc Graw-Hill, Inc., 1988.
52. Primus, R. J., “A Second Law Approach to Exhaust System Optimization,” SAE paper 840033.
53. Depcik, C., Assanisn, D. N., “A Universal Heat Transfer Correlation for Intake and Exhaust Flows in a Spark-Ignition Internal Combustion Engine,” SAE paper 2002-01-0372.
54. Chang, J., Guralp, O., Filipi, Z., Assanis, D., Kuo, T. W., Najt, P., and Rask, R., “New Heat Transfer Correlation for an HCCI Engine Derived from Measurements of Instantaneous Surface Heat Flux,” SAE paper 2004-01-2996.
55. Assanis, D. N., Filipi, Z., Gravante, S., Grohnke, D., Gui, X., Louca, L., Rideout, G., Stein, J., “Validation and Use of SIMULINK Integrated, High Fidelity, Engine-In-Vehicle Simulation of the International Class VI Truck”, SAE Paper 2000-01-0288.

56. Tuttle, J. H., “Controlling Engine Load by Means of Late Intake-Valve Closing”. SAE paper number 800794.
57. Tuttle, J. H., “Controlling Engine Load by Means of Early Intake-Valve Closing”. SAE paper number 820408.
58. Assanis, D. N., and B. Bolton, “Variable Valve Timing Strategies for Optimum Engine Performance and Fuel Economy,” ASME Paper 94-ICE-5, ASME ETCE Conference, New Orleans, LA, January 23-26, 1994.
59. Asmus, T., “Valve Events and Engine Operation,” SAE Paper 820749.
60. Soderberg, F., and Johansson, B., ”Load Control Using Late Intake Valve Closing in a Cross Flow Cylinder Head,” SAE paper 2001-01-3554.
61. Martins, J.G., Uzuneanu, K., Ribeiro, B.S., and Jasasky, O., “Thermodynamic Analysis of an Over-Expanded Engine”, SAE Paper 2004-01-0617.
62. Anderson, M. K., Assanis, D.N., and Filipi, Z.S., “First and Second Law Analyses of a Naturally-Aspirated, Miller Cycle, SI Engine with Late Intake Valve Closure”, SAE paper 980889.
63. Moro, D., Ponti, F., and Serra, G., “Thermodynamic Analysis of Variable Valve Timing Infuence on SI Engine Efficiency,” SAE paper 2001-01-0667.
64. Kamo, R., Mavinahally, N. S., Kamo, L., Bryzik, W., and Reid, M., “Emissions Comparisons of an Insulated Turbocharged Multi-Cylinder Miller Cycle Diesel Engine,” SAE paper 980888.
65. Bolton, B., and D. N. Assanis, “Optimum Breathing Strategies for Turbocharged Diesel Engines Based on the Miller Cycle Concept,” ASME PD-Vol. 64-8.2, pp. 253-

262, Second Biennial European Joint Conference on Engineering Systems Design and Analysis ESDA Proceedings, London, England, July 4-7, 1994.

66. Wilson, N. D., Watkins, A.J. and Dopson, C., “Asymmetric Valve Strategies and Their Effect on Combustion”, SAE paper number 930821.
67. Kattwinkel, T., Weiss, R., and Boeschlin, J.P., “Mechatronic Solution for Electronic Turbocharger”, SAE Paper 2003-01-0712, 2003.
68. Munz, S., Schier, M., Schmalzl, H.P., and Bertolini, T., “Design and Performance of an Innovative Electrically Driven Charging System”, Borg Warner Turbo Systems.
69. Jacobs, T., Assanis, D.N., and Filipi, Z., “The Impact of Exhaust Gas Recirculation on Performance and Emissions of a Heavy-Duty Diesel Engine”, SAE Paper 2003-01-1068, 2003.
70. Singer, D.A., “Comparison of a Supercharger vs. a Turbocharger in a Small Displacement Gasoline Engine Application”, SAE Paper 850244.